UNIVERSITÀ DI PARMA

DIPARTIMENTO DI SCIENZE DEGLI ALIMENTI E DEL FARMACO

DOTTORATO DI RICERCA IN

BIOFARMACEUTICA-FARMACOCINETICA

XXXIII CICLO

MANNITOL POLYMORPHS AS CARRIER IN DPIs FORMULATIONS: ISOLATION CHARACTERIZATION AND PERFORMANCE

Coordinator: Prof. MARCO MOR

Supervisor: Prof. RUGGERO BETTINI

Ph.D. Candidate: AYCA ALTAY BENETTI

SUMMARY

Introduction

1 Introduction

1.1 Pulmonary drug delivery

Pulmonary drug delivery has become one of the most accepted delivery systems for the treatment of respiratory disorder offering several benefits over oral and intra venous administration [1] [2]–[4]. The absence of the first pass effect and the typical enzymatic degradation of the gastrointestinal tract as well as the direct administration in the lung [1], [5] that often represents the site of action (such as in the case of diseases such as asthma and chronic obstructive pulmonary disease, COPD), allows a significant reduction of the administered dose, with concomitant reduced systemic exposure that, in turn, results in reduced side effects of the active ingredients. Inhalation has also been also proposed as a non-invasive route for the delivery of therapeutic drugs to treat systemic diseases [6]–[8]and for drugs that have low oral bioavailability, such as peptides and proteins, to achieve systemic effects [5], [9]–[11]. The advantages of this route of administration are therefore numerous; first of all, the lungs offer a large surface area available for drug absorption (1 m^2/kg in mammals) [12], highly vascularized and characterized by good epithelial permeability, ensuring a rapid onset of action [13], [14].

However, to exert its therapeutic activity the formulation must be constituted of respirable drug particles, capable to reach the lower airways [15].

Furthermore, a medicinal product intended to be administered in the respiratory tract is always a combination of a formulation and a device [16], therefore, its therapeutic effectiveness is the resulting function of several aspects including the formulation characteristics, the performance

of the inhalation device, the patient's inhalation technique and the physio-pathological characteristics of the airways [17]–[19].

The three main devices for the inhalation therapy management are nebulizers, pressurized, metered-dose inhalers (pMDIs) and dry powder inhalers (DPIs), the latter being the topic of the present thesis.

1.2 Dry powder inhalers

The development of DPIs arises from the need of finding alternatives to the pMDIs to overcome several problems related to these inhalers. The gas used as propellant in pMDIs dangerous for the environment being either reactive with the ozone (CFC) barrier or greenhouse gases (HFA). With DPIs the product is extracted from the inspiratory act thus, they do not require a propellant o any other external source for generating the aerosol; consequently, these products do not need coordination between aerosol delivery from the device and patient inspiration. Furthermore, solid particles have higher aerosolization efficiency than liquid products [20], [8] as well as greater physico-chemical stability. This latter aspect makes DPI, in principle, suitable for the administration of proteins and peptides [21]. Compared to pMDIs, DPIs afford lower speed in the actuation phase, leading to better deposition of the drug into the lower airways. Finally, this type of inhalers, unlike pMDI, can be used with high drug dosages up to 125 mg [22].

Given these advantages it is not surprising that DPIs have are more and more widely used in therapy.

The inhalation device is essential for the drug to effectively reach the lungs therefore, an ideal DPI (Figure 1.1.) should have a number of features to ensure reliability, clinical efficacy as well as easy and correct patient usability [23].

These features include:

- an easy to use, handy, portable and inexpensive device designed to deliver a high and reproducible Fine Particle Dose (FPD), and to provide an environment in which the drug can maintain its physico-chemical stability;
- accurate and uniform drug dose delivery over a wide range of respiratory rates, and constant throughout the life of the inhaler;
- an optimal drug particle size for delivery to the lung;
- suitability for a wide range of drugs;
- minimal adhesion between the formulation and the device;
- a favorable cost-effectiveness ratio and a feedback mechanism to inform the patient that the drug dose has been administered.

However, no DPI among those available on the market today possesses all these ideal characteristics [24].

Figure 1.1. Photographs of some currently available DPIs (A) Aerolizer™, (B) Easyhaler ™, (C) Turbohaler ™, (E) Novolizer ™, (F) Rotahaler ™, (G) Clickhaler ™, (H) MAGhaler ™, (I) Spinhaler ™, (J) Handihaler ™. Reproduced with permission from [24].

1.3 Factors that affect the transport and deposition of active ingredients

It has been reported that the deposition of particles in the respiratory tree can be effected by: low respiratory rate promotes aerosol deposition in the lower airways, higher frequencies increase the amount of powder deposited in the oropharynx and upper airways, the volume of inhaled air may affect the amount and depth of powder deposited in the lower airways [25]. Moreover, holding the breath is crucial for optimal particle deposition. Thus, the anatomical features of the airways and their physiological functions can affect the final outcome of the inhalation therapy [26]. In particular, the presence of diseases or anatomical anomalies, such as airway remodeling stemming from fibrotic processes, can alter the deposition of the particles and affect the patient's ability to inhale the drug. In addition, some recent studies have shown that the geometry of the airway in children is apparently distinct from adults regardless the anatomical anomalies [27] and this distinguished anatomic behavior in upper airway geometry might have an influence on drug deposition in the lung. From a general stand point, the pulmonary deposition of the aerosol depends on three key mechanisms [25], [27], [28]: inertial impact, sedimentation and diffusion which operate in different mutual interaction for the inhalable drugs in the different segments of the respiratory tree. Finally, the speed at which the aerosol is generated can also affect the fraction transported to the lower respiratory tract. Aerosols generated at a very high speed tend to deposit mainly in the upper rather than lower airways. The slower flow minimizes oropharyngeal and upper respiratory tract deposition and increases distal transport and deposition [19]. All these aspects can be summarized in the parameters that describes the particles aerodynamic behavior which rely both on formulation as such and single drug particles.

Aerodynamic diameter, d_{ae}, is the ratio between the geometric diameter and the density of the particle: particles below 1 micron are labelled as extra fine, while particles between 1 and 5 microns are defined as fine particles. Particles below 5 microns constitute the respirable fraction. In general, particles larger than 5 μm are deposited in the upper airways (buccal cavity, larynx, trachea, bronchi) due to inertial impact, while particles with a d_{ae} <5 μm can pass through the upper airways and settle in the lower ones (terminal bronchioles, alveoli) by gravitational sedimentation and under the influence of Brownian motions [27].

Therefore, the smaller the size of the particles, the greater their penetrative capacity into the bronchial tree. However, too small particles with dimensions of less than 0.5 μm can be dragged by the air flow and exhaled [29].

In this respect, the aerodynamic characteristics of the drug particles, and in turn, the fraction of drug transported to the desired site of action, also depends on the physical properties of the particles themselves. [30]. Small dry particles have the potential to reach the lower respiratory tract, but they are also highly cohesive and have poor flow properties, due to the large surface area. In order to enhance the flow properties, small drug particles are blended with coarse carrier particles [1] and they form aggregates thanks to adhesive forces (Van der Walls, hydrogen bonding and electrostatic attraction) between particles. Those aggregates separate upon impaction with the upper airways, freeing the small particles of the API. This underlines the fact that powder formulation is an extremely important factor to achieve improved aerosol performance and effective lung deposition. There are various techniques and particle engineering methods employed to develop DPI formulations.

The interaction of micronized drug particles with larger carriers is used as a strategy in such techniques, so the strong difference in particle size affects adhesion interactions [15], [31]. Since the interaction between the drug and the carrier is surface-mediated, the forces of attraction are also strongly influenced by the topographical characteristics of the particles (such

as for instance the surface roughness or the porosity) and their physico-chemical properties; these aspects have been extensively investigated in particular for the carrier [21], [32], [33]. Interactions are also greatly affected by the relative humidity present in the environment, which promotes the formation of water layers and bridges between the particles, increasing their cohesivity and thus worsening their aerosolization performance [34]–[36] .

The surface properties strongly depend the orientation of the molecules on the surface of the crystals and therefore, on the crystalline form both of the drug and the carrier, although the great majority of the studies available in literature focus mainly on the carrier [11]. This implies that the polymorphism of the carrier may play a crucial role in determining the adhesion forces between carrier and drug. As a paramount example in this respect a recent paper by Della Bella et al. [27] has put into evidence that the use of different lactose pseudopolymorph results in significantly different aerosolization profiles both with hydrophilic and lypophilic model drugs.

2 Aim

The first aim of the present thesis was to produce different polymorphs of mannitol in kinetically stable form and to investigate their solid-state and physico-chemical properties in view of its possible use as a carrier in dry powder inhalers as an alternative to lactose (Chapter 1). Once, the kinetically stable form of the mannitol was obtained, the second aim was to investigate the effect of formulations parameters on capsule filling and aerosolization performance (Chapter 2).

Then, the stability and producibility of a model protein was evaluated in an inhalable formulation containing mannitol and obtained by spray drying (Chapter 3).

Chapter I

1 Introduction

1.1 Polymorphism

Polymorphism is defined as the ability of a material to crystallize into multiple crystalline structures with different molecular arrangements within the lattice [37]. This phenomenon corresponds to that of allotropy of simple elements such as carbon, but at the level of more complex organic molecules. However, it differs from dynamic isomerism, which concerns chemically different molecules in both solid and liquid state; the difference between the various forms of polymorphs, in fact, occurs only in the solid state [38]. In some cases, particularly in the pharmaceutical field, the molecules in the crystalline structure are closely linked to one or more molecules solvent, which is typically water (hydrated material), which becomes an integral part of the structure via hydrogen bonding. The loss of solvent molecules may result in a collapse or conformational rearrangement with transformation of the original crystal form to a new form, called anhydrous. The capability of a material to crystallize both, in solvated and non-solvated form is defined of pseudopolymorphism [39].

It should be noted that the substantial difference at the level of the crystal lattice between the various forms also entails different structural and thermodynamic properties. Indeed, some of the key issues concerning polymorphic systems are the stability of crystalline form whose change is associated with temperature, pressure and other conditions to which it may be exposed. The stability of each polymorphic form in fact depends on its own free energy, described by the Gibbs equation [39]:

$$G = H - TS \qquad \text{(Eq 1.1)}$$

where G is the Gibbs free energy, H is the enthalpy, T is the absolute temperature and S is the entropy. Since S is always positive, G is a function that tends to decrease steadily.

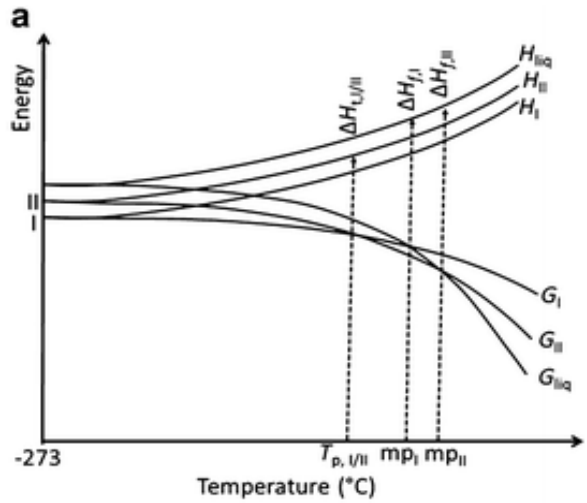

Figure 1.2. Gibbs equation diagram for a system of two polymorphs. Reproduced with permission from [39].

The resulting diagram (Figure 1.2.) is a complex representation of the interconversion among the various phases (liquid and polymorphic solids), that occurs at the intersections between the free energy curves. This illustrates how the less stable forms tend to transform into more stable forms with lower energy [39]. The kinetic and thermodynamic events in which this transformation takes place however are polymorph specific. Thus, the presence of a stable polymorph in nature does not inevitably imply that a metastable polymorph cannot be prepared. Pharmaceutical scientist and companies pay a great deal of attention to crystal polymorphism, due to the fact that it can lead to considerable differences in physico-chemical properties and solid-state form, which may extensively impact on the manufacturability, performance and quality of the drug product [40]. A metastable form is thermodynamically unstable, but it may be isolated and exploited as a result of the relatively slow rate of transformation. In the pharmaceutical manufacturing the metastable form is occasionally preferable for its particular attributes, such as enhanced solubility, preferable behavior over milling and compression or lower hygroscopicity. Nevertheless, a metastable form has a natural (thermodynamically

driven) propensity to convert into the stable form. This transformation is frequently detrimental to the effectiveness of the formulation [41], [42]. Some studies focused on the rate of formation of stable and metastable polymorphs in order to ensure that the polymorphic transition relies upon the processing conditions and the relative stability of the polymorphs forms.

For example, Bernstein et al. [43] using supersaturations to estimate the speed of formation of a metastable polymorph that might be equal to that of stable polymorph during concomitant polymorph development [44]. Black et al. [45] designed the growth rates with implementation to dimorphic p-aminobenzoic acid (pABA). A different approach by Croker and Hodnett predicted that the formation of the metastable polymorphs might be driven by its lower critical free energy in comparison to the corresponding stable polymorph [46]. In the formulation development the detection of transition rate might be crucial for controlling the processing conditions as well as to master the effect of different structural properties of the overall performance of the medicinal product.

1.1.1 Structural properties

The crystalline structure is the fundamental property of each polymorphic form. It is characterized by blocks containing elements that are symmetrical to each other and with a certain structural organization that is repeated regularly along the three dimensions in space. These blocks are called unit cells (Figure 1.3.) Thus, crystalline structure can be described as a three-dimensional structure, consisting of cells of identical units, each of which is uniquely defined by its three-unit cell axes a, b, c and by the three angles α, β and γ, between these axes [37].

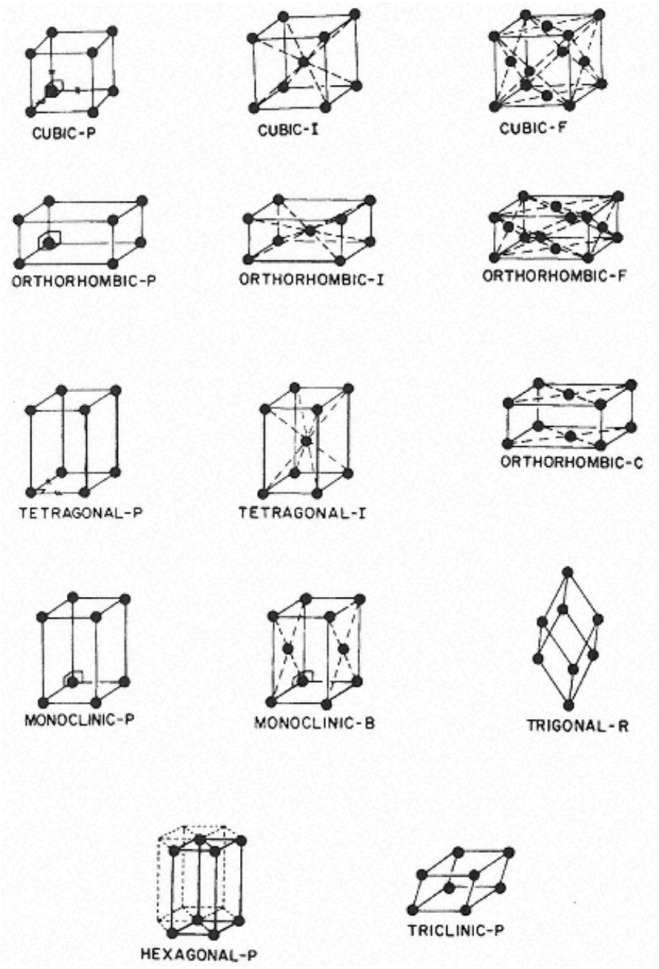

Figure 1.3. Structure of unit cells

When describing crystals and their structures it is important to differentiate between crystal forms and crystal habits. The first choice implies the identification of the different structures in which a crystal can occur (for example Form I or Form α) based on the atoms/molecules spatial disposition and their relevant thermodynamic relationship [37], [47]. The second is to describe the shape of a particular crystal, its morphology, which mainly dependent on kinetic factors such as the growth along certain directions and inhibition along others. It is important to underline that a different habit (external structure) does not necessarily indicate a differ in the polymorphic form (internal structure), but that both internal structure and external form contribute to the properties of each crystal [37], [47].

1.1.2 Pharmaceutical polymorphism

In the pharmaceutical field, solids presenting polymorphism are quite common. They generally show different dissolution rates as well as a different stability at various temperatures. Notwithstanding, some stable polymorphs may demonstrate poor solubility in aqueous solution which is an important issue in the pharmaceutical fields [48], [49] stemming from the different thermodynamic properties that are likely among the most important polymorphism-related properties of the material (Table 1.1)[40], [47].

Table 1.1. Different properties of polymorphic forms.

Packing/physical properties	- Density - Refractive index and optical properties - Electrical and thermal conductivity - Hygroscopicity
Thermodynamic properties	- Melting and sublimation temperature - Glass transition (T_g) temperature (amorphous forms) - $U_{\text{internal energy}}$ - Enthalpy - Heat capacity - Entropy - Free energy and chemical potential - Thermodynamics - P_{vapour} - Solubility (kinetic and thermodynamic)
Spectroscopic properties	- Electronic transitions (UV-Vis spectra) - Vibrational transitions (IR and Raman spectra) - Rotational transitions - Nuclear magnetic resonance
Kinetic properties	- Dissolution rates - Solid-state rates and kinetics - Rate of transition and crystal growth
Surface properties	- Surface area and energy - Interfacial tension - Habit
Mechanical properties	- Hardness - Tensile strength - Compressibility - Easy handling, flow properties and miscibility

These different properties affect the formulation, processing and storage of the pharmaceutical product in different ways. For this reason, it is important to understand the relationship between the crystal structure and its properties in order to optimize the formulation and manufacturing procedures just as it is important to have tools to quantify the different polymorphic forms [49].

Habit-related aspects such as particle size and shape can in fact affect mixing, compression and recrystallization, but also the stability, the dissolution rate and therefore the bioavailability of a solid formulation [44], [47], [50], [51].

As already stated, with DPIs, the different crystalline form of the carrier influences the interaction with the active ingredient and therefore the final aerosolization performance [11].

1.2 Systems used in carrier-based formulation

Inhalable powders must be coarse to facilitate the handling phases, including the dosage of the device, but at the same time fine to reach in lower airways. The problem can be solved by mixing the micronized drug with a carrier whose physical properties such as size, shape, roughness, can modify the behavior of the dry powder [30].

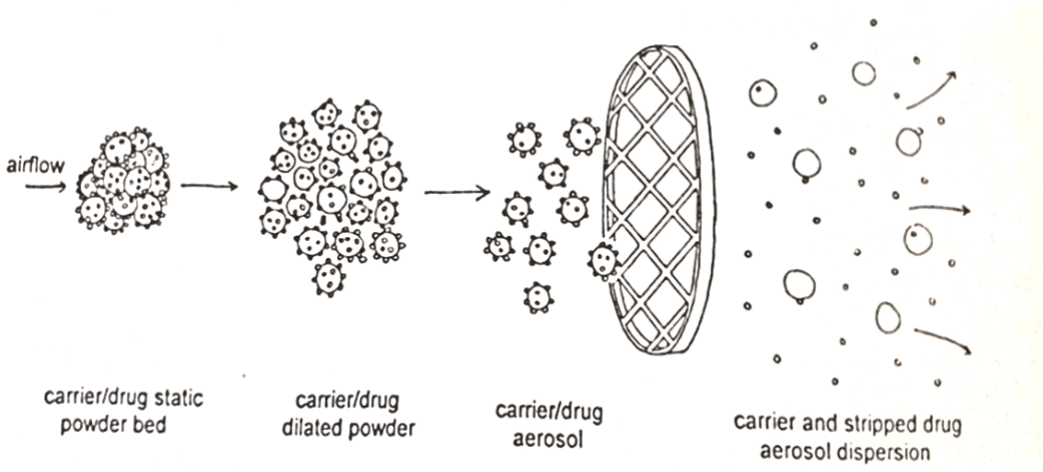

Figure 1.4. Schematic representation of the aerosolization process of a carrier-based formulation. Reproduced with permission from [52].

Homogenous mixture can be achieved by adding progressive quantities of the substances when the ratio between drug and excipient is suitable such as in the case of powder for inhalation used for treating asthma or COPD in which the drug is typically 1 or 2 % by weight of the whole formulation. Generally, this is done by mixing the active ingredient with a similar volume of carrier; this step can be repeated until all the drug particles are distributed over coarse carrier particles (Figure 1.4) [30], [32], [52]. The obtaining of a homogeneous mixture and the efficient aerosolization that leads to the deposit of the drug particles in the deep parts of the airways, are the two sides of the same coin, where the carrier surface characteristics represent the main tool for addressing both the technological an biopharmaceutical problems [31], [53], [54]. Carrier-based formulation enhances the flow properties of cohesive micronized drug particles and consequently physical properties of those coarse carrier particles (porosity, roughness, particle size distribution, surface energy and charges) have a considerable impact on the aerodynamic performances of inhalable mixtures.

1.2.1 Relevance of carrier selection

Lactose is one of the most widely used excipients as a diluent in many solid pharmaceutical preparations [5], [55]–[58]. A diluent facilitates to distribute the active ingredient powder and therefore give volume and consistency. It must be inert and biocompatible and must have appropriate technological properties according to the defined use (e.g. flowability, compactability etc.).

One problem that may be related to use concerns the more and more widespread intolerance towards this substance. To frame the problem correctly, it is necessary to distinguish allergy from intolerance [59]. Allergy is an immune-mediated phenomenon (IgE-mediated or cell-mediated) that involves milk proteins (mainly casein, lactalbumin, lactoglobulin). In its most

common form (IgE-mediated) it manifests itself with systemic symptoms (urticaria/angioedema, rhinitis, bronchospasm, vomiting/diarrhea, sometimes shock) immediately after ingestion of milk (mainly cow, but also of other mammals) and milk derivatives [60], [61].

Intolerance does not depend on immunological phenomena and concerns milk sugars. It is due to a deficiency, often congenital, of lactase (an enzyme present in the intestine responsible for breaking down lactose into glucose and galactose) which causes lactose malabsorption [62]. It manifests itself exclusively with gastrointestinal symptoms a few minutes after ingestion of milk and dairy products and does not involve additional risks.

In the carrier-based formulation, lactose improves both the mixing efficiency and the dispersion of the drug within the lower airways. Upon aerosolization (Figure 1.4) the micronized drug particles detach from the carrier particle surface and are transported in the airways while lactose particles are coarse enough (> 50 microns) to be deposited in the oropharynx and then passes into the stomach after being swallowed [5], [53], [63].

The quantities used for this purpose (some preparations contain a maximum of 12.5 mg) are not capable of causing clinically significant reactions in lactose intolerant subjects, who manifest symptoms only above a certain individual dose-threshold (always in the order of grams) [64]. Generally, about 12-18 grams of lactose, equivalent to the content of 240-350 mL of milk, is needed to induce symptoms of lactose intolerance, but some patients may experience symptoms even after taking three grams [60].

The lactose present in active ingredients can be synthetic (pure lactose) or, more often, extracted from milk. In the second case, preferred because it is less expensive, there may be traces of proteins potentially recognizable by allergy sufferers [61]. This potential risk in reality seems to occur very rarely. The risk of allergic reaction to lactose containing formulations and in particular to inhalable ones is limited to subjects with extremely high allergic reactivity. It

also seems extremely remote, and in any case not documented, the possibility that repeated inhalation of small quantities of cow's milk proteins present in inhalable formulations could accentuate the chronic bronchial inflammation typical of asthma or induce in subjects allergic to milk [61], [62], [64].

On the other hand, mannitol (Figure 1.5) is a natural chiral alditol belonging to the category of hexahydric alcohol that is a stereoisomer of sorbitol and was originally isolated from the secretions of the flowering ash (Fraxinus ornus) [65]. In the inhalable formulation, mannitol alone is used for the treatment of cystic fibrosis [66], but also as an excipient for solid formulations for oral use (tablets and granules) and has been proposed as carrier in formulations for DPI as an alternative to lactose [34], [67]. Compared to lactose, it has some advantages: it is less hygroscopic and has no reducing function, a property that allows it to be used also in association with peptides and proteins.

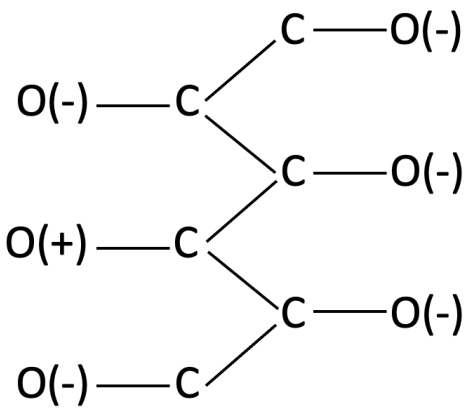

Figure 1.5. Chemical structure of D-mannitol.

It is reported in the literature that mannitol can exist in three anhydrous polymorphic forms (α, β and δ) and in a hemihydrate form [68], [69]. These depend on the crystallization conditions: type of solvent used, concentration, temperature and rate of cooling. The molecule can assume

six different staggered conformations thanks to the freedom of rotation of the bonds (Figure 5) [70] . Only three of these, however, are able to minimize the repulsion between the oxygen atoms that are on the same side of the carbon chain and therefore have a lower energy. In all three polymorphic forms the molecules have the same conformation and in none of these the terminal oxygen atom is aligned with the carbon chain [69]–[71]. The polymorphism is therefore determined by the different arrangements of the hydrogen bonds that are established with the surrounding molecules.

Beside mannitol and lactose, trehalose is another possible carrier which has been drowning the attention by the pharmaceutical scientist involved in drug delivery systems for the lung [9], [72]–[74]. It has been identified as the main chemical substance produced by different types of plants, spores, crustaceans and some species of animal organisms, called cryptobionts [75]. It has been observed that the presence of trehalose in solution increases the denaturation temperature of proteins and inhibits their precipitation in the formulation or during the production of solid formulation [76]. This disaccharide also prevents the chemical and physical degradation that may occur in the carrier-based formulations [76].

Two hypotheses have been described according to which the use of sugars or sugar alcohols would allow greater stabilization of proteins during the transformation of a solution into a solid powder such as in the freeze drying or in spray drying process [77]–[80]. The theory of vitrification, according to which the immobilization of the protein at the level of the amorphous and glassy matrix of the sugar would reduce the degradation of the protein itself [73], [77]. In fact, in the glassy solid-state structural changes are delayed, and only small molecular movements may occur, such as rotations and vibrations of the amino acid side chains. The second theory is water replacement, in which stabilization is due to the formation of hydrogen bonds between the hydroxyl groups of the sugar and the protein, that replace the hydrogen

bonds between water and protein lost during drying process ultimate assisting the native structures of the protein to remain unchanged [35], [73], [81].

2 Aim

The main aim of the present thesis was to produce different polymorphs of mannitol in kinetically stable form and to investigate their solid-state and physico-chemical properties on the *in vitro* aerosolization performance in view of its possible use as a carrier in dry powder inhalers as an alternative to lactose.

As many DPIs imply the use of hard capsules, a second aim was to investigate the effect of capsule filling parameters and physico-chemical properties of the filling material on the microdosage filling process.

The last aim involved the investigation of a model protein candidate in a potentially inhalable formulation containing mannitol obtained by spray drying technique.

The first part of the research work was organized in two distinct phases.

The first phase was dedicated to the production and isolation of each polymorphic form with particular attention to the development of methods for the kinetic stabilization of the metastable forms α and δ. Each polymorph was characterized in terms of purity of the powder, thermal behaviour water content, stability, surface morphology and particle size.

In the second step, the performance of each polymorphic form as a carrier in an DPI was evaluated. Mixtures of mannitol α, β or δ were then prepared with two different active ingredients, namely, salbutamol sulphate and budesonide, chosen as hydrophilic and lipophilic drug model respectively.

The rationale behind this part of the project was the production of different carrier surface characteristics, stemming from the different molecular arrangement in then crystal structure without changing the carrier itself (keeping the primary chemical structure). This would allow, in principle, to "extract" information on drug-carrier interaction due to specific solid-state

properties and eventually to exploit these properties to produce a DPI with improved aerosolization performances.

This part of the study was carried out *in vitro* with the using an Andersen Cascade Impactor, to estimate the amount of drug able to reach the lung level (fine particle fraction - FPF%). Aerosolization was performed using two devices with different resistance to introduce a further element capable to put into evidence the de-aggregation features of the drug-carrier mixtures. Finally, the mannitol-based carrier performances were compared to those lactose-based formulations which, as already stated, represent the benchmark of the presently available DPIs.

3 Material and methods

3.1 Material

Pearlitol® 200SD and Pearlitol® 160C were obtained from Roquette, France. Micronised salbutamol sulfate (SS) and budesonide (BUD) were supplied from Fagron, Bologna, Italy and by Chiesi Farmaceutici, Parma, Italy respectively. Lacto-Sphere® MM50 (sieved α-lactose monohydrate, d_{V50} = 53.1 μm) was provided by Micro-Sphere SA (Switzerland).

3.2 Methods

3.2.1 Crystallization techniques of D-mannitol

Recrystallization of mannitol was carried out in order to isolate kinetically stable mannitol polymorphic forms with techniques suitable for manufacturing scale-up.

Hydrate form recrystallization

The hydrate and β forms were prepared by freeze-drying a water solution of Pearlitol® 200SD at the concentrations of 4 % and 18 % w/v using a laboratory freeze-drier (Alpha 2-4 LSC Plus, Martin Christ Gefriertrocknungsanlagen GmbH, Osterode am Harz, Germany).

The following conditions afforded hydrate form as characterized below: (1) Preparation of the D- mannitol solution 4% w/v in purified water and equilibration at -20 °C for 3 hours (2) Freezing at -45 °C for 20 minutes, (3) Primary drying at -15 °C for 2 hours, then, 0 °C for 1 hour, then, 10 °C for 2 hours 0.100 mbar, (4) Secondary drying at 25 °C for 4 hours at 0.100 mbar.

Since this form was not stable enough as it rapidly dehydrated forming the β polymorph an attempt was made to increase its stability at ambient temperature; thus, a small amount of CaCl

(1% w/w of mannitol) was added to the water solution and submitted to the above-described process of freeze-drying.

β form recrystallization

The β form of mannitol, which is the thermodynamically stable one, was prepared using two different methods.

The first was similar to the method used to obtain the hydrated form from freeze drying, but with a longer time (10 hours instead of 4 hours) in the secondary drying phase (25 ^{o}C - 0.100 mbar).

The second method implied for the use of an acetone as anti-solvent. 4.5 g of mannitol Pearlitol® 160C were weighed and dispersed in an Erlenmeyer flask containing 25 mL of ultrapure water (18% w/v). The solution was placed on a magnetic plate for 2 hours until complete mannitol dissolution and then filtered (PTFE 0.45 μm) using a vacuum pump. 25 mL of acetone were then added to the water solution of mannitol, under magnetic stirring for 4 hours. The precipitate was then filtered using the same type of a filter and placed in an oven at 30° C for 12 hours until complete drying [69].

α form recrystallization

For the preparation of the mannitol α form, 1 g of Pearlitol® 200SD and different amount of PVA (0, 1 or 2% w/w of mannitol) were weighed and transferred in an Erlenmeyer flask and brought into solution in 125 mL of methanol on a heated magnetic plate at a temperature of 60° C for 2 hours. The solution was then filtered (PTFE 0.45 μm) under vacuum and placed into an ice bath for 30 minutes under stirring. The obtained mannitol precipitate was finally filtered (PTFE 0.45 μm) and dried in an oven at 30° C for 12 hours [69].

δ form recrystallization

The δ form was obtained by crystallization in presence of PVP, thus modifying the method proposed by Cares-Pacheco et al. and Vanhoorne et al. [69], [83]. For all samples, the same filtration and storage conditions were applied, that is a Büchner filtration with a 0.45 μm pore size of PTFE membrane (ALBET®, Spain) followed by storing in desiccator with silica gel.
4.5 g of mannitol Pearlitol®160C were weighed and dispersed in the presence of PVP K30 (from 0.5 to 3% w/w of mannitol) in 25 mL of ultrapure water in an Erlenmeyer flask. The solution was placed on a magnetic plate for 2 hours until complete mannitol dissolution and then filtered (PTFE 0.45 μm) using a vacuum pump. 25 mL of acetone were then added to the water solution of mannitol, under magnetic stirring for 4 minutes. The obtained mannitol precipitate was finally filtered with (PTFE 0.45 μm) and dried in an oven at 30° C for 12 hours [69].

3.2.2 Solid state characterization

The solid state and physical characteristics of the mannitol phases were assessed by X-Ray diffraction on powder (XRPD), differential scanning calorimetry (DSC), dynamic vapor sorption (DVS), laser light diffraction and scanning electron microscopy (SEM). In order to identify unambiguously the crystalline phase of the recrystallized mannitol, the Cambridge Crystallographic Database was used to obtain the X-ray Powder Diffraction beamline of pure mannitol crystals [84], [85]. The diffraction pattern of the pure crystalline phase was obtained by downloading the data file related to then relevant crystal phase in ".cif " format from the Cambridge Crystallographic Database (CCD). This file was processed using the Mercury 4.0.0 software (Cambridge Crystallographic Data Centre, UK), to calculate the powder pattern of the

forms of mannitol. Subsequently, data have been converted into Microsoft Excel format and compared to those obtained experimentally.

3.2.2.1 X-ray diffraction on powders

The analysis was performed with a MiniFlex diffractometer (Rigaku, Japan) using Cu Kα radiation (λ= 1.5418 Å) generated with 30 kV. The samples were put into the aluminum sample holder until it was completely covered by powder and then gently compacted with a glass slide in order to obtain an even surface. The goniometer was set at a scanning rate of 1.5° min^{-1} (step size = 0.05°) over the 2θ range 2-35°. Each measurement was carried out in triplicate.

3.2.2.2 Particle size distribution

The particle size distribution of the mannitol powders was measured by laser light diffraction (Spraytec, Malvern, UK). Powders were dispersed in cyclohexane at the concentration of 1 % w/v in the presence of 0.1% w/v of Span 85 and sonicated for 3 min (8510, Branson Ultrasonics Corporation, USA). Particle size distributions for three dispersions of each powders were performed with an obscuration level of at least 10%. Data were expressed in terms of equivalent volume diameter (Dv) for $10^{th}/50^{th}/90^{th}$ percentiles: Dv(10), Dv(50), and Dv(90) respectively. The amplitude of the distribution was expressed by means of the span value, defined as:

$$Span = (Dv(90)- Dv(10))/ Dv(50) \qquad \text{(Eq 1.2)}$$

3.2.2.3 Differential scanning calorimetry

A DSC 821e (Mettler Toledo, Switzerland) driven by STARe software (Mettler Toledo) was employed to investigate the thermal behavior of mannitol forms in the temperature range between 25°C and 200° at the heating rate of 10°C/min. The instrument was previously calibrated with Indium (onset of melting T_m = 156.48°C, enthalpy of melting ΔH_m = -28.60 J g^{-1}). Samples of about 5-8 mg were placed in a 40 µL aluminum pan with a pierced cover and heated under a flux of dry nitrogen (100 mL/min).

3.2.2.4 Thermogravimetric analysis

Thermogravimetric analyses performed with the TGA/DSC1 instrument (Mettler Toledo, Switzerland) was used to evaluate the water content of the powders based on their weight loss due to heating. Samples of about 5-8 mg sample were weighed in 40 µL aluminum pan and heated in the temperature range between 25 and 100°C at the heating rate of 10°C/min under nitrogen flow at 80 mL/min.

3.2.2.5 Scanning Electron Microscopy

The morphology of the different mannitol polymorphs was investigated via scanning electron microscopy using a FESEM SUPRA™ 40 (Carl Zeiss, Germany). Each powder sample was deposited on adhesive black carbon tabs pre-mounted on aluminum stubs in order to allow the dispersion of the charge and coated with a gold film of about 60 nm. The particles in excess were gently removed with a nitrogen flow. The samples were analyzed under high vacuum

conditions (1.33×10^{-2} Pa for 30 min) and the images were collected at different magnifications using an accelerating voltage of 1 kV.

3.2.3 Preparation of adhesive mixtures

All blends were prepared with 1% active ingredient content on the final weight. In order to investigate the better and faster method of preparation, the "sandwich" method (or layering, which consist in placing a fraction of the excipients in the blender, then layering the active ingredient over the surface of the excipient, and finally putting the remaining part of the excipient on the top of the powder bed) and the geometric dilution method were compared. The same mixture was prepared following the two methods using a Turbula® blender and five samples of each mixture were collected every five minutes to be analyzed via HPLC. The mixture was considered homogeneous when the coefficient of variation (calculated as the percentage of the ratio between standard deviation and mean value on the five measurements) was lower than 5%. The method that ensured better yield and shorter preparation time was geometric dilutions. Therefore 2 g of each mixture (model drug and different mannitol polymorphs) were prepared using this method, by mixing for one hour at 40 rpm.

3.2.4 In vitro aerodynamic assessment

The aerodynamic assessment of the blends was performed using an Andersen Cascade Impactor (ACI; Copley Scientific, UK) employing two devices with different resistance RS01® (RPC Plastiape Spa, Italy) and the prototype NESAT® (Bormioli Pharma Srl, Italy). The effective cut-off diameters (ECD) of each stage were recalculated according to Stokes's law using the ECDs referring to a flow of 28.3 l/min [86] :

$$D_Q = D_{28.3} \cdot \sqrt{\frac{28.3}{Q}} \qquad \text{(Eq 1.3)}$$

where D refers to the cut-off diameter at the flows Q used during *in-vitro* test.

The pre-separator, having 10 µm of *cut off* diameter was equipped with a liquid trap (10 mL of ultrapure water) in order to capture non-inhalable large particles. The micro orifice collector (MOC) was equipped by type A/E glass filter (Whatman, UK). To avoid particle bounce, ACI plates were coated with 1% (w/v) glycerol in methanol for SS and 2% (w/v) Tween 20 in ethanol for BUD, allowing solvent evaporation before ACI assembling. The device was connected by a rubber mouthpiece adapter to the ACI and an air stream generated by a VP 1000 vacuum pump (Erweka, Germany) was set to have a pressure drop behind the impactor of 4 kPa and 4 L of the air volume; thus, 4 s at a flowrate of 60 L/min or 5.1 s at a flowrate of 48 L/min were used for RS01® and NESAT® respectively. A capsules size 3 (Quali-V® Qualicaps Europe, Spain) were manually filled with 20.0 ± 0.2 mg of powder.

After the aerosolization process, the capsule was removed from the device, the deposition test was repeated until six capsules had been discharged. At the end of the test the drug deposited at the various levels (capsule and device, rubber and throat, pre-separator, stage 0, 1, 2, 3, 4, 5, 6, 7 and filter) was collected with a mixture of acetonitrile: water (6:4 v/v) for BUD and with distilled water for SS. The residual part of drug in the capsule device, rubber adaptor, throat and pre-separator were collected in a 50 mL flask each whereas the drug deposited on the plates and filter were washed in crystallizers containing 10 mL of solvent. The drug solutions obtained by washing the capsule, device and filter were also sonicated for 5 minutes and filtered with RC filters to ensure homogeneity. The concentration of SS and BUD in each sample was determined by the HPLC. Each formulation was tested three times.

The obtained data were processed with Microsoft Office Excel 16.16.21 (Microsoft Corp., USA) and KaleidaGraph (version 4.5.4 Sinergy Software, USA) softwares to obtain the

aerodynamic parameters: the Emitted Dose (ED) which is the amount of drug discharged from the device after inhalation; the Emitted Fraction (%), calculate as the ratio between the emitted dose and the loaded dose in the capsule; the fine particle dose that corresponded to the amount of drug recovered in the stages of impactor; the Fine Particle Fraction (FPF%) calculated as the ratio between fine particle dose and emitted dose and the Mass Median Aerodynamic Diameter (MMAD) which is the diameter that separates the aerosolized particles in two populations with equal weight. MMAD was determined by plotting the cumulative percentage of mass less than the cut-off diameter for each stage on a probability scale versus the relevant aerodynamic diameter of the stage on a logarithmic scale. MMAD corresponds to the slope of the line obtained by linear regression of the experimental points.

3.2.5 High Performance Liquid Chromatography (HPLC)

The samples collected from the aerodynamic studies were loaded into vials for the HPLC analysis, performed using an Agilent 1200 LC Series (Agilent Technologies, USA), driven by a ChemStation software A.04.02, using a UV detector set at the wavelength of 220 and 254 nm for salbutamol sulphate and budesonide respectively. The applied analytical methods differed between budesonide and salbutamol. As for salbutamol sulphate, the mobile phase was prepared from 6 g of KH_2PO_4 in 800 mL of ultrapure water. After neutralizing to pH 7 with 10M NaOH, the solution was brought to volume of 1 L and filtered with a 0.45 μm CA-filter (Sartorius Stedim Biotech GmbH, Gottingen, Germany). The phosphate buffer solution was mixed with methanol (4:6 v/v) to obtain the final mobile phase that was pumped at 0.6 mL/min, through Supelcosil^{TM} LC-18 column (25 cm x 4.6 mm, 5 μm) kept at 30° C; 50 μL of sample solution were injected and the retention time was 5.6 minutes. The analytical method was

assessed in terms of linearity of response (AUC *vs* concentration) in the concentration range 4 - 40 μg/mL; Limit of d Quantification; Limit of Detection, evaluated as:

$$LOD = 3.3\ \sigma/slp \qquad \text{(Eq 1.4)}$$

$$LOQ = 10\ \sigma/slp \qquad \text{(Eq 1.5)}$$

Here σ and the *slp* are the standard deviation and the slope respectively of the regression line of the absorbance *vs* concentration experimental points. In the set conditions LOQ was = 1.04 μg /mL and LOD resulted = 0.31 μg/mL.

For budesonide the mobile phase was a mixture of acetonitrile: water (6:4 v/v). The flow was set at 0.75 mL/min through an Atlantis® dC18 column (150 mm x 3.9 mm); 50 μL of sample solution was injected and the retention time was 3.3 minutes. Also, in this case the analytical method was assessed in terms of linearity of response in the concentration range 4 - 40 μg/mL (LOQ = 0.32 μg/mL; LOD = 0.097 μg/mL).

3.2.6 Preliminary cell toxicity

Cell viability was measured in terms of mitochondrial activity using the 3-(4,5-dimethylthiazol-2-yl)-2,5-dyphenyltetrazolium bromide (MTT) assay on a human lung cancer cell line, Calu3 (ATCC® HTB-55®) [87]. Cells at passage 36 were seeded into 96-well plates (VWR Tissue culture plates, VWR International, Italy) at a density of 3 x 10^4 cells/well in 200 μl of culture medium composed of MEM (Minimum essential medium, Gibco®, Thermo Fisher scientific, USA) with the addition of 10% fetal bovine serum (FBS, Heat inactivated, Aurogene s.r.l. Italy) 1% penicillin/streptomycin solution (100x Aurogene s.r.l. Italy) and 1% of non-

essential amino acid solution (MEM NEAA, Gibco®, Thermo Fisher scientific, USA). Cells were left to settle and form a monolayer for three days before performing the viability assay.

The powder samples were dissolved in Hanks buffered salt solution (HBSS, Gibco, Thermo Fisher scientific, USA) + 30 mM HEPES (>99.5% H3375, Sigma-Aldrich, Italy). Before the test, growth medium was removed and 150 µl of each solution to be tested were added to each well and left for (4 hours or) 24 hours at 37°C, 5% CO_2. After incubation, solutions were gently removed and 150 µl of 1 mg/mL solution of thiazole blue tetrazolium bromide (M2128, Sigma-Aldrich, USA) in HBSS+ 30 mM HEPES were added and left for 2 hours at 37°C, 5% CO_2. After removing the solution, precipitated formazan crystals were dissolved in 120 µl DMSO for each well, under shaking, for 10 min in the dark. Absorbance of samples was read at 570 nm by means of a plate reader Spark® (Tecan, Switzerland). The concentrations of mannitol, PVP or PVA to be tested were chosen on the basis of a rough estimate of the amount of each component, in terms of respirable fraction, that could reach the lungs following an inspiration from a capsule loaded with about 20 mg of excipient, which was set at 2 mg. This amount is supposed to be dissolved in the available volume of lung lining fluid, whose estimate is between 10 and 30 mL [14]. On these bases, and assuming the worst-case scenario (more concentrated solution) 0.2 mg/mL mannitol was considered as reference concentration to be evaluated and a viability assay was executed over 8 concentrations following a serial dilution of two, covering and exceeding this value. As a consequence, PVP and PVA, when taken alone, were tested at concentrations reflecting their relative ratio with mannitol during crystallization, namely 1% w/w and 2% w/w respectively, with a final reference concentration of 2 µg/mL and 4 µg/mL. HBSS + 3mM HEPES was chosen as a solvent for powder as well as negative control for the test: viability of cells was expressed as percentage with respect to untreated negative control as mean value + standard deviation (n=4).

The statistical analysis was performed with Microsoft Office Excel 16.16.21 software employing a two-tailed unpaired t-test with significance level fixed at *p*-value = 0.05. Standard deviation was used to indicate experimental variability.

4 Results and discussion

4.1 Solid-state and physical characteristics assessment of mannitol crystallized forms

The purpose of this part of the project was to investigate whether mannitol powders in different crystal phases could affect the aerosolization behavior of two model active pharmaceutical ingredient (API) when said mannitol particles were used as carried in adhesive mixture. To this aim, starting from the work of Cares-Pacheco et al. [69] (for α form) and Vanhoorne et al. [67], [83] (for δ form), modified crystallization procedures were developed in order to isolate four mannitol solid phases suitable for the production of binary mixtures with the selected micronized API in terms of kinetic stability, and physical characteristics such as shape and particle size distribution.

The obtained mannitol solid phases were, first of all unequivocally identified by comparing their powder X-ray diffraction patterns with the those relevant to α, β, δ and hydrate form obtained from the CCD. Figure 6, 7, 8 and Figure 9 reports the PXRD patterns of the crystallized mannitol α, β, δ and hydrate forms in comparison with the relevant theoretical one from CCD.

Considering the α form (Figure 1.6) in the absence of PVA [69] the diffraction pattern substantially differed from that obtained from CCD, while the addition of 2% PVA resulted in a good matching with the reconstructed pattern as testified in particular by the presence of the diagnostic peaks at 8.98°, 10.52°, 13.24° and the most intense at 16.84° *2Theta*. At 1% PVA the presence of the latter peak at low intensity suggest the formation of a mixture of phases rather than pure α form as also indicated by the absence of the peaks at 8.98° and 10.52° *2Theta*. Thus, 2% PVA appears to be the lower polymer concentration suitable for obtaining

the stable α form.; although the use PVA in formulation for inhalation has already been proposed [88] it is worth underlying that PVA has not yet been approved for such application; therefore, a low concentration of PVA in the carrier would be beneficial to reduce the polymer burden that by reach the respiratory tree, although it should be considered that most of the carrier deposition in the oropharyngeal region and is eventually swallowed .

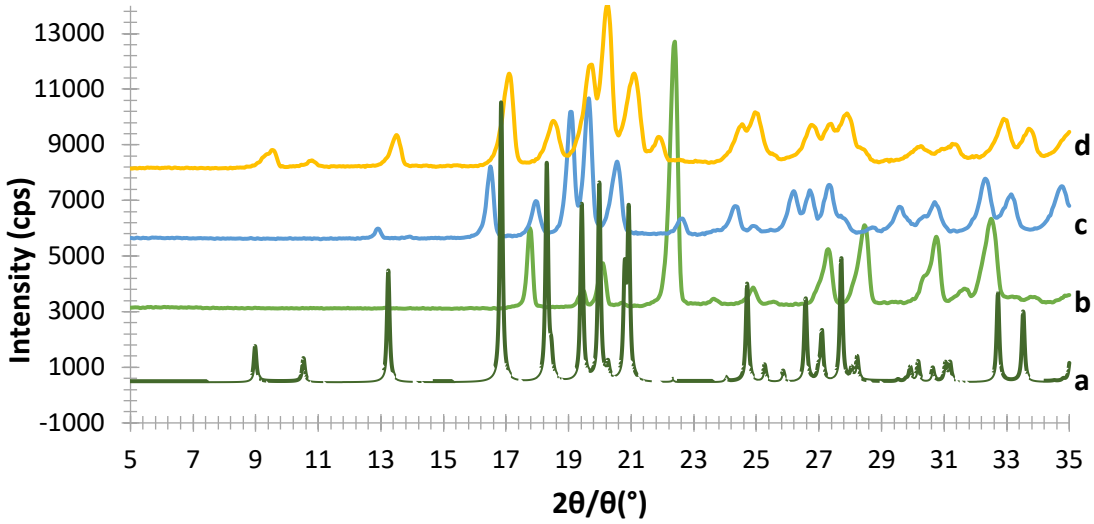

Figure 1.6. PXRD patterns of mannitol α form (d) prepared in saturated methanol solution using 2% of PVA (c) 1% of PVA (b) without PVA (a) CCD reference.

As for the supposed β form (Figure 1.7), the superimposition with the pattern reconstructed from CCD data was quite good for the powders obtained with both crystallization methods in particular for the characteristic peaks at 10.06°, 14.22°, the most intense peak at 23.02° and the one at 20.10° *2theta*.

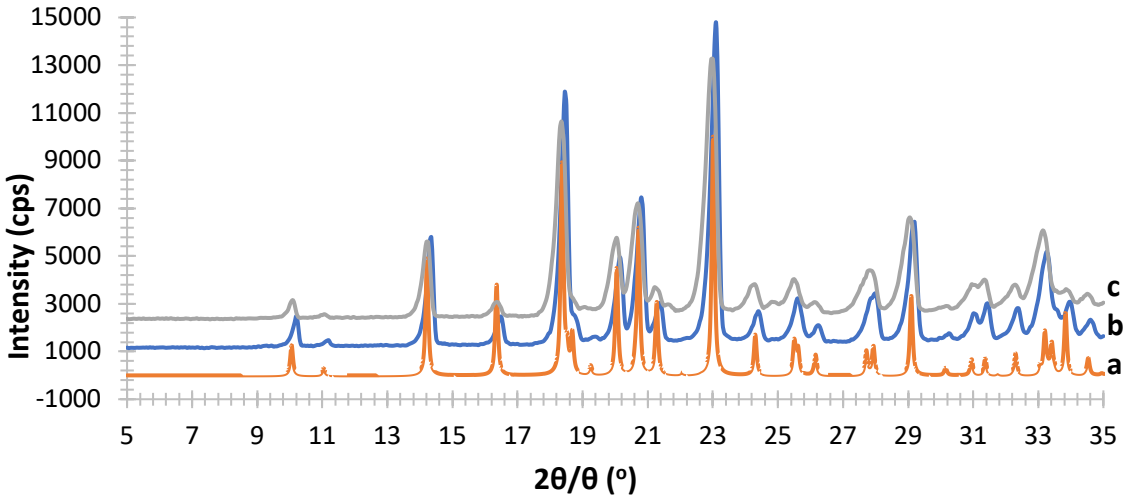

Figure 1.7. PXRD patterns of mannitol β the form (c) obtained using acetone as an antisolvent. (b) freeze drying technique (a) CCD as a reference.

The PXRD patterns obtained from CCD for the δ form is reported in Figure 8 along with those obtained from the powders prepared by modifying the method propose by Vanhoorne et al. [67], [83] who added 5% of PVP to get stable mannitol δ form. Similarly, to the approach adopted for the δ form the rationale here was to figure out what was the lower amount of polymer necessary to obtain crystallographic pure (and possibly kinetically stable) δ form in order to limit at the minimum the polymer potentially reaching the airways. Thus, five different PVP concentration s (from 0 to 3 % w/w of mannitol) were investigated (Figure 1.8.).

Without PVP, as well as with 0.5 % w/w polymer, the highly intense peak at 9.26° *2theta* which is characteristic of the δ form could be observed; however, in the trace from CCD no peaks are present in the 9.5-18.5° *2theta* e region, whereas 0 and 0.5% PVP-containing powders afforded small peaks at 13.24° and 16.84° *2theta*, likely ascribable to the presence of traces of the α form. These two peaks disappeared as the PVP concentration increased, being 1% w/w PVP

the minimum polymer concentration to get crystallographic pure δ form. This powder did not differ from those containing 2% and 3% PVP.

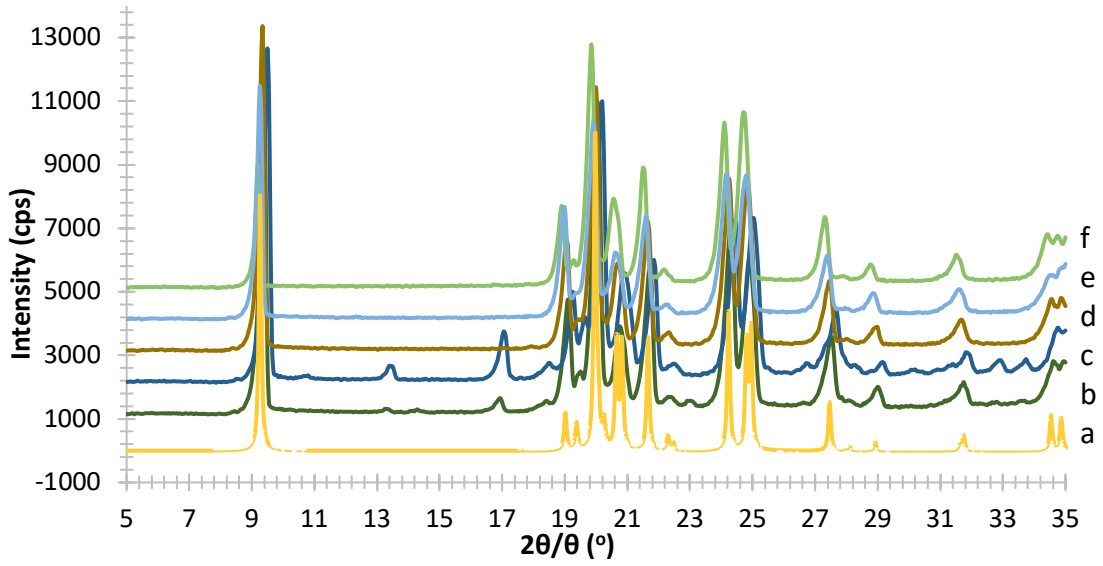

Figure 1.8. PXRD patterns of mannitol δ form (f) obtained using acetone as an antisolvent with 3% PVP (e) 2% PVP (d) 1% PVP (c) 0.5% PVP (b) without PVP (a) CCD as a reference.

It is worth underscoring that the amount of polymer added both in the case of PVA and PVP was below the sensitivity of the diffractometer, thus, it was not possible to speculate about the solid-state characteristics of the polymer in the carrier particles.

The hydrate form of mannitol was obtained by freeze-drying with final drying at 25 ºC for 4 hours at 0.100 mbar [85]. An hemihydrate form was isolated (Figure 1.9), however this form was not stable enough as it easily dehydrated at room temperature converting into the anhydrous form [89]. For this reason, its crystalline form was characterized but it was not used for the preparation of adhesive mixtures with the drug used in the second phase of research.

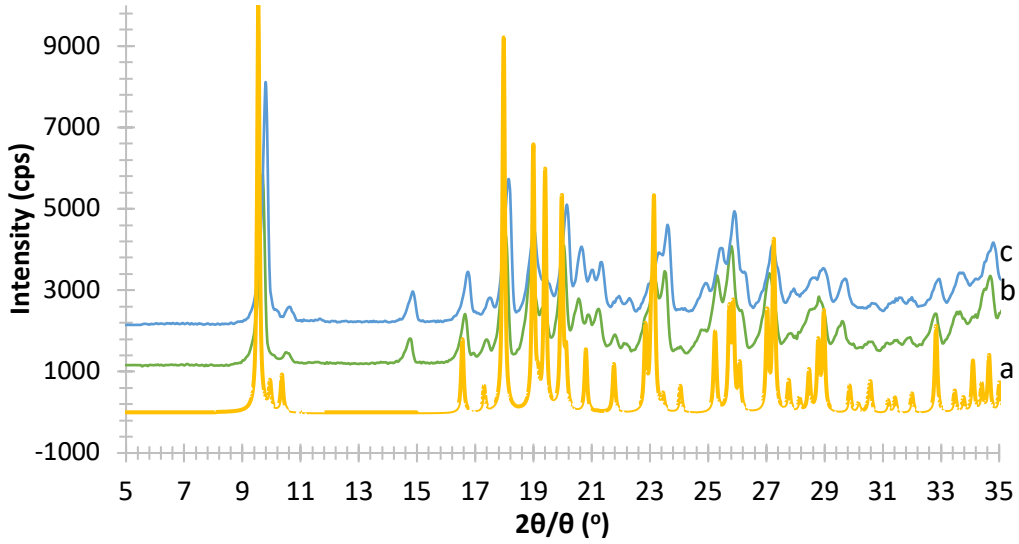

Figure 1.9. PXRD patterns of mannitol hemihydrate forms (c) obtained by freeze drying using 1% of CaCl (b) without any additional component in mannitol water solution (a) CCD as a reference.

The hydrate nature of the crystal was confirmed by DSC (Figure 1.10) that showed a fairly broad endothermic event (onset 62.9 ± 0.1, peak 64.0 ± 0.1) ascribable to the pseudopolymorphic transition (release of water molecule from the hydrate crystal) followed by a final melting with onset at 164.5 ± 0.2. TGA analysis indicated a weight loss of 5.4 ± 0.4 at the temperature range 25-80°C, thus confirming the loss of half molecule of water per molecule of mannitol (theoretical value 4.7% w/w).

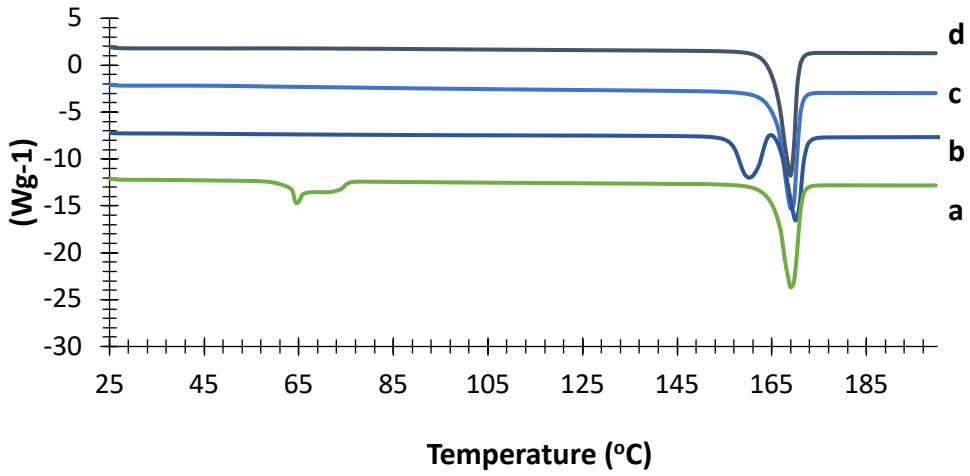

Figure 1.10. DSC traces of crystallized mannitol forms: (a) hydrate; (b) δ form (1% PVP); (c) β form; (d) α form (2% PVA).

Figure 1.10 reports also the DSC traces of the other mannitol forms: δ mannitol showed an onset melting temperature of 155.4 ± 0.4 °C and at the peak of 157.1 ± 0.2 °C. This endothermic event was followed by a small exotherm ascribable to the recrystallization and a final melting at 165.2 ± 0.5 °C (onset). As for the α mannitol the onset melting temperature was at 164.4 ± 0.1 °C and the peak at 165.6 ± 0.1 °C; the β form showed an onset temperature of fusion at 165.2 ± 0.5 °C with the peak at 166.0 ± 0.5 °C. All these data were in good agreement with those reported by Cares-Pacheco and co-workers [69].

4.2 Stability of crystallized α and δ mannitol

XRPD was used to study the stability of α and δ forms over time (Figures 1.11 and 1.12 respectively). The crystallized powders were stored in glass vials stoppered and clamped at a

temperature of 40° C, 75% RH for up to 24 months. XRPD analyses were performed to verify the evidence possible solid-phase changes.

As for the α form, although the peaks appeared slightly translated from one time sample to another (likely due to preferential orientation phenomena), the patterns were substantially similar as no new peaks appeared with 12 months. However, 24 months storage afforded small peaks at 15° and 23.1° *2theta*, likely ascribable to the presence of traces of the β form. In the case of δ form, the pattern recorded after 1 month or 12 months storage were practically superimposed to that recorded at time zero. After 24 months storage, small peaks were detected at 10.95°, 15.15° and 23.85° *2theta*, ascribable also here to the presence of traces of the β form.

Therefore, it can be stated that both polymorphic forms were stable in the considered time interval for 12 months under accelerated stability conditions.

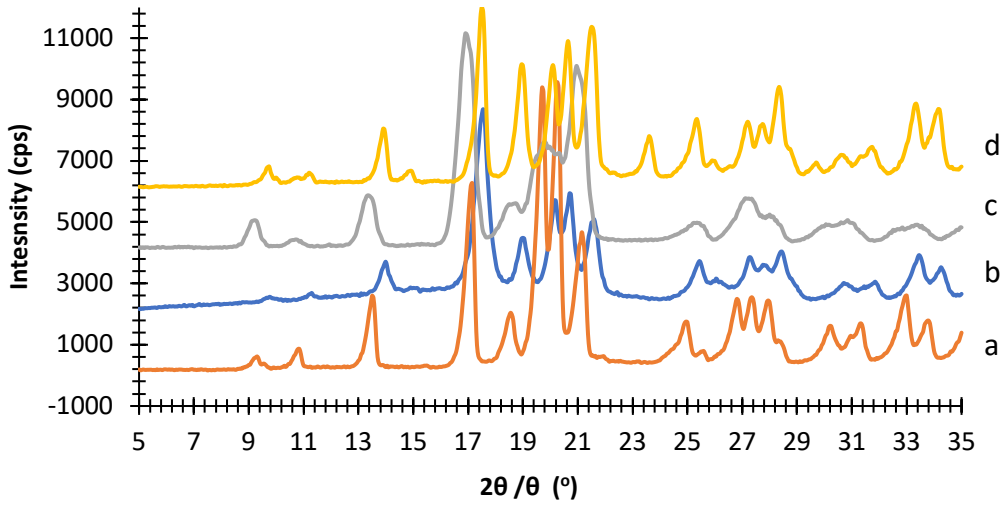

Figure 1.11. PXRD patterns of mannitol α form recorded at (a) time zero; (b) 1 month (c) 12 months (d) 24 months storage at 40 °C and 40% RH.

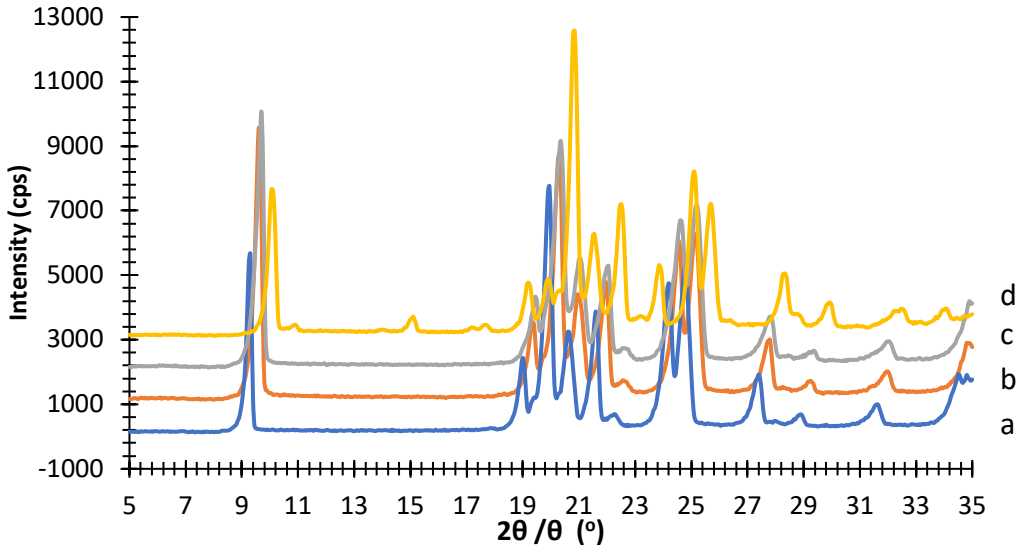

Figure 1.12. PRXD patterns of mannitol δ form recorded at (a) time zero; (b) 1 month (c) 12 months (d) 24 months storage at 40 °C and 40% RH.

4.3 Particle size distribution and morphology

The particle size distribution (PSD) of the powders of the recrystallized mannitol polymorphs was determined by laser light scattering. The obtained data are summarized in Table 1.2.

It was observed that β form showed the smallest particle size distribution with the majority of the particle having a size lower than 30 µm, while α and δ forms (as well as the hydrate) afforded similar PSD with a median volume diameter around 23 µm. In view of a possible use of these powders as carried in adhesive mixtures, these figures are lower compared to the typical median diameters of lactose carriers which ranges between 50 and 150 µm.

Table 1.2. Particle size distribution expressed as equivalent volume diameters (Dv, μm) and Span ± standard deviation.

Mannitol	Dv_{10}	Dv_{50}	Dv_{90}	Span
β form	2.90 ± 0.29	11.11 ± 1.75	28.87 ± 1.15	2.34 ± 0.17
δ form	6.21 ± 0.86	23.05 ± 1.85	57.93 ± 1.50	2.24 ± 0.18
α form	6.83 ± 0.42	22.68 ± 2.11	45.36 ± 3.32	2.98 ± 0.75
hydrate form	6.83 ± 1.17	22.68 ± 2.72	58.14 ± 1.35	1.60 ± 0.07

The morphology of the mannitol forms was assessed by scanning electron microscopy. SEM pictures are presented, as an example in Figure 1.13. In all cases more or less prismatic crystals were obtained with the α form showing higher amounts of fine particulates aggregated to form threadlike crystals. β form has a higher size distribution with some elongated and needle shaped crystals.

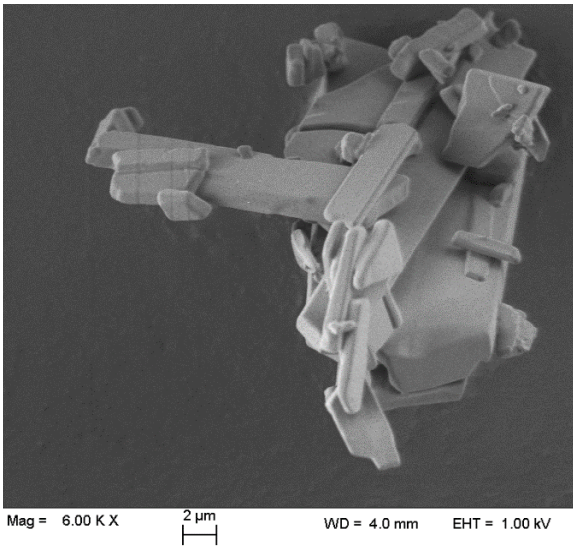

δ form

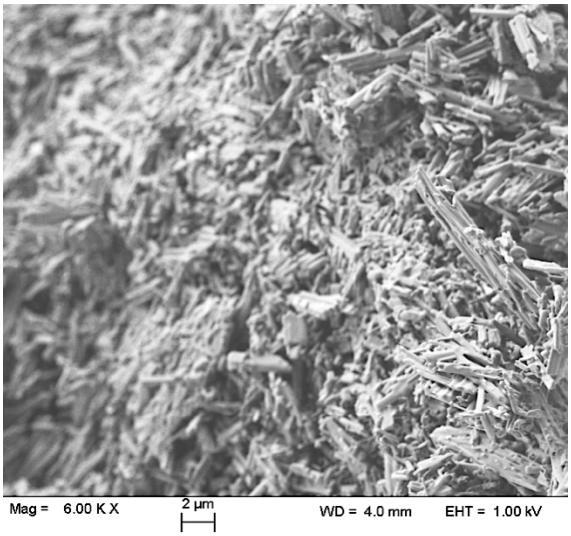

α form

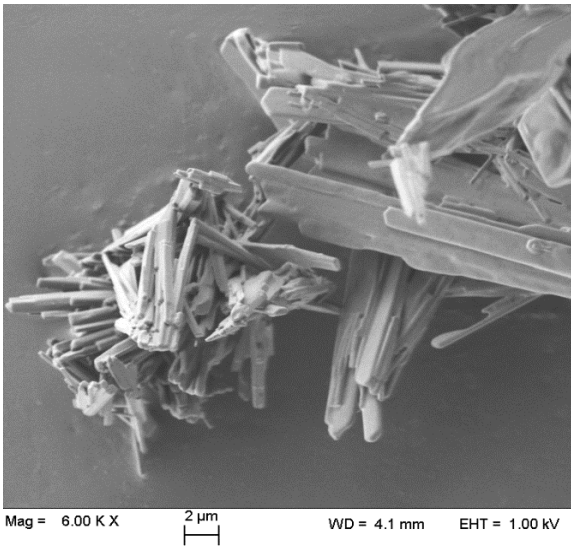

hydrate form

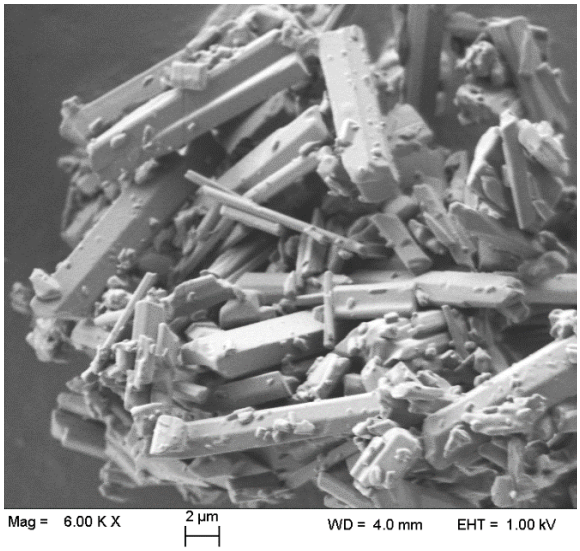

β form

Figure 1.13. SEM images of mannitol forms taken at 6000x magnification.

4.4 Invitro aerodynamic assessment of selected drugs

The adhesive mixtures of selected drugs with the different mannitol forms (Table 1.3) were used to study the aerosolization performance with mid (RS01®) and low (NESAT®) resistance devices.

Table 1.3. Percentage composition of the adhesive mixtures prepared with different mannitol polymorphs and lactose MM50 as reference. Drug content and loaded powder doses in capsules (mean, standard deviation, CV%, n=5).

	Drug	Drug Content (%)	Loaded dose (mg)
MM50	SS	0.82 ± 0.03 (3.67)	20.1 ± 0.2 (0.96)
MM50	BUD	0.70 ± 0.02 (2.86)	20.3 ± 0.1 (0.41)
δ form	SS	1.01 ± 0.04 (3.92)	20.1 ± 0.1 (0.26)
δ form	BUD	0.85 ± 0.03 (3.81)	20.0 ± 0.1 (0.38)
β form	SS	0.93 ± 0.03 (3.14)	20.2 ± 0.2 (0.84)
β form	BUD	0.99 ± 0.04 (4.04)	20.0 ± 0.1 (0.32)
α form	SS	0.83 ± 0.04 (4.83)	20.1 ± 0.1 (0.24)
α form	BUD	0.87 ± 0.01 (1.57)	20.0 ± 0.1 (0.26)

4.4.1 Effects of mannitol polymorphs on salbutamol sulphate deposition

Table 1.4 reports the deposition parameters of SS from adhesive mixture prepared α, β and δ mannitol polymorphs in comparison with those obtained from MM50, aerosolized with RS01 device.

Different mannitol forms lead to different SS deposition profiles. The mixtures prepared with the β form afforded an almost complete delivery of the loaded dose. In terms of FPF there was no significant difference between α and β form, while the mixture SS with the δ form gave rise to a lower deposition of fine particles on the impactor ($p = 0.01$ compared to both formulations

with α and β form).

On the other hand, after actuation of the blends containing MM50 lactose, more drug particles were retained in the inhaler device and capsules (16.26 ± 3.92 %) than in the case of the blends with δ mannitol forms (3.67 ± 2.11 %). For example, more than 80% of the total dose of the formulations with lactose was emitted from the inhaler while more than 90% of drug emission was achieved after aerosolization of the formulations containing the δ form. Despite the high emitted dose, most of the emitted powder was constituted by a coarse fraction as indicated by the percentage of the loaded dose deposited in the pre-separator: 38.64 ± 12.8 % for blends with lactose, 47.41 ± 3.73 % for the formulations with δ form and 47.98 ± 14.23 % and 51.81 ± 1.24 %, for the formulations with α and β form respectively.

A study from Kaialy and coworkers [90] indicated that there was a significant difference between recrystallized and commercial (β form) mannitol in terms of aerodynamic performances when salbutamol sulphate was used as a model drug. According to their *in vitro* aerodynamic test via multi-stage liquid impinger, FPF values of the SS blend with recrystallized mannitol were considerably higher than FPF of the SS blend with commercial mannitol [90]. However, the solid state of their recrystallized mannitol showed that it was a mixture of α, β and δ forms and not a single stable phase. On the other hand, the study of Boshhiha and Urbanetz showed that there was not difference between commercial lactose and mannitol when SS was used as a model drug [91].

Table 1.4. Deposition parameters of salbutamol sulphate from adhesive mixture prepared with lactose MM50, α, β and δ mannitol polymorphs in an ACI after aerosolization at 60 L min^{-1} with RS01 device [Mean, SD, n.3].

	ED (µg)	**Recovery (%)**	**Emitted fraction (%)**	**FPD (µg)**	**FPF (%)**	**MMAD (µm)**
MM50	128.8 ± 14.9	96.2 ± 11.6	80.1 ± 12.7	10.0 ± 2.5	8.4 ± 1.7	3.6 ± 0.1
δ form	173.6 ± 29.6	92.4 ± 17.5	90.4 ± 18.5	16.0 ± 1.6	9.3 ± 2.4	4.1 ± 0.0
β form	200.5 ± 6.9	99.6 ± 3.3	97.6 ± 3.2	29.8 ± 1.9	13.9 ± 0.7	4.7 ± 0.5
α form	136.4 ± 16.2	99.0 ± 9.0	81.7 ± 9.0	21.8 ± 4.8	13.4 ± 4.3	4.1 ± 0.1

When the aerosolization was performed with the NESAT® device (Table 1.5), mixtures prepared with α showed a slightly higher emitted fraction compared to δ and β although the differences were not statistically significant. On the other hand, as for the case of aerosolization with RS01, the mixture with the β form gave rise to a higher dose deposition of fine particles compared to the mixture with lactose MM50 ($p = 0.021$) The deposition of mixtures with the δ and β forms took place mostly in the stage zero of the impactor compared to lactose MM50 ($p = 0.04$, $p = 0.01$ respectively). The formulation of α form showed 81.7 % of emitted fraction with device RS01, while it was 90.5% with NESAT®.

α and β forms had similar dispersibility regardless of the devices used while, some effect of the device type and resistance (although not dramatic) could be observed for formulations prepared with lactose MM50 and mannitol δ form.

Table 1.5. Deposition parameters of salbutamol sulphate from adhesive mixture prepared with lactose MM50, α, β and δ mannitol polymorphs in an ACI after aerosolization at 48 L min^{-1} with NESAT® device [Mean (SD), n.3].

	ED (µg)	Recovery (%)	Emitted fraction (%)	FPD (µg)	FPF (%)	MMAD (µm)
MM50	147.4 ± 7.4	104.3 ± 5.5	96.0 ± 6.2	14.6 ± 1.9	13.5 ± 3.3	3.9 ± 1.2
δ form	196.6 ± 20.6	98.8 ± 8.0	95.1 ± 5.6	13.2 ± 1.5	6.5 ± 0.1	5.7 ± 0.4
β form	182.8 ± 31.9	97.4 ± 14.4	90.3± 12.5	21.0 ± 3.0	11.1 ± 3.7	4.5 ± 0.0
α form	150.2 ± 22.8	95.5 ± 14.2	90.5 ± 13.4	18.0 ± 5.5	11.9 ± 6.0	4.0 ± 0.1

4.4.2 Effects of mannitol polymorphs on budesonide deposition

The values relevant to the aerosolization performance of budesonide with RS01 and NESAT® devices are reported in Table 1.6 and 1.7 respectively. With both devices, trends similar to those already presented for SS were observed, with the only significant difference that, in the case of BUD, the values of FPD, FPF were much higher than those recorded for SS while the MMADs were significantly smaller.

The BUD deposition profile from RS01 device were not significantly different between the α and β form, while the mixture BUD with the form δ afforded a lower deposition of fine particles on the impactor ($p = 0.01$ for RS01®). Moreover, the deposition profiles of budesonide from MM50 mixtures showed a significantly lower fine particle dose on the filter compared to the blends with α and β forms ($p = 0.02$, $p = 0.004$ respectively). Those are partly in agreement with those reported in the study of Nokhodchi and coworkes, who showed that the highest FPF % of budesonide was obtained with the formulation of mannitol, compared to the other carriers (sorbitol, maltitol, xylitol, dextrose) attributed a better aerosolization performance due to the elongated shape of the carrier rather than to its specific surface chemistry [90],[92].

Table 1.6. Deposition parameters of budesonide from adhesive mixtures prepared with lactose MM50, α, β and δ mannitol polymorphs in an ACI after aerosolization with RS01 device at 60 L min^{-1} [Mean (SD), n.3].

	ED (µg)	**Recovery (%)**	**Emitted fraction (%)**	**FPD (µg)**	**FPF (%)**	**MMAD (µm)**
MM50	93.9 ± 3.5	99.0 ± 3.6	87.3 ± 2.0	36.2 ± 0.2	26.6 ± 1.3	1.6 ± 0.2
δ form	111.8 ± 12.0	93.1 ± 4.5	78.4 ± 3.5	26.3 ± 8.2	19.6 ± 3.2	2.9 ± 0.4
β form	141.2 ± 15.0	91.2 ± 9.4	71.3 ± 7.6	104.7 ± 7.2	58.1 ± 3.9	1.8 ± 0.1
α form	122.0 ± 14.3	98.0 ± 8.4	76.5 ± 8.6	84.0 ± 14.6	53.5 ± 5.1	1.8 ± 0.1

With the NESAT® device very similar figures were observed except for the performance of the mixture prepared with the mannitol β form that afforded significantly higher FPD and FPF relative to RS01.

Table 1.7. Deposition parameters of budesonide from adhesive mixtures prepared with lactose MM50, α, β and δ mannitol polymorphs in an ACI after Aerosolization with NESAT® device at 48 L min^{-1} [Mean (SD), n=3].

	ED (µg)	**Recovery (%)**	**Emitted fraction (%)**	**FPD (µg)**	**FPF (%)**	**MMAD (µm)**
MM50	105.0 ± 14.9	90.0 ± 5.5	76.8 ± 9.7	48.0 ± 2.8	39.1 ± 3.4	2.1 ± 0.2
δ form	117.6 ± 9.9	90.7 ± 3.6	71.7 ± 5.0	47.1 ± 10.6	32.0 ± 9.2	1.7 ± 0.1
β form	168.5 ± 16.8	95.3 ± 9.2	85.0 ± 8.7	108.0 ± 18.0	57.7 ± 11.8	1.8 ± 0.1
α form	142.3 ± 2.7	98.4 ± 3.4	89.5 ± 1.7	87.3 ± 0.8	55.8 ± 1.5	2.0 ± 0.2

These results clearly indicate that the manipulation of the mannitol solid-state can have an impact on the in vitro deposition of two model drugs in relevant adhesive mixtures. Formulations prepared with α and β polymorphs behave similarly affording better aerosolization performance with respect to the formulations prepared with δ mannitol

polymorphs or the reference lactose MM50. In the case of β form, the better performance might be ascribed to the small particle size distribution and in particular to the greater percentage of micronized particles (see Table 1.2) as, for lactose, it is common knowledge that the presence of fines improves the aerosolization performance [15], [31], [93]. However, this is not the case for the mixture prepared with mannitol α polymorphs that showed a particle size distribution practically superimposable to that of mannitol form δ. Thus, the observed differences observed among mannitol polymorphs performance are more likely to be ascribed to the different characteristics of the particle surface solid state rather than to a physical property such as the size, whereas this latter cannot be excluded *a priori* when considering the comparison with lactose (Dv50 = 53 μm vs nearly 23.05 μm for α and δ mannitol).

4.5 Preliminary cell toxicity

As previously stated, despite the use PVA in formulation for inhalation has already been proposed [88] it is worth underlying that neither the PVA nor the PVP have been approved as excipient for inhalation. Moreover, taking into consideration the particle size distribution of the mannitol powders proposed here as carried for inhalation (Table 1.2) it would not be unlikely that some small carrier particle would reach de lung while the biggest one would deposit in the oropharynx and be swallowed. Thus, it is worth raising a concern about the possible toxic effect of the two polymers at the adopted concentration in the mannitol carrier.
As reported in the experimental part, the concentrations of mannitol, PVP or PVA to be tested were taken based on the estimate of the amount of each component potentially reaching the lungs following an inspiration from a capsule loaded with about 20 mg of excipient, which, on the base of the in vitro aerosolization results, was set at 2 mg. It was assumed that this amount

would dissolved in the available volume of lung lining fluid, which has been reported to range between 10 and 30 mL [14]. A worst-case scenario (more concentrated solution) was assumed, thus, 0.2 mg/mL mannitol was considered as reference concentration to be evaluated in the cell viability assay. PVP and PVA alone were taken as reference and tested at concentrations of 2 μg/mL and 4 μg/mL respectively reflecting their relative ratio with mannitol in the solid particle (1% w/w and 2% w/w respectively).

Figure 1.14 reports the cell viability values obtained from the MTT test after 4 and 24 hours contact of Calu-3 cell with all forms of mannitol, as well as PVP and PVA alone.

It can be observed that the crystallized mannitol polymorphs had no deleterious effect on cell viability as no significant difference could be detected between negative control cells and treated cells at all concentrations considered, up to 16 times above the reference value. These results suggests that not only the recrystallized mannitol, but also PVA and PVP could be considered as relatively safe excipients even for lung administration in accordance with other data reported in literature for PVA [94] and PVP [95], [96].

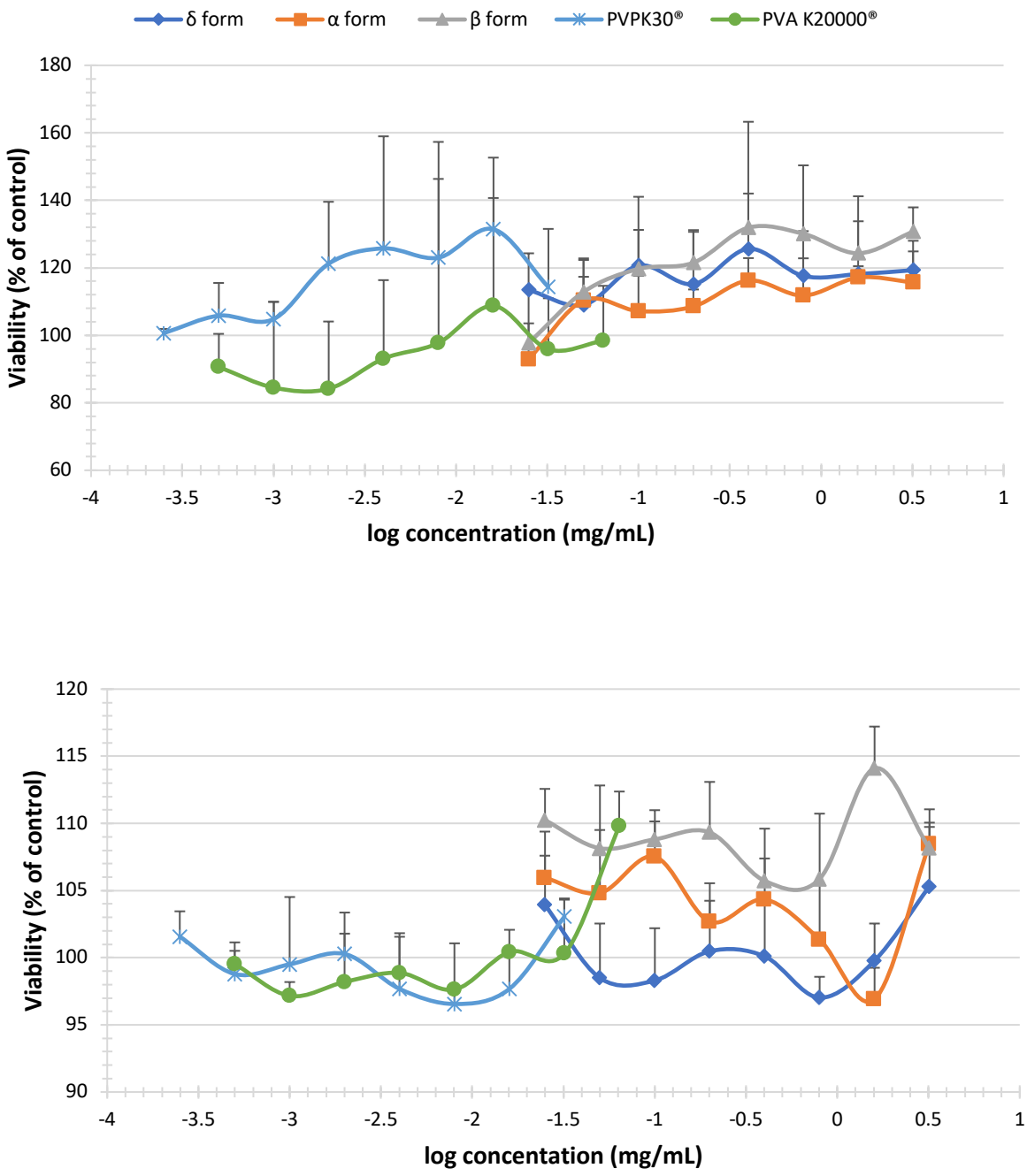

Figure 1.14. Viability assay for Calu3 cell lines. Upper panel: after 4hours, contact. Lower panel: after 24 hours contact. The bars represent the standard deviations.

5 Conclusion

From the data presented in the present chapter it can be concluded that mannitol polymorphs can be produced with simple processes easy to scale up at industrial scale which imply the doping with small amounts of selected polymers. The polymorphic metastable forms are kinetically stable for at least one year 40 °C 75% R.U. which suggest a longer stability time at ambient temperature and their possible use as carrier for the preparation of binary adhesive mixture for pulmonary delivery of low dose micronized active ingredients. On the contrary the pseudopolymorphic form, namely mannitol hemihydrate, tends very rapidly to convert into β form which represent the thermodynamically stable one at standard conditions.

Although the particle size distribution of the crystallized mannitol polymorphs was not optimized, their aerosolization performance is very positive, for both the model drug tested.

As for lactose, also mannitol affords better aerosolization performance with the active ingredient lipophilic in nature relative to hydrophilic one.

Differently from lactose, the aerosolization of the best performing mannitol polymorphs are not affected by the device resistance.

These results indicated that as observed for lactose, [31] also in the case of mannitol the surface physico chemical properties stemming from the different crystal structure represent a tool for modulating the carrier-drug interaction and, in turn, the aerosolization performance.

Finally, the crystallized carriers proved to be safe toward lung cell in a wide range of possible concentrations, thus supporting the idea of using this excipient in DPI formulations.

Chapter II

1 Introduction

1.1 Quality by Design tools: DoE

Quality by design (QbD) is a method to develop a product or a process based on the evaluation of all critical its parameters. This way of thinking was developed by the quality pioneer Dr. Joseph M. Juran [97]. QbD principles were also defined by Woodcock as a way to obtain a high-quality drug product free of contamination and defects [98]. Over decades the studies have showed that the quality must be built in the manufacture of the product and not simply checked afterwards. Pharmaceutical approach of QbD was described in ICH Q8 (R2) (Pharmaceutical Development), ICH Q9 (Quality Risk Management), and ICH Q10 (Pharmaceutical Quality System) [97], [99].

Design of experiment is part of the QbD tools (Figure 2.1) used with the identification of the main process variables and their effect on product quality. After the definition of the critical process parameters, the formulation and/or the process can be designed to ensure that those factors can be controlled within acceptable ranges [100].

One of the aim of QbD is to reduce the number of experiments needed according to four principles: controlling, randomization, replication and blocking [101].

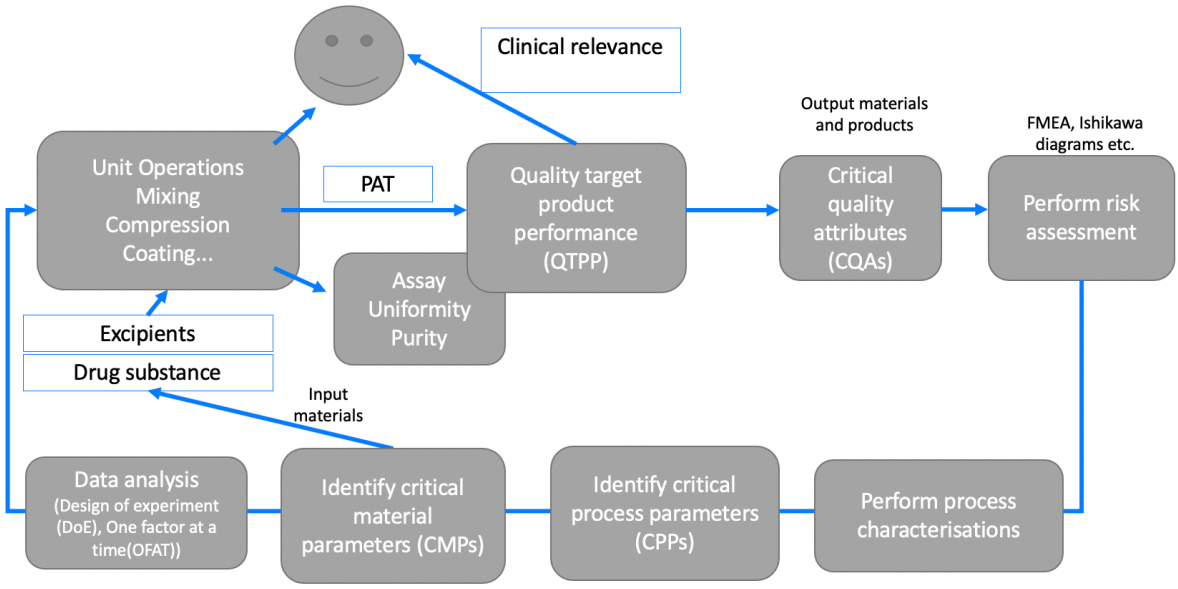

Figure 2.1. Quality by design tools (PAT =Process analytical technology).

According to QbD-based approach the procedure of experimental phases does not include only the combination of four principles but also the critical material attributes (CMSs), critical process parameters (CPPs) and critical quality attributes (CQAs) in formulation and manufacturing processes. The combination of CMAs and CPPs is a sort of junction to CQAs which is a thorough investigation of scale-up principles for pharmaceutical companies. Once the identification of CQAs has been done, the next step is to assess which parameters lead to the desired product quality [99]. The quality of a drug product can be identified with different attributes such as content uniformity, physical properties, dissolution profile, water and residual content, degradation profile.

The aim of this part of the PhD project was to investigate through a QbD-based approach the capsule filling process with powder containing polymorphs of mannitol intended for use in DPIs. In fact, this specific application poses some specific issues related, in particular, to the low dosage (few mg or µg of active ingredient) and the influence of the filling process (in particular of the tamping) on the aerosolization performance.

Several studies deal on micro-dosed capsule filling techniques for DPIs [102]–[104], but no

literature is available to show the possible effect on this process and the subsequent aerosolization of the polymorphism of a carrier such as mannitol.

Design of Experiments copes with the CMAs and CPPs in order to compile a reasonable set of experiments used to analyze statistically the formulation and process responses as CQAs [105].

1.2 The role of capsules for DPIs

As mentioned before, the aerosolization performance of a dry powder inhalation device depends not only on the powder formulation but also on the device used. Single-dose dry powder inhalers, which use a capsule to store and dispense the drug formulation [17], [106], are widely used. Therefore, the capsule may play a role in the aerosolization of the powder and in the dispersion of the micronized drug during inhalation.

Devices that use capsule offer several advantages, such as the ease of use for the patient and accurate dispensing of the drug dose [23], [107]. After inhalation, the patient can check the capsule to verify that the administration has taken place correctly and, if necessary, repeat the maneuver. On the other hand, the presence of the capsule increases the number of steps needed to load the dose compared to a multidose DPI, even if the loading techniques are quite intuitive. The capsules must be pierced before inhalation. The emission of powder from the device and the aerodynamic performance are linked to the intrinsic resistance of the device, to the emptying of the capsules which is related, in turn to the capsule movement (rotation, shaking, vibration) [108]. Capsules can be opened by cutting or via needles that pierce the capsule. The latter is the most common method, with the number and location of puncture points varying according to the DPI used. In addition, other factors, such as the size of the hole, the volume of the capsule housing chamber, the geometry of the mouthpiece and the structure of the grid can affect the performance of the product [93], [109].

There are several types of hard capsules used for inhalation on the market, which follow the evolution of capsules in oral drug administration. The primary material used for the capsules is gelatin, as it exhibits good film-forming properties and can easily dissolve in biological fluids at body temperature. The film produced is homogeneous and very strong and the gelatin capsules can easily withstand the mechanical stresses of the filling and packaging operations. However, gelatin comes from animal sources, is not completely chemically inert and contains water (about 13-16 % w/w) which acts as a plasticizer. These properties lead to incompatibility with some compounds, especially with hygroscopic drugs, and to fragility at low relative humidity.

These disadvantages have led to the development of capsules made from plant-based polymers, used to avoid the risk of transmissible bovine spongiform encephalopathy and used in cases where consumers do not take capsules made of gelatin for religious, cultural or dietary reasons. Hypromellose (hydroxypropyl methylcellulose, HPMC), a chemically inert material that reduces the risk of incompatibility with some active ingredient, is nowadays commonly used to produce capsules. These capsules have a low moisture content (about 2-4 % w/w) thus, they can be used with hygroscopic drugs and or moisture sensitive formulations. HPMC capsules have also been shown to be less likely to shrink or become brittle when stored in low humidity conditions. They can also be easily punctured to allow for optimal and reproducible drug release from the capsule. In addition, it was also noted that the size of the capsule used to disperse the powder does not have a significant effect on the overall performance of the inhaler. The reduction of the capsule size has led to a small increase in the overall levels of turbulence generated in the device, but this is not sufficient to affect the dispersion of the powder [110].

1.3 Capsule filling process and compactability

1.3.1 Compactability

Compressibility is the ability of a powder material to be transformed into a tablet under the effect of compaction pressure [111]. The compression and compaction processes are strongly influenced by the physical form of the material, i.e. whether it is amorphous or crystalline. As it was mentioned before, different crystals include salts, polymorphs, hydrates and solvates, each of which has different outer crystalline habits (needles or prisms), melting point and mechanical properties. Amorphous materials tend to plastic deformation and crystalline materials to break (crumbling). The surface and the roughness of the material has to be investigated in order to understand the compactability of solid particles which are held together by interfacial forces, which are also known as long range attractive forces; these forces include: electrostatic forces, Van der forces Waals and hydrogen bonds (among the excipients capable of forming hydrogen bonds there are simple sugars and polysaccharides such as cellulose and starches). These last two forces are the ones that make the greatest contribution during compression.

Many active ingredients are ionizable and have an asymmetrical charge distribution. Some materials have permanent dipoles and the interaction forces are due to the attraction between the negative pole of one molecule when it is in contact with the positive pole of another. The molecules that take part in these interactions are considered polar [112]. Materials can change shape during compaction, this can alter the properties of the compact powder including chemical stability and dissolution.

It has been observed that the crystalline habit can influence compaction through its effect on the orientation of the crystals during the compression phase [34], [111], [113].

Equidimensional crystals are usually preferred because they are handled better and have better characteristics such as flow, compactability and compressibility. In addition, the crystalline habit deeply influences surface-dependent properties such as drying, dissolution,

sedimentation, dispersibility, mixing and bulk density. Furthermore, the change of the crystalline habit can alter the particle size distribution and the surface/roughness characteristics: the change in crystallin habit modify the contact area and the alignment of the particles during the compression of the powder.

To study the compression behavior of solids, the T factor (S_{Fmax} / F_{max}) is devised, which considers the compressibility S_{Fmax} and tablettability (tensile strength/Fmax) of solids. In this case, F_{max} is the maximum force of the upper punch and S_{Fmax} is the displacement of the punch at F_{max}. In addition, plastic and elastic deformation was considered in the calculation of the T factor. A high T factor value for a material indicates good compactability [114].

In a study on paracetamol [111], an active ingredient known for its poor tablettability properties, it was possible to achieve different crystalline habits varying the crystallization via solvent, temperature and additives (polymers such as HPMC); different crystalline habits were obtained: raw, spherical, irregular paracetamol and flat in shape, which exhibited exactly the opposite behavior [111], [113], [114]. Each prepared material was compressed directly and without the addition of excipients. Compressing rough, irregular or flat-shaped paracetamol crystals produced very weak compacts that had no measurable tensile strength. Conversely, spherical crystals led to the formation of very strong compacts under the same operating conditions. Therefore, the manipulation of the crystals has proved to be an effective tool for the production of crystals with optimal physical-mechanical properties for compression.

In the literature there are a few studies on compactability of carriers for DPIs formulation [102], [115]. Thus, taking into consideration that the so call Zanasi process for capsule filling implies a phase of powder compaction, this part of the thesis aimed to investigate this aspect in reference to capsule filling process parameters together with different types of capsules and carriers (lactose and mannitol).

1.3.2 Relevance of capsule filling process

Properties of materials that can affect the capsule filling process include:

- particle size, which affects the flow and cohesion of a powder (smaller particles show greater cohesion),
- size distribution (considered critical in capsule filling mainly due to its impact on the compressibility of powders),
- flowability of the powder (greater variability in weight with cohesive powders that do not flow easily).

Furthermore, it is known that the powders produced by spray drying and sieved show a better behavior during the filling than those grounded and micronized [115].

The filling speed of the capsules has a moderate impact on the final weight of the capsules. Typically, higher speeds mean higher fill weights, resulting in higher powder compaction. One possible explanation is that when using a lower filling rate, more powder is more likely to be lost during the compacted powder transfer step to the capsule body than at a higher filling rate. Furthermore, the inhomogeneity of the powder bed is a critical factor since any compaction or trapped air can cause a variability of the final weight. In any case, powder bed uniformity, fill weight and weight variability strongly depend on powder characteristics and instrument settings [103].

In general, it is possible to state that content uniformity varies less with high content, while with low dose filling, flow and the friction characteristics will be decisive. In this case the dosator is also important, since it allows to dispense a decidedly smaller quantity with the only decrease in diameter.

Giving these premises, it appears reasonable to consider the capsule filling process as a critical step for the efficacy of the DPIs formulation and there are no systematic studies yet available, meaning that the equipment plays quite a dominant role in filling process [102].

2 Aim

The aim of this part of the thesis project was to evaluate the effect of different types of capsules on the in vitro aerosolization performance of DPIs in relation to the type of carrier used. The research work was organized in three phases.

In preliminary phase, the process of capsule filling through a semi-automatic bench top capsule filling apparatus was set. Thereafter, the filling was studied using two different types of carrier (lactose and mannitol) to evaluate the effect of the different carrier characteristics on different types of capsules. Lactose and mannitol were used in two different particle distributions: 90-125 μm and <10 μm. Particles between 90 and 125 μm were obtained by sieving while particles less than 10 μm were prepared by air jet milling. Formulation parameters were investigated via a full factorial design in order to achieve a better knowledge of their effect on the response of interest. The filling process was evaluated taking as CQAs the coefficient of variation on the final weight of the capsule, as well as the Emitted Fraction and the Fine Particle Fraction obtained upon aerosolization. These last parameters were obtained from an *in vitro* aerosolization assessment using a Fast Screening Impactor (FSI).

The parameters obtained from the first DoE were used for the second phase in which two different model drugs, one lipophilic (beclomethasone dipropionate) and one hydrophilic (salmeterol xinafoate) were used to further investigate and identify possible interactions with the carrier and the capsule.

The aerosolization performance was carried out via FSI to assess if different types of capsules had any significant effect on aerosolization performance.

In the third phase the effect of mannitol polymorphism on the filling process of different hard capsules for inhalation on the aerosolization performance was investigated.

The capsules were initially filled with two different commercially available carriers, lactose and β mannitol. Then the filling of the capsules was studied with the three polymorphs of

mannitol (α, β and δ) crystallized as described in Chapter 1, at different size distribution and force applied in the dosing tube during the compaction phase.

3 Material and methods

3.1 Material

Pearlitol® 100SD and Pearlitol® 160C were obtained from Roquette, France. Salmeterol xinafoate (SAL) was supplied from Sigma-Aldrich (Germany) and beclomethasone dipropionate (BDP) was obtained from Chiesi Farmaceutici (Italy). Lacto-Sphere® MM50 and MM3 (sieved and micronized α-lactose monohydrate, d_{V50} = 53.1 μm, d_{V50} = 2.5 μm, respectively) was provided by Micro-Sphere SA (Switzerland). Lactose Lactohale 100 (LH100) was obtained from DFE Pharma, Italy. The capsules for DPIs were supplied from Capsugel Lonza Pharma & Biotech, Switzerland (Conisnap white, Vcaps plus, Conisnap transparent, Gelatin- PEG 2.5% DPI, Vcaps DPI, Vcaps plus DPI).

3.2 Methods

3.2.1 Full factorial design of experiment

All parameters used for the DoE were standard coded, i.e. the value of each variable was transformed into a value ranging from -1 to 1. This step was necessary to scale all variables to the same range in order to neutralize the effects stemming from the different size of the parameters relevant to each variable, thus avoiding erroneous interpretation of their effect.

3.2.1.1 Design of experiment for capsule filling

A full factorial experimental design was used in order to investigate the effect of the different type of capsules, of two different carriers and of the relevant particle size distribution, using the design of experiment obtained by R-based Chemometric Agile Tool (CAT) software [116]. Each variable was considered at different levels (Table 2.1):

Table 2.1. Variables and relevant levels adopted in the design of experiment for capsule filling with lactose and mannitol.

Selected variables	**Number of levels**	**Levels**
Type of capsules	6	Conisnap white, Vcaps Plus, Conisnap, DPI PEG 2.5%, DPI Vcaps, DPI Vcaps Plus
Filling material	2	Lactose (1) and Mannitol (-1)
Particle size distribution (PSD) (μm)	2	90-125 (1) and <10 (-1)
Dosage (mg)	3	10 (-1), 20 (0) and 30 (1)

The capsules tested presented different composition in terms of materials and water content as reported in Table 2.1.1 where the relevant coding adopted for each capsule type in the DoE is also presented.

Table 2.1.1. Composition and water content of capsules as well as the relevant scaling.

	Material	**Water content (%)**	**Coding for DoE**
Conisnap® white	Gelatin	15.1	0.9852
Vcaps® Plus	HPMC	3.5	-0.7333
Conisnap®	Gelatin	14.9	0.9556
DPI PEG 2.5%	Gelatin (97.5%) + PEG (2.5%)	15.2	1
DPI Vcaps®	HPMC	3.1	-0.7926
DPI Vcaps® Plus	HPMC	1.7	-1

Each type of capsules was classified using the water content as reported in the relevant certificate of analysis provided by the producer.

Then all variables were placed into the matrix of design of experiment, which consist of 72 experiments (Table 2.1.2); each run was performed in triplicates.

Table 2.1.2. Matrix of the design of experiments for capsule filling with lactose and mannitol.

Experiment number	Capsule Type	Filling material	PSD (µm)	Dosage (mg)
1	0.9852	1	-1	-1
2	-0.7333	1	-1	-1
3	0.9556	1	-1	-1
4	1	1	-1	-1
5	-0.7926	1	-1	-1
6	-1	1	-1	-1
7	0.9852	-1	-1	-1
8	-0.7333	-1	-1	-1
9	0.9556	-1	-1	-1
10	1	-1	-1	-1
11	-0.7926	-1	-1	-1
12	-1	-1	-1	-1
13	0.9852	1	1	-1
14	-0.7333	1	1	-1
15	0.9556	1	1	-1
16	1	1	1	-1
17	-0.7926	1	1	-1
18	-1	1	1	-1
19	0.9852	-1	1	-1
20	-0.7333	-1	1	-1
21	0.9556	-1	1	-1
22	1	-1	1	-1
23	-0.7926	-1	1	-1
24	-1	-1	1	-1
25	0.9852	1	-1	0
26	-0.7333	1	-1	0
27	0.9556	1	-1	0
28	1	1	-1	0
29	-0.7926	1	-1	0
30	-1	1	-1	0
31	0.9852	-1	-1	0
32	-0.7333	-1	-1	0
33	0.9556	-1	-1	0
34	1	-1	-1	0
35	-0.7926	-1	-1	0
36	-1	-1	-1	0

37	0.9852	1	1	0
38	-0.7333	1	1	0
39	0.9556	1	1	0
40	1	1	1	0
41	-0.7926	1	1	0
42	-1	1	1	0
43	0.9852	-1	1	0
44	-0.7333	-1	1	0
45	0.9556	-1	1	0
46	1	-1	1	0
47	-0.7926	-1	1	0
48	-1	-1	1	0
49	0.9852	1	-1	1
50	-0.7333	1	-1	1
51	0.9556	1	-1	1
52	1	1	-1	1
53	-0.7926	1	-1	1
54	-1	1	-1	1
55	0.9852	-1	-1	1
56	-0.7333	-1	-1	1
57	0.9556	-1	-1	1
58	1	-1	-1	1
59	-0.7926	-1	-1	1
60	-1	-1	-1	1
61	0.9852	1	1	1
62	-0.7333	1	1	1
63	0.9556	1	1	1
64	1	1	1	1
65	-0.7926	1	1	1
66	-1	1	1	1
67	0.9852	-1	1	1
68	-0.7333	-1	1	1
69	0.9556	-1	1	1
70	1	-1	1	1
71	-0.7926	-1	1	1
72	-1	-1	1	1

3.2.1.2 Design of experiment for drug respirability test

A further, similar full factorial DoE was used in order to optimize the different type of capsules filling with two different carriers of the two different model drugs (Table 2.2 and Table 2.2.1.).

Table 2.2. Variables and relevant levels adopted in the design of experiment for capsule filling with lactose and mannitol and two model drugs.

Selected variables	**Number of levels**	**Levels**
Type of capsules	6	Conisnap white, Vcaps Plus, Conisnap, DPI PEG 2.5%, DPI Vcaps, DPI Vcaps Plus*
Filling material	2	Lactose LH100 (1) and Mannitol 100SD (-1)
API	2	Salmeterol xinafoate (1) and Beclomethasone dipropionate (-1)
Dosage of API (mg)	2	Low dose (-1) and High dose (1)

* See Table 2.1.1. for the coding of the levels relevant to capsule type.

Table 2.2.1. Composition of design matrix for drug respirability test.

Experiment number	**Capsule type**	**API**	**Filling material**	**Dosage of API**
1	0.9852	1	1	-1
2	-0.7333	1	1	-1
3	0.9556	1	1	-1
4	1	1	1	-1
5	-0.7926	1	1	-1
6	-1	1	1	-1
7	0.9852	1	1	1
8	-0.7333	1	1	1
9	0.9556	1	1	1
10	1	1	1	1
11	-0.7926	1	1	1
12	-1	1	1	1
13	0.9852	1	-1	-1
14	-0.7333	1	-1	-1
15	0.9556	1	-1	-1

16	1	1	-1	-1
17	-0.7926	1	-1	-1
18	-1	1	-1	-1
19	0.9852	1	-1	1
20	-0.7333	1	-1	1
21	0.9556	1	-1	1
22	1	1	-1	1
23	-0.7926	1	-1	1
24	-1	1	-1	1
25	0.9852	-1	1	-1
26	-0.7333	-1	1	-1
27	0.9556	-1	1	-1
28	1	-1	1	-1
29	-0.7926	-1	1	-1
30	-1	-1	1	-1
31	0.9852	-1	1	1
32	-0.7333	-1	1	1
33	0.9556	-1	1	1
34	1	-1	1	1
35	-0.7926	-1	1	1
36	-1	-1	1	1
37	0.9852	-1	-1	-1
38	-0.7333	-1	-1	-1
39	0.9556	-1	-1	-1
40	1	-1	-1	-1
41	-0.7926	-1	-1	-1
42	-1	-1	-1	-1
43	0.9852	-1	-1	1
44	-0.7333	-1	-1	1
45	0.9556	-1	-1	1
46	1	-1	-1	1
47	-0.7926	-1	-1	1
48	-1	-1	-1	1

3.2.2 Air jet milling

Micronized particles were obtained by jet milling (JM) using a Labo Mill (FPS, Italy) spiral jet mill. Compressed air injection and grinding pressures of 6.5 bar and 5.5 bar were used

respectively and a maximum of 20 minutes of operation was necessary to achieve the desired size reduction at a fixed feed rate of 1g/min.

3.2.3 Minima® capsule filling machine

Minima® (IMA Bologna) is a semi-automatic bench top capsule filling machine designed for capsules intending both inhalation and oral use.

The main parts of the machine are reported in Figure 2.3:

1- dosage valve

2- regulator of the dosage value (mm)

3- regulator of the final height of the piston

4- value of the final height of the piston (mm)

5- locking piston for dosator

6- dosator (with different diameters)

7- insertion/expulsion devices

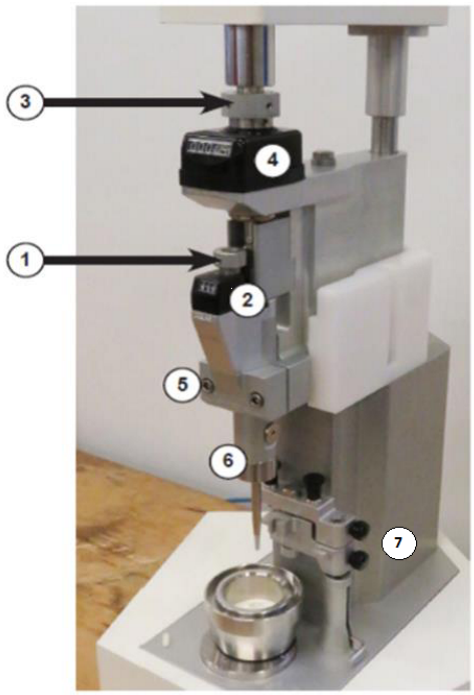

Figure 2.2. Minima® bench top capsule filling equipment.

The capsule is inserted in a special housing that can be adapted to the size of the selected capsule. Before filling, the head and the body of the capsule are separated. After filling, they are assembled thanks to a small side knob that allows to push the body towards the head, establishing the definitive closure.

At the bottom of the equipment the powder bed container is located. The powder bed is manually filled with a certain quantity of powder, chosen according to the type of filling: in fact, the height of the powder bed affects the dosage. The powder bed is also mounted on a rotating disc divided into four sections, which allows the container to be rotated at 90° after the powder withdrawal by the dosator; in this way, the piston does not pick up the powder in the same position, avoiding a decrease in the amount of powder used to fill the capsule.

The path of the piston towards the powder bed can be decreased or increased placing metal discs of different thickness below the underlying part of the container in order to reduce the distance between the piston and the bottom of the container and, consequently, increase the compactness of the powder sampled by the dosator.

3.2.4 Preparation of adhesive mixtures

Mannitol and lactose were sieved to obtain a particle size distribution in the range of 90-125 μm. Both carriers were mixed with two different drugs at two different dosage: salmeterol xinafoate up to 0.1% and 0.5% on the final weight; beclometasone dipropionate up to 1% and 5% of the final weight. Therefore 10 grams of each mixture were prepared using the geometric dilution method. Each sample was mixed in Turbula® (WAB, Basel Switzerland) for 1 hour at 40 rpm.

3.2.5 *In-vitro* aerodynamic assessment

The in vitro aerosolization performance of lactose and mannitol powders was investigated

using a Fast Screening Impactor (FSI, MSP Corporation, UK). This impactor divides the particles delivered by the inhaler into two stages: CFC, Coarse Fraction Collector, which captures coarse particles having aerodynamic greater than 5μm, and FFC, Fine Fraction Collector, where particles with an aerodynamic diameter lower than 5 μm are collected. 10 mL of washing solution were added before analysis at the CFC level, to simulate the humidity of the respiratory tract.

A single dose inhalation device with intermediate resistance, RS01® was used to perform the aerosolization test. Through a pump the air flow was set at 60L/min for 4.0 seconds in order to generate a pressure drop of 4 kPa for 4 L of air volume. (Erweka VP1000 GMBH pump, Germany; TPK flow regulator Copley, Copley Scientific Limited, UK).

At the end of the process, the drug deposited at the various levels was collected using different washing solutions: methanol/water (50/50 v/v) for salmeterol xinafoate; water/acetonitrile (60/40 v/v) for beclomethasone dipropionate and different washing volumes:

- Capsule and device: 25 mL;
- Induction Port (IP): 5 mL;
- CFC: 20 mL;
- FFC:10 mL.

The drug solutions obtained by washing the capsules and filter were placed in an ultrasonic bath for 5 minutes and subsequently filtered using a regenerated cellulose membrane.

3.2.6 High performance liquid chromatography

The samples collected from the aerodynamic studies were loaded into vials and analyzed by HPLC, performed using an Agilent 1200 LC Series (Agilent Technologies, USA), driven by ChemStation software v. A.04.02.

Salmeterol xinafoate: The mobile phase was prepared using 6 g of CH_3COONH_4 in 1 L of ultrapure waters filtered with 0.45 μm cellulose acetate filter. A Supelcosil ™ C18 column (25 cm x 4.6 mm, 5μm) at 25° C was used with a 0.8 mL/min flow, an injection volume of 20 μL, 8 minutes running time and a 250 nm wavelength. The analytical method was validated in terms of response linearity (AUC vs concentration) in the concentration range 4 - 42 μg/mL (LOQ = 0.065 μg/mL; LOD = 0.020 μg/mL).

Beclomethasone dipropionate: an Atlantis® dC18 column (15 cm x 3.9 mm, 3 μm) was used for the analysis with a mobile phase of acetonitrile: water (70:30 v/v). The flow was set at 0.8 mL/min, the chromatographic run time at 6 minutes and the detector wavelength at 258 nm. The column was thermostated at 40 °C and the volume injected for each sample set at 50 μL. The analytical method was validated in terms of response linearity (AUC vs concentration) in the concentration range 6-83 μg/mL (LOQ = 0.062 μg/mL; LOD = 0.019 μg/mL).

The collected data were processed with Excel to calculate ED (Emitted dose), EF% (Emitted Fraction), FPD (Fine Particle Dose) and FPF% (Fine Particle Fraction) in order to assess the aerodynamics parameters of the powder and the aerosolization performance of drug-carrier mixtures.

3.2.7 True density measurement by helium pycnometer

An automatic helium pycnometer (AccuPyc II 1340, Micromeritics, USA) was used to calculate the true density of the powder. Analysis was performed for all three mannitol polymorphs. The samples were placed in a 1 cm^3 standard chamber were carried out on different powder samples. Helium was used as an inert gas displacing medium. The samples were sealed in the instrument compartment of known volume and weight, the appropriate pressure of inert gas allowed, and then expanded into another internal volume. The pressure before and after the expansion was measured and used to calculate the sample volume.

Dividing this volume by the weight of the samples (1.3-1.5 g) gives the density. Measurements were carried out in triplicate.

3.2.8 Compactability

3.2.8.1 Heckel Equation

The Heckel equation is one of the most useful mathematical tools to describe the compaction properties of pharmaceutical powders. Important material properties like tensile strength and porosity) of the powders can be derived via the Heckel analysis. Two types of Heckel analyses are commonly used. One is the so called "out-of-die" or "zero-pressure" method which consists in collecting data after the expulsion of the compacted powder, the other is the "in-die" or "at-pressure" method which it is used during compaction. Since particles undergo elastic deformation under pressure, which tends to lower the porosity of the powder bed, the "out-of-die" method describes the consolidation and compaction of the powders more accurately than the "in-die" method. However, Heckel's "in-die" analysis is the most widely used due to the rapid and easy data collection [117].

The analysis was performed by compacting mannitol powders using the Styl'One Evolution compression simulator (Medel'Pharm, France) equipped with 6.5 mm round shaped punches. The equipment, which has a single station for die and punches, is conceived to simulate rotary tablet presses using Advanced ANALIS® software. The movement of the upper and lower punches is electronically controlled, and the force exerted by the punches on the powder bed is measured by sensors. Compacts were obtained at an average compressive force value of 0.5 kN. The powder true density value, obtained by pycnometric measurements, was used in the Heckel equation (Eq. 2.1, 2.2). According to this equation a linear relationship exists between the compression pressure and the natural logarithm of the reciprocal of the powder bed porosity [117]:

$$In\left(\frac{1}{(1-\rho)}\right) = kP + a \quad (2.1)$$

where ρ is the relative density of the material and therefore 1-ρ represents the porosity, P is the applied compression pressure, and *a* and *k* are constants of densification specific to the powder due to the initial arrangement of the particles under compression.

In a typical Heckel profile, obtained by plotting ln [1 / (1-ρ)] as a function of P, it is possible to distinguish three regions, namely a nonlinear initial part (Region I), followed by a linear (Region II), and finally a non-linear region (Region III) (Fig. 1).

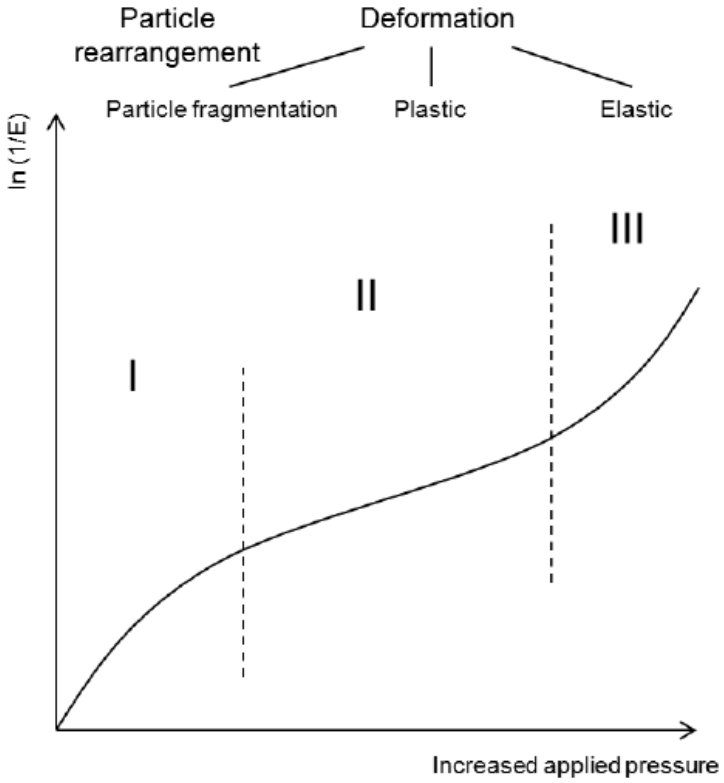

Figure 2.3. Schematic illustration of the three different regions characterizing the Heckel profile. Reproduced with permission from [118].

$$P_y = \frac{1}{k} = 3\sigma_0 \quad (2.2)$$

From the linear region (Region II), the inverse of the slope (parameter *k*) is calculated [119] as in equation 2.2. This is referred as the Heckel parameter or the yield pressure, P_y, and it is commonly used as an indication of the plasticity or hardness of the particles constituting the powder bed. This assumption originated from an empirical relationship between the parameter *k* and the yield strength (σ_0).

Obviously since the Heckel relationship applies a range of pressures causing irreversible deformation of the powder bed, which would not be the case in capsule filling, in the present work, this approach was used only to estimate the compaction behavior of the tested powders but exploring only the very initial part of the Heckel curve.

3.2.8.2 Bulk and tapped density of powder

The bulk and tapped densities were determined in triplicate and average value was calculated according to Ph. Eur. 10th Ed. (2.9.34. Bulk density and tapped density of powders) using a tap density tester (Erweka, Germany).

Carr Index (or Compressibility Index, CI%) values were calculated to express the flowability of the microparticles as:

$$CI(\%) = 100\left(\frac{\rho \text{ tapped} - \rho \text{ bulk}}{\rho \text{ tapped}}\right) \quad (2.3)$$

A similar index was defined also with the Hausner Ratio (HR):

$$HR = \frac{\rho \text{ tapped}}{\rho \text{ bulk}} \quad (2.4)$$

where *ρtapped* is the tapped density of the powder and *ρbulk* is the freely settled bulk density of the powder. These parameters were determined on 20 g of powder in a 25 mL cylinder and were interpreted as in Table 2.3.

Table 2.3. Carr's index and Hausner Ratio as an indication of powder flow (according to Ph. Eur. 10th Ed.).

Carr's index (%)	Type of flow	Hausner Ratio
5-15	Excellent	1.00-1.18
12-16	Good	1.19-1.25
18-21	Fair to passable	1.26-1.34
23-35	Poor	1.35-1.45
33-38	Very poor	1.46-1.59
>40	Extremely poor	>1.60

3.2.8.3 Angle of repose

The flowability of the powders was also determined by measuring the static angle of repose. 15 g of powder were introduced into a 10 mL graduated cylinder, transferred to a funnel with a diameter of 1 mm, placed at a height of 4 cm from the bench surface. The distance between the neck of the funnel and the tip of the cone was kept at 4 cm. The powder was dropped onto the surface to form a cone whose height and diameter of the base were measured to calculate the tangent of the angle of repose according to equation 2.5.

$$tan\ \alpha = \frac{h}{r} \quad \text{(Eq. 2.5)}$$

h = height of the cone formed by the powder,

r = radius of the base circumference of the cone formed by the powder.

The angle of repose a was then calculated by computing the inverse trigonometric function *arctangent* of the value obtained from equation 2.5.

The correspondence between angle of repose and powder flow properties as for Ph. Eur. Is reported in table 2.4.

Table 2.4. Angle of repose as an indication of powder flow (according to Ph. Eur. 10th Ed.).

Type of flow	**Angle of repose (degree)**
Excellent	25-30
Good	31-35
Fair to passable	36-40
Passable	41-45
Poor	46-55
Very poor	56-65
Extremely poor	>66

4 Results and discussion

4.1 Capsule filling parameters

4.1.1 Powder characterization

To set up the capsule filling method, mixtures with fine and coarse lactose particles were prepared with sieved lactose MM50 as carrier of Lacto-Sphere® MM3(D_{v50} = 2.5µm) as micronized particles mimic the active ingredient at three different concentration. The lactose MM50 was previously sieved through a 38 µm mesh sieve in order to eliminate the fine fraction. The sieving was carried out twice: the fine part of the first sieving was eliminated and the remaining fraction having size ≥ 38 µm was subjected to a second sieving. Each cycle lasted 60 minutes. To verify that the fine fraction had been correctly eliminated, the powders obtained were subjected to laser diffractometry according to the method described in Chapter 1 (3.2.2.2. Particle size distribution). Lactose mixtures were then prepared by adding Lacto-Sphere® MM3 at 2%, 5% and 10% w/w, respectively, to sieved lactose MM50. The previous sieving of the carrier resulted in an accurate control of the dose of fines in the mixture.

The "sandwich" method (Chapter 1, 3.2.3. Preparation of adhesive mixtures) was used to prepare 15 g of each mixture by mixing in Turbula® for 40 minutes.

For each mixture (fine content 2%, 5%, 10% w/w) the flow properties were determined in order to describe the behavior of the powder on the basis of the quantity of fine fraction loaded. The obtained results are reported in Table 2.5.

Table 2.5. Angle of repose, Carr Index and Hausner ratio values of MM3-MM50 mixtures. Mean values ± standard deviation.

MM3 content (%w/w)	Angle of repose [°]	Carr's Index [%]	Hausner Ratio
2	58.9 ± 2.7	34.6 ± 1.6	1.5 ± 0.1
5	57.0 ± 3.6	34.7 ± 1.7	1.5 ± 0.0
10	52.1 ± 0.9	32.0 ± 0.8	1.5 ± 0.0

According to European Pharmacopeia, if the angle of repose is greater than 50°, the flow capacity of the powder is not acceptable, therefore those three mixtures showed poor flowability. The angle of repose is also influenced by the operating conditions; therefore, it is not a reliable method for determining the smoothness of a powder. Free-flowing powders will have both density values very close to each other; poor flowing powders, on the other hand, will be characterized by lower apparent density values and a greater difference between the two densities, because of the greater interactions between particles. These differences are reflected in the Carr's index and in the Hausner ratio, that also indicate the flowability of the powders (Tab. 2.3).

4.1.2 Filling method

The capsule filling method was firstly standardized by verifying the suitability of the method's parameters suggested by the producer of Minima® (hereinafter referred to as IMA method) for microdosing intended for DPI capsules. To this end, 15 capsules (with an average weight of 15 mg) were filled with the suggested method that assumed the following parameters:

- Diameter of dosator: 2.5 mm;
- Regulator of the dosage value: 5 mm;
- Final height of the piston: 25 mm.

The content of the obtained capsules was aerosolized in the FSI with the RS01® device to

evaluate the EF% and FPF% by determining the difference of the mass between each capsules, devices and filters before and after the actuation of DPI.

The obtained results, reported in Figure 2.3 indicate the lack of relationship between fine powder dose in the mixture and emitted dose (Figure 2.4a), as it would have been expected. For the FPF no relation with the dose of fines was evidenced too (Figure 2.4b). In this latter case, a positive, negative or neutral relationship (no variation) was expected, whereas the higher FPF was obtained, as for EF, with the powder containing the intermediate dose of fines. Thus, the method was modified as follow and coded as UNIPR method:

- Diameter of dosator: 2.5 mm;
- Regulator of the dosage value: 25 mm;
- The final height of the piston: 3 mm.

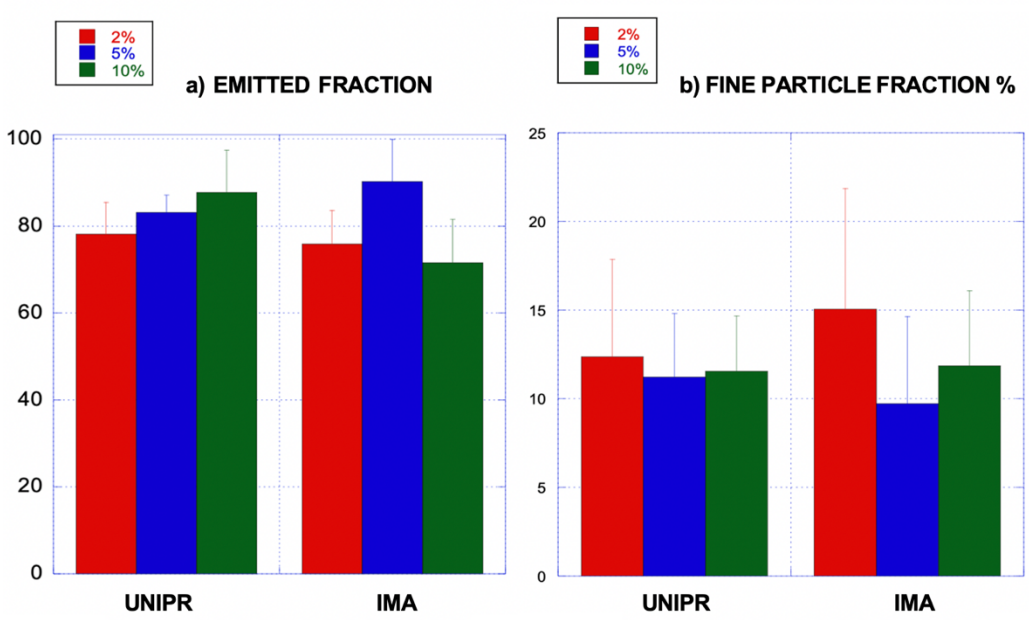

Figure 2.4. Emitted Fraction, EF % Panel a) and Fine Particle Fraction, FFP % (panel b) obtained by aerosolization with RS01 device of lactose binary mixtures containing 2%, 5%, 10% by weight lactose fine prepared by filling the capsule with IMA and UNIPR methods.

The new set-up afforded a linear relationship between the fine fraction and the emitted fraction. Furthermore, Fig. 2.4b shows constant FPF%, meaning that the amount of respirable particles was proportional to the emitted dose, and in turn to the loaded dose. EF% calculated for the UNIPR and IMA methods was not significantly different for the 2% mixture and the 5% mixture (value of p, evaluated by T test 0.49 and 0.65 respectively). The 10% mixture showed significantly different results (p value = 0.002) between the two methods. As for FPF% not statistically different values were obtained (p=0.34, p=0.80 and p= 0.66 for the 2%, 5% and 10 % fine in the mixture respectively).

According to these results, UNIPR method was therefore selected for the subsequent filling studies.

4.2 Design of Experiment

4.2.1 Particle size distribution analysis

The aim was to investigate the effects of type and properties of formulation components on the aerosolization performance. The size distribution of the micronized lactose (obtained from LH100®) and mannitol (obtained from 100SD®) particles was determined by laser light diffraction. The results obtained are summarized in Table 2.6 in comparison with the original particle size distribution of the parent material.

Table 2.6. Particle size distribution of mannitol 100SD and lactose LH100 powders before and after jet milling.

Powder	Dv_{10}(µm)	Dv_{50}(µm)	Dv_{90}(µm)	Span
Mannitol 100SD	55.70	112.09	189.08	2.126
Mannitol_jet milled	2.02	5.91	13.19	1.284
Lactose LH100	63.95	117.90	197.01	2.137
Lactose_jet milled	2.64	6.75	12.68	1.342

The micronization of lactose and mannitol led to powders with similar particle size distribution. As previously stated, in order to eliminate the effect of the size in the comparison between lactose LH100 and mannitol 100SD, these two carriers were sieved in order to obtain similar particle size distribution in the interval of interest between 90-125 µm.

Lactose and mannitol were selected in order to investigate the effect of their sensitivity to humidity on different types of capsules with different water contents. The type and properties of formulation components were investigated using design of experiment to study the effect of capsule water content on the aerosolization performance using the RS01® device. The results obtained are shown in Table 2.7.

Table 2.7. Values of response variables (RSD of the weight of the capsules ED, EF, FPD and FPF) obtained from an *in vitro* aerosolization study using FSI. For capsule code see Table 2.1.1.

Run order	Capsule type	Filling material	PSD (µm)	Dosage (mg)	RSD (%)	EF (%)	ED (mg)	FPD (mg)	FPF (%)
70	Conisnap white	Lactose	<10	10	2.7	92.93	9.1	1.5	16.57
71	Vcaps Plus	Lactose	<10	10	4.1	87.3	10.07	1.8	17.84
10	Conisnap	Lactose	<10	10	9.57	88.72	9.3	1.43	15.47

12	DPI PEG 2.5%	Lactose	<10	10	6.07	88.26	9.53	1.23	12.88
59	DPI Vcaps	Lactose	<10	10	3.53	91.13	9.77	1.63	16.78
1	DPI Vcaps Plus	Lactose	<10	10	4.36	89.74	9.73	1.47	15.03
34	Conisnap white	Mannitol	<10	10	1.46	87.91	9.2	1.77	19.35
67	Vcaps Plus	Mannitol	<10	10	4.77	88	9.1	1.83	20.1
45	Conisnap	Mannitol	<10	10	4.4	94.76	10.17	1.87	18.4
48	DPI PEG 2.5%	Mannitol	<10	10	1.41	90.25	9.8	1.5	15.45
23	DPI Vcaps	Mannitol	<10	10	3.02	93.74	9.97	1.63	16.41
39	DPI Vcaps Plus	Mannitol	<10	10	1.07	95.04	10.23	1.97	19.3
4	Conisnap white	Lactose	<10	20	5.48	84.5	17.53	2.53	14.44
8	Vcaps Plus	Lactose	<10	20	2.74	89.39	18	2.4	13.37
57	Conisnap	Lactose	<10	20	4.74	84.98	17.7	2.63	14.91
2	DPI PEG 2.5%	Lactose	<10	20	0.54	87.99	18.8	2.97	15.78
63	DPI Vcaps	Lactose	<10	20	2.17	87.8	18.2	2.27	12.47
21	DPI Vcaps Plus	Lactose	<10	20	3.75	88.91	18.1	2.7	14.9
11	Conisnap white	Mannitol	<10	20	6.4	88.96	18.07	2.57	14.29
17	Vcaps Plus	Mannitol	<10	20	2.61	94.81	19.23	3.03	15.77
7	Conisnap	Mannitol	<10	20	5.77	89.8	17.97	2.87	15.96

60	DPI PEG 2.5%	Mannitol	<10	20	3.72	93.62	19.03	3.27	17.23
26	DPI Vcaps	Mannitol	<10	20	2.57	91.94	18.37	2.4	3.08
41	DPI Vcaps Plus	Mannitol	<10	20	3.31	95.2	19.9	2.7	13.61
37	Conisnap white	Lactose	<10	30	2	93.27	30.13	3.93	13.07
44	Vcaps Plus	Lactose	<10	30	5.47	92.41	27.8	3.7	13.31
58	Conisnap	Lactose	<10	30	4.12	92.16	27.97	3.73	13.35
20	DPI PEG 2.5%	Lactose	<10	30	5.2	91.64	25.67	3.2	12.47
35	DPI Vcaps	Lactose	<10	30	3.82	90.19	28.37	3.8	13.4
13	DPI Vcaps Plus	Lactose	<10	30	4.98	91.3	28.43	3.57	12.57
56	Conisnap white	Mannitol	<10	30	1.57	92.12	28.87	4.1	14.18
18	Vcaps Plus	Mannitol	<10	30	5.96	94.46	27.77	4.77	17.3
43	Conisnap	Mannitol	<10	30	3.86	97.06	26.17	4.23	16.14
62	DPI PEG 2.5%	Mannitol	<10	30	4.84	91.38	27.23	3.47	12.75
14	DPI Vcaps	Mannitol	<10	30	7.42	94.62	28.9	3.47	15.58
22	DPI Vcaps Plus	Mannitol	<10	30	5.71	93.77	26.47	2.63	9.74
19	DPI Vcaps Plus	Lactose	90-125	10	1.45	97.77	10.33	0.07	0.64
33	Conisnap	Lactose	90-125	10	3.84	97.17	10.23	0	0

38	Vcaps Plus	Lactose	90-125	10	0.95	94.91	9.97	0.1	0.98
40	Conisnap white	Lactose	90-125	10	2.71	95.08	10.13	0.13	1.32
64	DPI Vcaps	Lactose	90-125	10	2.03	99.34	10.2	0	0
69	DPI PEG 2.5%	Lactose	90-125	10	0.54	97.5	10.37	0.1	0.96
29	DPI PEG 2.5%	Mannitol	90-125	10	2.5	98.41	10.43	0.37	3.44
46	DPI Vcaps	Mannitol	90-125	10	1.13	96.08	9.83	0.18	1.78
47	Vcaps Plus	Mannitol	90-125	10	5	97.79	10.17	0.47	4.55
54	DPI Vcaps Plus	Mannitol	90-125	10	3.47	97.43	10.13	0.37	3.68
55	Conisnap white	Mannitol	90-125	10	1.52	99	9.97	0.27	2.69
65	Conisnap	Mannitol	90-125	10	5.21	94.49	10	0.23	2.24
3	DPI Vcaps Plus	Lactose	90-125	20	0.77	100	19.87	0.07	0.34
9	DPI PEG 2.5%	Lactose	90-125	20	1.51	98.2	19.87	0.17	0.84
24	Conisnap	Lactose	90-125	20	1.52	98.32	19.47	0.17	0.85
50	DPI Vcaps	Lactose	90-125	20	1.81	99.5	19.8	0.1	0.5
66	Conisnap white	Lactose	90-125	20	0.57	99.18	20.1	0.2	0.99
68	Vcaps Plus	Lactose	90-125	20	1.32	97.34	19.57	0.03	0.18
28	DPI Vcaps	Mannitol	90-125	20	1.99	97.78	20.5	0.5	2.42
30	Vcaps Plus	Mannitol	90-125	20	2.81	100	20.27	0.4	1.98

31	Conisnap	Mannitol	90-125	20	1.02	100	20.47	0.73	3.53
32	DPI PEG 2.5%	Mannitol	90-125	20	1.99	99.66	20.2	0.83	4.18
49	DPI Vcaps Plus	Mannitol	90-125	20	0.47	98.54	20.37	0.57	2.8
52	Conisnap white	Mannitol	90-125	20	0.44	100	20.9	0.43	2.07
6	DPI Vcaps	Lactose	90-125	30	0.19	99.35	30.73	0.17	0.54
16	DPI PEG 2.5%	Lactose	90-125	30	2.46	99.23	30.3	0.1	0.34
25	Conisnap	Lactose	90-125	30	0.7	99.89	29.63	0.3	1.01
36	Conisnap white	Lactose	90-125	30	1.42	99.12	30.33	0.17	0.55
42	Vcaps Plus	Lactose	90-125	30	1.9	99.14	30.57	0.13	0.44
51	DPI Vcaps Plus	Lactose	90-125	30	0.92	99.68	31.13	0.17	0.53
5	Vcaps Plus	Mannitol	90-125	30	1.45	98.77	29.73	0.87	2.94
15	DPI PEG 2.5%	Mannitol	90-125	30	1.42	99.24	30.47	1.03	3.39
27	Conisnap	Mannitol	90-125	30	0.81	99.78	30.87	1.17	3.78
53	Conisnap white	Mannitol	90-125	30	0.82	98.58	30.3	0.47	1.54
61	DPI Vcaps Plus	Mannitol	90-125	30	2.5	99.44	28.8	0.83	2.82
72	DPI Vcaps	Mannitol	90-125	30	2.55	99.34	29.53	0.93	3.16

By analyzing the data shown in table 2.7, it is possible to observe that the use of carriers with particle sizes less than 10 μm increased the FPF, while carriers with dimensions between 90-

125 μm determined a greater EF but lower FPF. Furthermore, using this last particle size, a reduction in the coefficient of variation of the capsule weight was observed.

An increase in filling improved the EF but determined a decrease in the FPF. From the analysis of the data shown in the table it is possible to deduce that, on average, the best performances were obtained by using mannitol as carrier. This is further supported by the observation that in three experiments an EF value of 100% was noted using mannitol with dimensions in the 90-125 range and filling of 20 mg. On the contrary, two capsules that use lactose as carrier, show minimal values in the FPF.

The relative standard deviation (RSD %) of the weight of the filled capsules were calculated from the ratio between the standard deviation and the mean, obtained from the fillings carried out in triplicate. The obtained data were subsequently analyzed, by multi linear regression. The same statistical treatment was applied also to the aerosolization parameters.

In detail, the statistical evaluation of the effect of the different variables on RDS% evidenced that only the particle size distribution had a significant effect on the capsule filling weight variability (Figure 2.5). Particles between 90-125 μm showed a lower value than particle smaller than 10 μm ($p<0.001$). The other variables examined did not lead to any significant effect. As for the second order terms, only the interaction between PSD and dosage afforded a significant effect although at the lower level ($p=0.046$). The interaction of third and fourth order were not considered on purpose in order to improve the potency of the model.

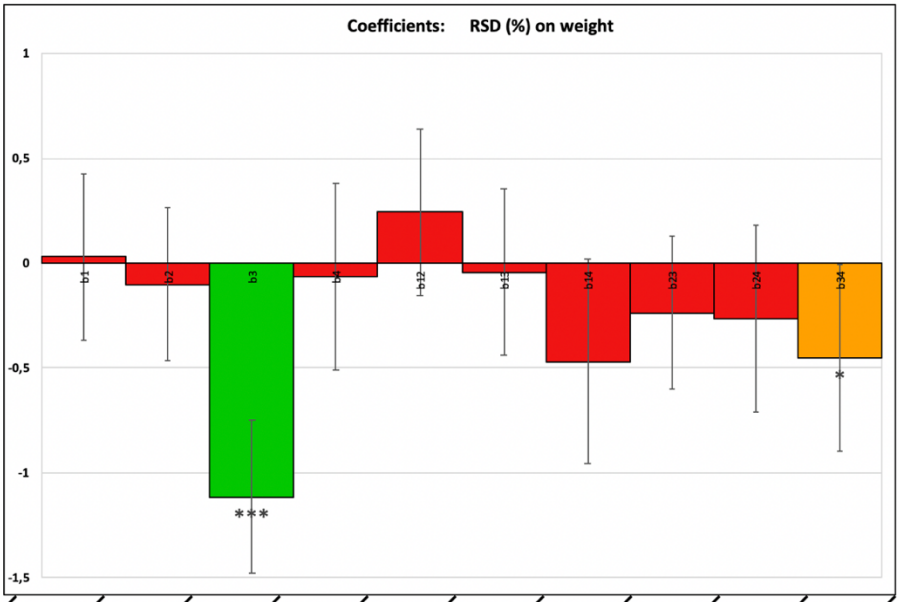

Const.	b1	b2	b3	b4	b12	b13	b14	b23	b24	b34
2.913338	0.032075	-0.100394	-1.11515	-0.06587	0.242704	-0.04198	-0.46952	-0.23556	-0.26292	-0.45208
Const signf.	0.872285	0.583791	7.40E-08	0.768959	0.226577	0.833383	0.058325	0.199856	0.242149	0.046631

Figure 2.5. Effect of individual variables on the RSD (%).

In the case of EF (%), the effect of the carrier, the particle size distribution and the dosage were highly significant whereas the effect of the type of capsule was not significant ($p > 0.05$) Figure 2.6).

When mannitol was used instead of lactose, an increase in EF% value is observed. Moreover, an increase in the dosage resulted in a higher emitted fraction. Finally, the variable most affecting EF% was the PSD: EF increased with the PSD.

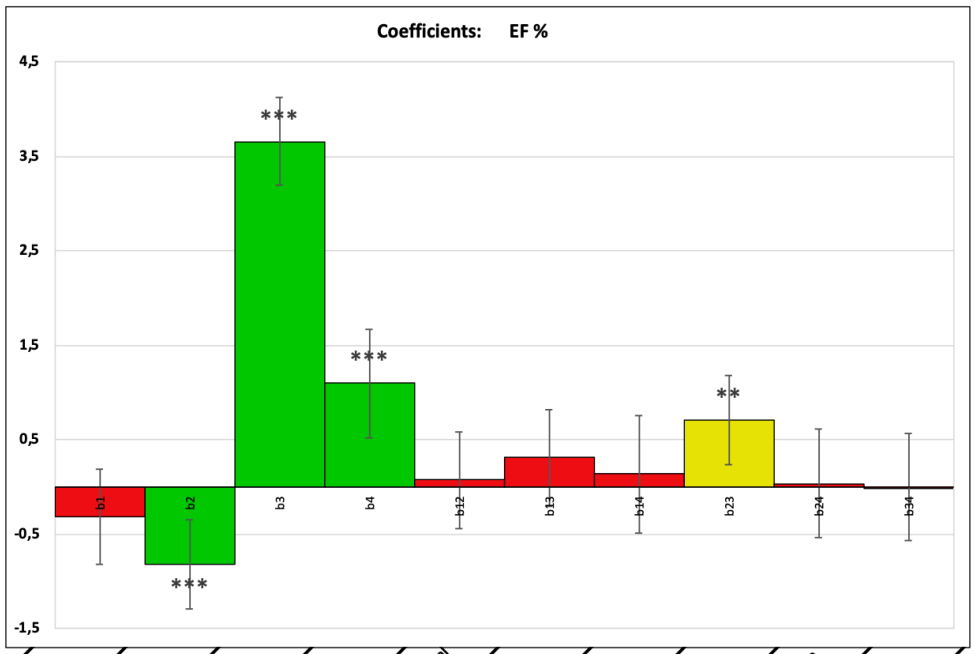

Const.	b1	b2	b3	b4	b12	b13	b14	b23	b24	b34
94,814818	-0,312707	-0,8167567	3,6586927	1,0986198	0,0756178	0,3141572	0,1374584	0,71125	0,0389583	-0,000208
Const signf.	0,2245672	0,0008947	5,00E-23	0,0002987	0,7677115	0,2224516	0,6612361	0,0033782	0,89190303	0,9994203

Figure 2.6. Effect of individual variables on the EF (%).

Considering the two-way interactions, only in the case of the filling material and particle size a positive interaction could be evidenced on EF% (p= 0.003), as evidenced also by the slight curvature of the response surface presented in Figure 2.7.

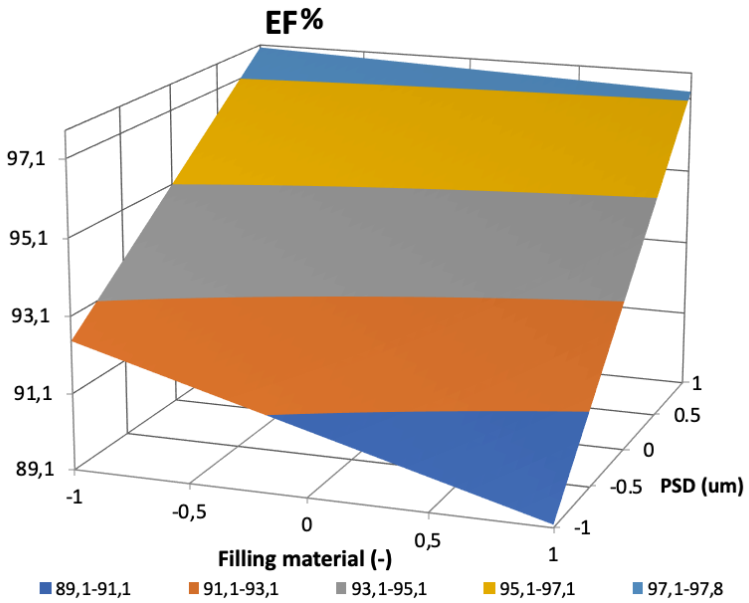

Figure 2.7. Response surface of filling material and particle size distribution on the EF(%).

The fine particle fraction (Figure 2.8) was also significantly affected by the filling material, the particle size distribution, and the dosage. The use of mannitol determined an increase for FPF%. The reduction of the particle size as well as of the dosage led to higher respirability. Again, when the two-way interactions were considered, a significant effect was observed only for filling material and particle size.

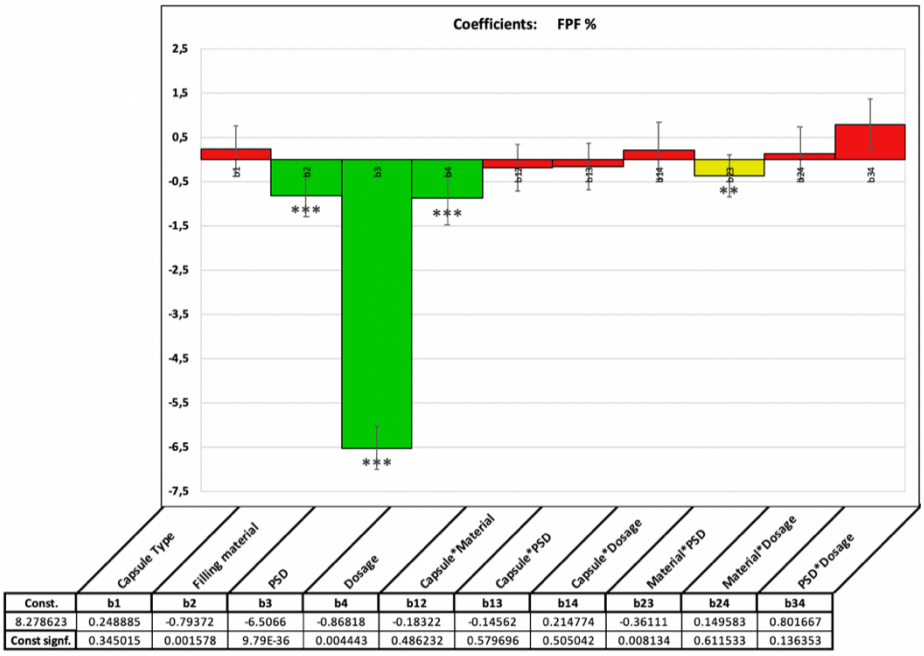

Const.	b1	b2	b3	b4	b12	b13	b14	b23	b24	b34
8.278623	0.248885	-0.79372	-6.5066	-0.86818	-0.18322	-0.14562	0.214774	-0.36111	0.149583	0.801667
Const signf.	0.345015	0.001578	9.79E-36	0.004443	0.486232	0.579696	0.505042	0.008134	0.611533	0.136353

Figure 2.8. Effect of individual variables on the FPF (%).

In this respect, as it is shown in Figure 2.9, the higher fine particle fraction value was obtained with mannitol with smaller particle size distribution. Whereas the lower fine particles fraction was observed in the case of lactose with larger particle size distribution.

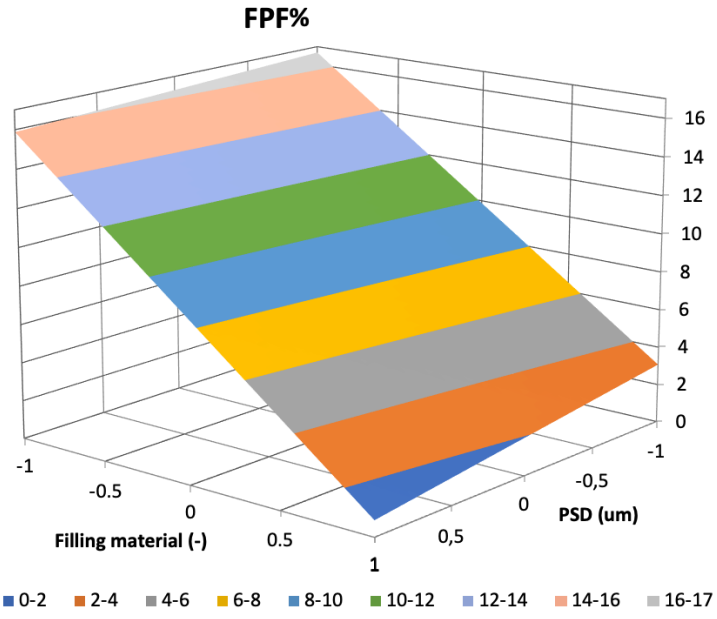

Figure 2.9. Response surface on FPF% of filling material and particle size distribution.

These results are in agreement with the finding of Monckedieck and co-workers [120] who claimed that micronized mannitol particles had an important effect on the FPF, due to their different shape and surface roughness.

4.3 Aerodynamic assessment with model drugs

4.3.1 Adhesive mixture with beclomethasone dipropionate (BDP)

A further Design of Experiment was carried out in order to assess the effect of several formulation parameters on the aerosolization performance in terms of emitted dose, fine particle dose and fine particle fraction.

Adhesive mixtures containing 1% and 5% w/w BDP were prepared using lactose or mannitol with the same particle size distribution (90-125 μm). The blends were mixed with Turbula® using geometric dilution. *In vitro* respirability test was performed using one capsule for each loading dose of BDP.

The analysis of the drug content was performed according to the procedure described in Chapter 1, paragraph 3.2.2.2.

Table 2.8 summarizes the actual BDP content and loaded powder dose for the capsule samples prepared for the *in vitro* respirability test.

Table 2.8. Percentage composition of the BDP mixtures, drug content and actual loaded powder doses in capsules filled with 10 mg of powder. Mean values ± standard deviation, RSD% between parenthesis (n=3).

	BDP (%)	**Carrier (%)**	**Drug Content (%)**	**Loaded powder dose (mg)**
BDP 1% – mannitol	1	99	0.77 ± 0.03 (3.51)	10.3 ± 0.3 (3.17)
BDP 5% – mannitol	5	95	5.00 ± 0.08 (1.53)	10.7 ± 0.2 (1.47)
BDP 1% – lactose	1	99	0.93 ± 0.01 (0.78)	10.9 ± 0.2 (2.33)
BDP 5% – lactose	5	95	5.12 ± 0.19 (3.76)	10.6 ± 0.1 (1.31)

Figure 2.10 shows the results of *in vitro* aerosolization of the mixture containing BDP 5%; data relevant to mixture with mannitol are depicted in Figure 2.10a, while those of the mixture with lactose are in Figure 2.10b.

For mannitol mixtures there was not a significant variation between the capsule types for drug distribution at the various levels of the impactor. On the contrary, with lactose-based mixtures larger variation between the drug distribution was observed with the various capsule types. In particular, the gelatin-based capsules presented a greatest deposition of the drug in the CFC level and consequently lower drug amount in the FFC.

In general, fine particle fraction of lactose-based mixture was lower than mannitol-based mixture regardless of the capsule type.

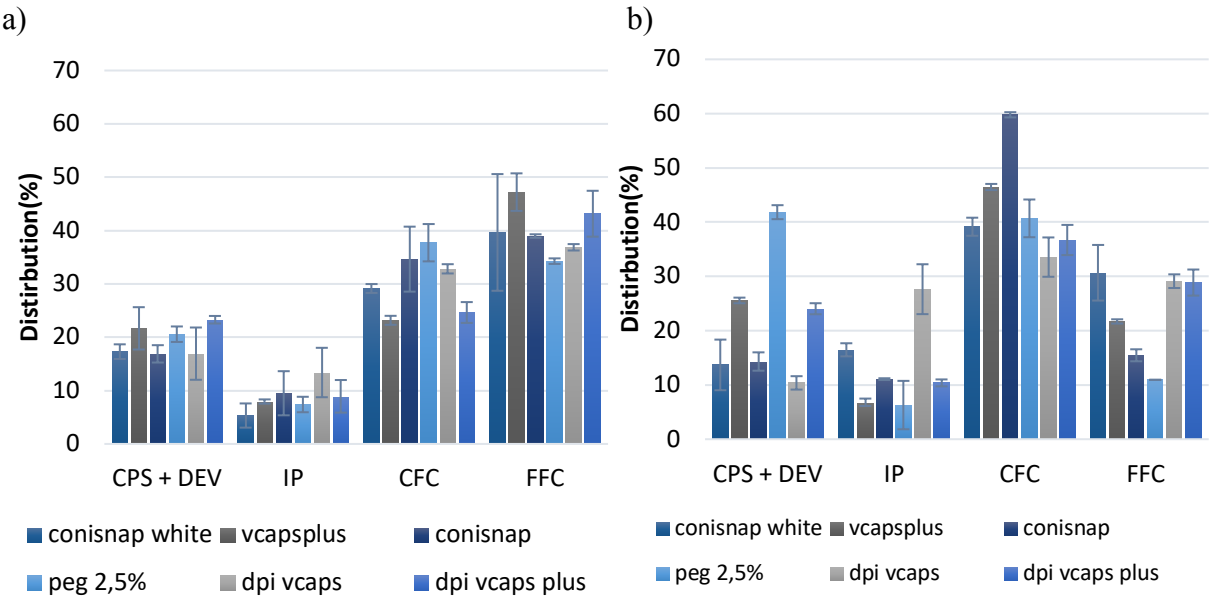

Figure 2.10. Distribution of BDP from BDP 5% - mannitol mixture (a) and BDP 5% - lactose mixture (b). Capsule and device (CPS + DEV), Induction Port (IP), Coarse Fraction Collector (CFC) and Fine Fraction Collector (FFC). The bars represent the standard deviation.

The aerosolization parameters calculated from data reported in Figure 2.9 are summarized in Table 2.9 and Table 2.10 for mannitol and lactose-containing mixtures respectively.

The fine particle fraction values were calculated both considering the emitted dose and the metered dose in order to put into evidence also any possible effect depending on the loaded dose. These data confirmed the better in vitro respirability of BDP carried by mannitol particles compared to lactose: FPF% in the case of mannitol-containing mixtures ranging from 43 and 60 % depending upon capsule type, with higher values observed with HPMC capsules. In the case of lactose-containing mixture the BDP FPF% ranged from 18 and 38% with no clear dependence on the composition of the capsule (either gelatin or HPMC).

Table 2.9. Aerosolization parameters of BDP 5% mannitol mixtures. Mean ± standard deviation (n = 3).

Capsule type	Metered Dose (µg)	ED (µg)	EF (%)	FPD (µg) <5 µm	FPF (%) <5 µm	FPF (%) (Metered Dose)
Conisnap® white	500.0 ± 114.3	362.5 ± 14.6	74.1 ± 14.0	192.0 ± 9.4	53.1 ± 4.7	39.6 ± 10.9
Vcaps® Plus	472.6 ± 56.4	371.3 ± 62.9	78.3 ± 4.0	224.1 ± 43.2	60.2 ± 1.4	47.2 ± 3.5
Conisnap®	417.8 ± 34.9	391.9 ± 21.3	83.1 ± 1.6	183.9 ± 15.2	46.9 ± 1.3	39.0 ± 0.3
DPI PEG 2.5%	502.1 ± 1.7	398.5 ± 9.0	79.4 ± 1.5	172.0 ± 2.0	43.2 ± 1.5	34.3 ± 0.5
DPI Vcaps®	407.4 ± 30.5	339.2 ± 45.3	83.1 ± 4.9	150.1 ± 8.8	44.5 ± 3.4	37.0 ± 0.6
DPI Vcaps® Plus	468.2 ± 2.1	359.2 ± 5.0	76.7 ± 0.7	202.0 ± 19.2	56.3 ± 6.1	43.2 ± 4.3

Table 2.10. Aerosolization parameters of BDP 5% lactose mixtures. Mean ± standard deviation (n = 3).

Capsule type	Metered Dose (µg)	ED (µg)	EF (%)	FPD (µg) <5 µm	FPF (%) <5 µm	FPF (%) (Metered Dose)
Conisnap® white	553.1 ± 71.3	479.1 ± 87.4	86.3 ± 4.7	171.5 ± 50.2	35.4± 4.0	30.7 ± 5.1
Vcaps® Plus	578.6 ± 18.1	433.9 ± 15.1	75.0 ± 0.3	125.7 ± 6.2	29.0 ± 0.4	21.7 ± 0.4
Conisnap®	539.2 ± 32.9	465.3 ± 24.1	86.3 ± 0.8	83.2 ± 0.9	17.9 ± 1.1	15.5 ± 1.11
DPI PEG 2.5%	564.6 ± 4.5	327.1 ± 2.9	57.9 ± 1.0	61.8 ± 0.6	19.0 ± 0.4	10.9 ± 0.0
DPI Vcaps®	594.6 ± 67.6	537.9 ± 74.3	90.4 ± 2.3	173.6 ± 27.2	32.2 ± 0.6	29.1 ± 1.3
DPI Vcaps® Plus	452.0 ± 30.6	343.1 ± 18.7	76.1 ± 1.0	130.8 ± 19.7	38.0 ± 3.7	28.8 ± 2.4

The aerosolization performance was assessed also for the low BDP dose mixtures. Figure 2.11 reports the results of *in vitro* aerosolization of BDP 1% with lactose and mannitol.

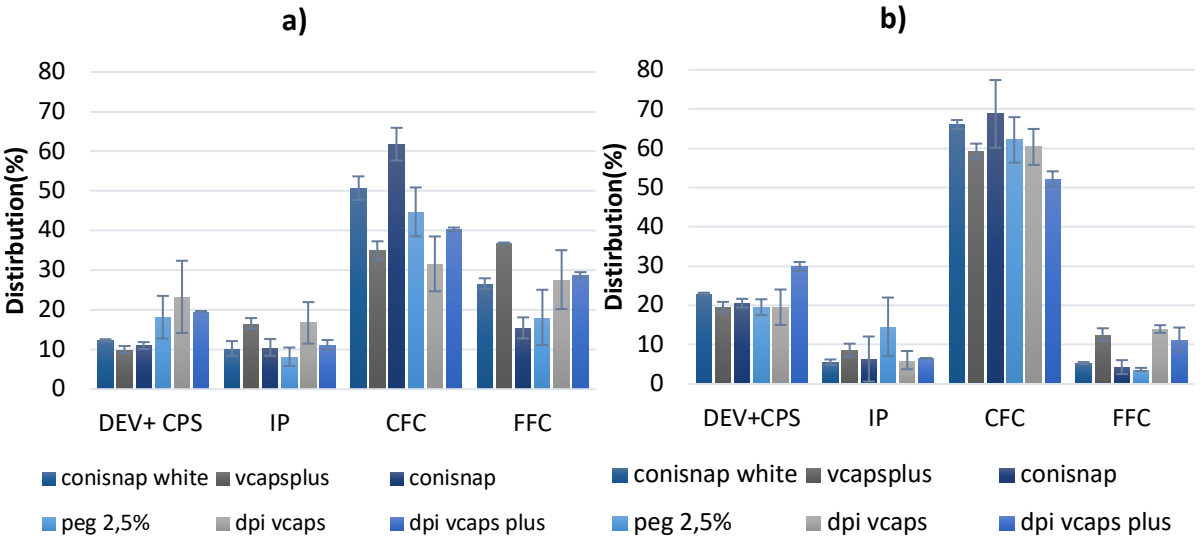

Figure 2.11. Distribution of BDP from BDP 1 % - mannitol mixture (a) and BDP 5% - lactose mixture (b). Capsule and device (CPS + DEV), Induction Port (IP), Coarse Fraction Collector (CFC) and Fine Fraction Collector (FFC). The bars represent the standard deviation.

The relevant parameters are shown in Table 2.11 and Table 2.12 for mannitol and lactose mixtures respectively.

The data reported in Figure 2.11 indicate that the reduction of the dose, determined an increase in the difference between the amount deposited in the CFC relative to FFC. This was particularly evident in the case of lactose-containing mixture that presented very high CFC deposition irrespectively of the type of capsule.

Again the better performance in terms of FPF was obtained with HPMC capsules both for mannitol and lactose mixture; overall, mannitol-containing-mixtures performed better than lactose-containing ones.

Table 2.11. Aerosolization parameters of BDP 1% mannitol mixtures. Mean ± standard deviation (n = 3).

Capsule type	Metered Dose (µg)	ED (µg)	EF (%)	FPD (µg) <5 µm	FPF (%) <5 µm	FPF (%) (Metered Dose)
Conisnap® white	90.6 ± 1.7	79.2 ± 1.3	87.6 ± 0.2	24.1 ± 0.7	30.4 ± 1.4	26.7 ± 1.3
Vcaps® Plus	95.7 ± 2.3	84.6 ± 0.9	88.4 ± 1.1	35.2 ± 0.6	41.6 ± 0.3	36.8 ± 0.2
Conisnap®	101.3 ± 1.1	89.0 ± 0.3	87.8 ± 0.7	27.8 ± 2.8	31.3 ± 1.3	27.4 ± 2.7
DPI PEG 2.5%	108.3 ± 14.9	75.8 ± 6.1	71.4 ± 15.0	19.7 ± 4.4	25.0 ± 4.4	18.1 ± 7.0
DPI Vcaps®	86.8 ± 6.7	66.3 ± 13.0	76.0 ± 9.1	24.3 ± 8.3	36.1 ± 5.4	27.6 ± 7.4
DPI Vcaps® Plus	97.5 ± 1.2	78.3 ± 1.2	80.4 ± 0.1	28.1 ± 0.2	35.9 ± 0.9	28.8 ± 0.7

Table 2.12. Aerosolization parameters of BDP 1 % lactose mixtures. Mean ± standard deviation (n = 3).

Capsule type	Metered Dose (µg)	ED (µg)	EF (%)	FPD (µg) <5 µm	FPF (%) <5 µm	FPF (%) (Metered Dose)
Conisnap® white	94.6 ± 5.7	72.7 ± 0.4	77.0 ± 0.2	5.1 ± 0.5	6.9 ± 0.3	5.3 ± 0.3
Vcaps® Plus	108.4 ± 3.3	87.1 ± 4.1	80.4 ± 1.3	13.7 ± 2.2	14.1 ± 0.8	12.6 ± 1.6
Conisnap®	104.1 ± 3.1	82.7 ± 3.7	79.4 ± 1.1	4.5 ± 1.7	5.4 ± 2.3	4.3 ± 1.8
DPI PEG 2.5%	101.7 ± 0.9	81.8 ± 2.7	80.4 ± 2.0	3.7 ± 0.4	4.6 ± 0.4	3.7 ± 0.4
DPI Vcaps®	96.5 ± 12.1	77.6 ± 8.5	80.4 ± 1.3	13.6 ± 2.6	17.4 ± 1.5	14.0 ± 1.0
DPI Vcaps® Plus	106.9 ± 17.9	75.0 ± 13.7	70.1 ± 1.1	12.4 ± 5.3	16.1 ± 4.1	11.3 ± 3.1

4.3.2 Adhesive mixtures with salmetorol xinafoate (SAL)

Aerodynamic assessment was also carried out with adhesive mixtures prepared with 0.1% and 0.5% w/w of SAL and lactose or mannitol with the same particle size distribution (90-125 µm).

Table 2.13 reports the actual SAL content and loaded powder dose for the capsule samples prepared for the in vitro respirability test.

Table 2.13. Percentage composition of the SAL-containing prepared mixtures, drug content and actual loaded powder doses in capsules filled with 10 mg of powder. Mean values ± standard deviation, RSD% in parenthesis (n=3).

	SAL (%)	**Carrier (%)**	**Drug Content (%)**	**Loaded powder dose (mg)**
SAL 0.1% – mannitol	0.1	99.9	0.13 ± 0.01 (3.45)	10.1 ± 0.2 (2.7)
SAL 0.5% – mannitol	0.5	99.5	0.49 ± 0.01 (1.96)	10.7 ± 0.7 (4.5)
SAL 0.1% – lactose	0.1	99.9	0.16 ± 0.01 (2.34)	9.8 ± 0.3 (3.2)
SAL 0.5% – lactose	0.5	99.5	0.56 ± 0.02 (2.97)	10.6 ± 0.1 (1.31)

Figure 2.12 shows the results of the *in vitro* deposition in the FSI of SAL 0.5% mixtures aerosolized with different capsules; the relevant aerosolization parameters are reported in Table 2.14 and Table 2.15 for mannitol and lactose mixtures respectively.

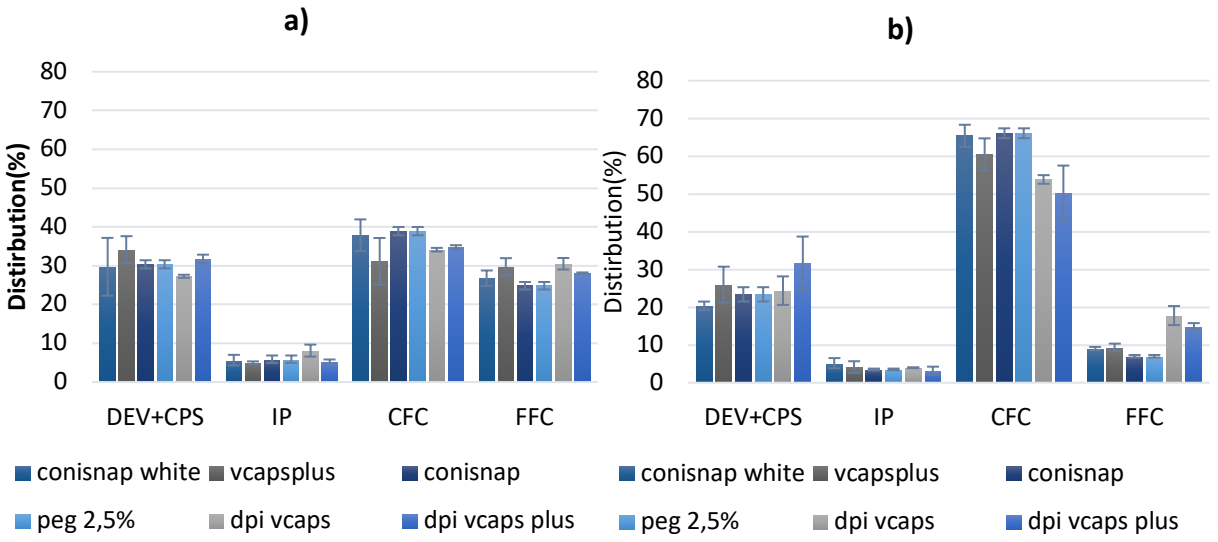

Figure 2.12. Distribution of SAL 0.5% - mannitol mixture (a) and SAL 0.5% - lactose mixture (b). Capsule and device (CPS + DEV), Induction Port (IP), Coarse Fraction Collector (CFC) and Fine Fraction Collector (FFC). The bars represent the standard deviation.

In the case of mannitol mixtures, the differences between the different capsule types with regard to deposition at the level of the CFC and FFC compartments were not observed. On the contrary in the case of lactose-containing mixtures a much greater deposition at the level of the CFC was observed. The HPMC capsule afforded better deposition in the FFC (implying a higher FPF%, Table 2.15) as apposite to CFC.

Table 2.14. Aerosolization parameters of SAL 0.5 % mannitol mixtures. Mean ± standard deviation (n = 3).

	Metered Dose (µg)	**ED (µg)**	**EF (%)**	**FPD (µg) <5 µm**	**FPF (%) <5 µm**	**FPF (%) (Metered Dose)**
Conisnap® white	47.4 ± 1.4	33.3 ± 4.5	70.3 ± 7.4	12.6 ± 1.3	38.2 ± 1.2	26.8 ± 2.0
Vcaps® Plus	47.2 ± 0.9	31.1 ± 2.2	65.9 ± 3.5	14.0 ± 0.8	45.3 ± 5.7	29.7 ± 2.2
Conisnap®	49.7 ± 4.2	34.6 ± 3.3	69.6 ± 1.1	12.4 ± 0.5	35.7 ± 1.9	24.8 ± 1.0
DPI PEG 2.5%	48.1 ± 1.0	36.2 ± 0.7	75.3 ± 3.0	12.0 ± 0.4	33.1 ± 0.6	24.9 ± 1.4
DPI Vcaps®	42.7 ± 1.3	31.0 ± 0.8	72.7 ± 1.5	13.0 ± 0.2	41.9 ± 1.8	30.5 ± 1.5
DPI Vcaps® Plus	50.3 ± 0.9	34.3 ± 0.1	68.3 ± 1.1	14.1 ± 0.2	41.2 ± 0.4	28.1 ± 0.2

Table 2.15. Aerosolization parameters of SAL 0.5 % lactose mixtures. Mean ± standard deviation (n = 3).

	Metered Dose (µg)	**ED (µg)**	**EF (%)**	**FPD (µg) <5 µm**	**FPF (%) <5 µm**	**FPF(%) Metered dose**
Conisnap® white	64.4 ± 0.8	51.3 ± 1.4	79.6 ± 1.1	5.8 ± 0.2	11.4 ± 0.7	9.1 ± 0.4
Vcaps® Plus	72.1 ± 1.2	53.3 ± 2.5	74.0 ± 4.8	6.8 ± 0.8	12.7 ± 2.2	9.4 ± 1.0
Conisnap®	66.7 ± 7.1	51.2 ± 6.7	76.6 ± 1.9	4.7 ± 0.7	9.1 ± 0.2	7.0 ± 0.3
DPI PEG 2.5%	64.5 ± 2.1	50.8 ± 0.5	78.8 ± 3.8	4.7 ± 0.0	9.3 ± 0.6	7.1 ± 1.0
DPI Vcaps®	60.3 ± 1.4	45.6 ± 1.3	75.6 ± 3.8	10.7 ± 1.3	23.5 ± 2.2	17.8 ± 2.5
DPI Vcaps® Plus	64.9 ± 8.9	44.1 ± 1.0	68.4 ± 7.07	9.7 ± 0.7	21.9 ± 1.0	14.9 ± 0.9

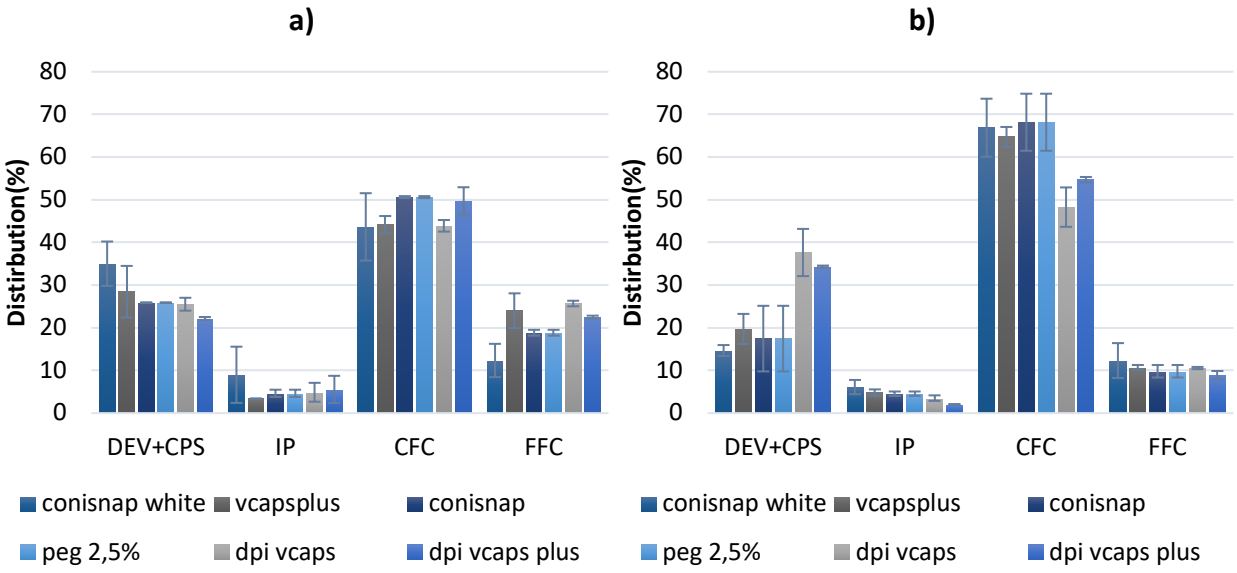

Figure 2.13. Deposition of SAL 0.1% - mannitol mixture (a) and SAL 0.1% - lactose mixture (b). Capsule and device (CPS + DEV), Induction Port (IP), Coarse Fraction Collector (CFC) and Fine Fraction Collector (FFC). The bars represent the standard deviation.

Figure 2.13 reports the results of the *in vitro* deposition in the FSI of SAL 0.1% mixtures aerosolized with different capsules; the relevant aerosolization parameters are reported in Table 2.16 and Table 2.17 for mannitol and lactose mixtures respectively.

Here the general trend was similar to that already described for the BDP when passing from the higher to the lower dosage, thus similar consideration applies.

Table 2.16. Aerosolization parameters of SAL 0.1 % mannitol mixtures. Mean ± standard deviation (n = 3).

	Metered Dose (µg)	**ED (µg)**	**EF (%)**	**FPD (µg) <5 µm**	**FPF (%) <5 µm**	**FPF (%) (Metered Dose)**
Conisnap® white	13.0 ± 0.4	8.5 ± 1.0	68.8 ± 4.7	1.6 ± 0.5	20.4 ± 4.4	12.3 ± 3.9
Vcaps® Plus	14.3 ± 0.5	10.2 ± 0.5	71.6 ± 6.1	3.4 ± 0.5	33.4 ± 2.7	24.0 ± 4.1
Conisnap®	12.7 ± 0.0	9.4 ± 0.0	74.1 ± 0.1	2.4 ± 0.1	25.4 ± 0.9	18.8 ± 0.7
DPI PEG 2.5%	14.3 ± 0.1	9.6 ± 0.1	67.0 ± 0.1	2.2 ± 0.2	22.7 ± 1.6	15.2 ± 1.0
DPI Vcaps®	13.8 ± 1.0	10.3 ± 0.5	74.5 ± 1.5	3.5 ± 0.2	34.5 ± 0.2	25.7 ± 0.7
DPI Vcaps® Plus	13.2 ± 1.0	10.3 ± 0.7	77.8 ± 0.3	3.0 ± 0.2	28.9 ± 0.3	22.5 ± 0.3

Table 2.17. Aerosolization parameters of SAL 0.1 % lactose mixtures. Mean ± standard deviation (n = 3).

	Metered Dose (µg)	**ED (µg)**	**EF (%)**	**FPD (µg) <5 µm**	**FPF (%) <5 µm**	**FPF(%) Metered dose**
Conisnap® white	14.6 ± 1.4	12.4 ± 1.2	85.9 ± 0.6	2.0 ± 0.9	11.6 ± 5.8	13.7 ± 4.8
Vcaps® Plus	14.2 ± 0.2	11.4 ± 0.6	82.2 ± 3.5	1.5 ± 0.1	13.4 ± 0.2	10.7 ± 0.5
Conisnap®	15.0 ± 1.5	12.4 ± 2.2	80.8 ± 7.7	1.5 ± 0.2	11.2 ± 1.3	9.8 ± 1.5
DPI PEG 2.5%	15.1 ± 0.4	9.2 ± 0.5	60.9 ± 4.8	0.7 ± 0.0	7.5 ± 0.6	4.6 ± 0.0
DPI Vcaps®	16.7 ± 1.5	10.4 ± 0.0	62.3 ± 5.5	1.8 ± 0.1	17.0 ± 1.1	10.6 ± 0.3
DPI Vcaps® Plus	14.3 ± 0.3	9.4 ± 0.2	65.7 ± 0.3	1.3 ± 0.1	13.6 ± 1.4	9.0 ± 0.9

4.3.3 Statistical evaluation of the data from FSI deposition

As it was mentioned before, the output parameters (EF and FPF) obtained from the design of experiments (Tables 2.12.12 and Tables 2.14-2.17) were statistically evaluated in order to highlight the effect of each single variable ad possible interaction effects. Table 2.18 summarizes the data matrix. Figure 2.14 and 2.15 report effects on Emitted fraction and fine particle fraction and the level of significant of the considered variables alone or in combination.

For EF% (Figure 2.14) the only statistically significant effect was observed for active ingredient, meaning that higher EF was obtained with BDP.

As for FPF% (Figure 2.15), capsule type, active ingredient type of carrier and dosage as well as the combination of active ingredient and dosage exerted a highly statistically significant effect.

Table 2.18. Drug distribution values obtained from an *in vitro* aerosolization study using the Fast Screening Impactor (FSI).

Run order	Capsule type	API	Filling material	Dosage of API	EF (%)	FPF (%)
3	Conisnap white	SAL	Lactose	low dose	85.88	11.63
9	Vcaps Plus	SAL	Lactose	low dose	82.21	13.37
15	Conisnap	SAL	Lactose	low dose	80.88	11.17
21	DPI PEG 2.5%	SAL	Lactose	low dose	60.91	7.52
27	DPI Vcaps	SAL	Lactose	low dose	62.36	16.99
33	DPI Vcaps plus	SAL	Lactose	low dose	65.67	13.63
39	Conisnap white	SAL	Lactose	high dose	79.64	11.38
45	Vcaps Plus	SAL	Lactose	high dose	74.02	12.71
1	Conisnap	SAL	Lactose	high dose	76.59	914
7	DPI PEG 2.5%	SAL	Lactose	high dose	78.83	9.06

13	DPI Vcaps	SAL	Lactose	high dose	75.61	23.47
19	DPI Vcaps plus	SAL	Lactose	high dose	68.36	21.88
25	Conisnap white	SAL	Mannitol	low dose	66.82	20.41
31	Vcaps Plus	SAL	Mannitol	low dose	71.55	33.43
37	Conisnap	SAL	Mannitol	low dose	74.14	25.74
43	DPI PEG 2.5%	SAL	Mannitol	low dose	66.97	22.66
4	DPI Vcaps	SAL	Mannitol	low dose	74.48	34.50
10	DPI Vcaps plus	SAL	Mannitol	low dose	77.82	28.94
16	Conisnap white	SAL	Mannitol	high dose	70.28	38.18
22	Vcaps Plus	SAL	Mannitol	high dose	65.86	45.30
28	Conisnap	SAL	Mannitol	high dose	69.64	35.67
34	DPI PEG 2.5%	SAL	Mannitol	high dose	75.34	33.00
40	DPI Vcaps	SAL	Mannitol	high dose	72.59	41.29
46	DPI Vcaps plus	SAL	Mannitol	high dose	68.27	41.16
5	Conisnap white	BDP	Lactose	low dose	76.95	6.95
11	Vcaps Plus	BDP	Lactose	low dose	80.39	14.06
17	Conisnap	BDP	Lactose	low dose	79.43	5.44
23	DPI PEG 2.5%	BDP	Lactose	low dose	80.44	4.60
29	DPI Vcaps	BDP	Lactose	low dose	80.45	17.42
35	DPI Vcaps plus	BDP	Lactose	low dose	70.05	16.10
41	Conisnap white	BDP	Lactose	high dose	86.31	35.44
47	Vcaps Plus	BDP	Lactose	high dose	74.99	28.95
6	Conisnap	BDP	Lactose	high dose	86.33	17.91
12	DPI PEG 2.5%	BDP	Lactose	high dose	57.94	18.90
18	DPI Vcaps	BDP	Lactose	high dose	90.33	32.24
24	DPI Vcaps plus	BDP	Lactose	high dose	75.96	38.03
30	Conisnap white	BDP	Mannitol	low dose	87.63	30.41
36	Vcaps Plus	BDP	Mannitol	low dose	88.42	41.67
42	Conisnap	BDP	Mannitol	low dose	86.47	31.28
48	DPI PEG 2.5%	BDP	Mannitol	low dose	75.90	25.03
2	DPI Vcaps	BDP	Mannitol	low dose	75.98	36.05

8	DPI Vcaps plus	BDP	Mannitol	low dose	80.39	35.87
14	Conisnap white	BDP	Mannitol	high dose	74.05	53.05
20	Vcaps Plus	BDP	Mannitol	high dose	78.34	60.23
26	Conisnap	BDP	Mannitol	high dose	83.11	46.90
32	DPI PEG 2.5%	BDP	Mannitol	high dose	79.38	43.18
38	DPI Vcaps	BDP	Mannitol	high dose	83.08	44.47
44	DPI Vcaps plus	BDP	Mannitol	high dose	76.50	56.95

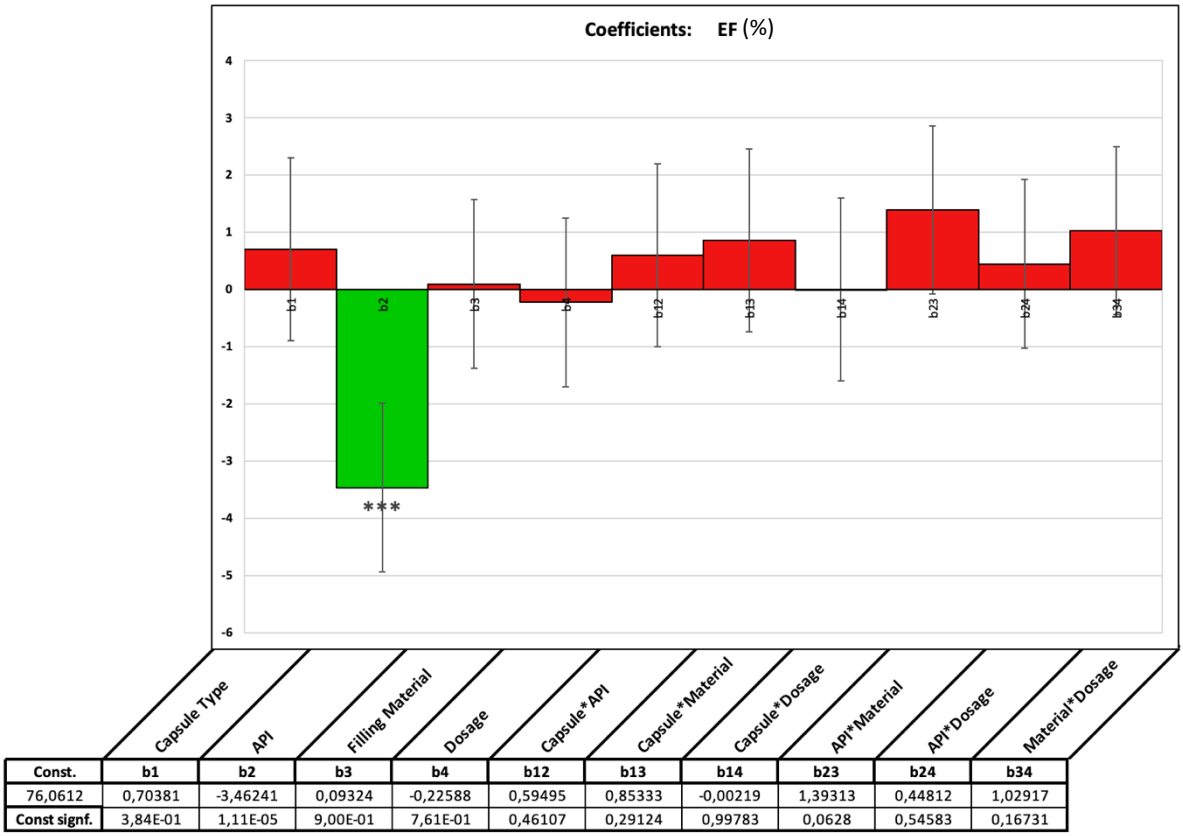

Const.	b1	b2	b3	b4	b12	b13	b14	b23	b24	b34
76,0612	0,70381	-3,46241	0,09324	-0,22588	0,59495	0,85333	-0,00219	1,39313	0,44812	1,02917
Const signf.	3,84E-01	1,11E-05	9,00E-01	7,61E-01	0,46107	0,29124	0,99783	0,0628	0,54583	0,16731

Figure 2.14. Effect of individual variables and their combination on the EF (%)

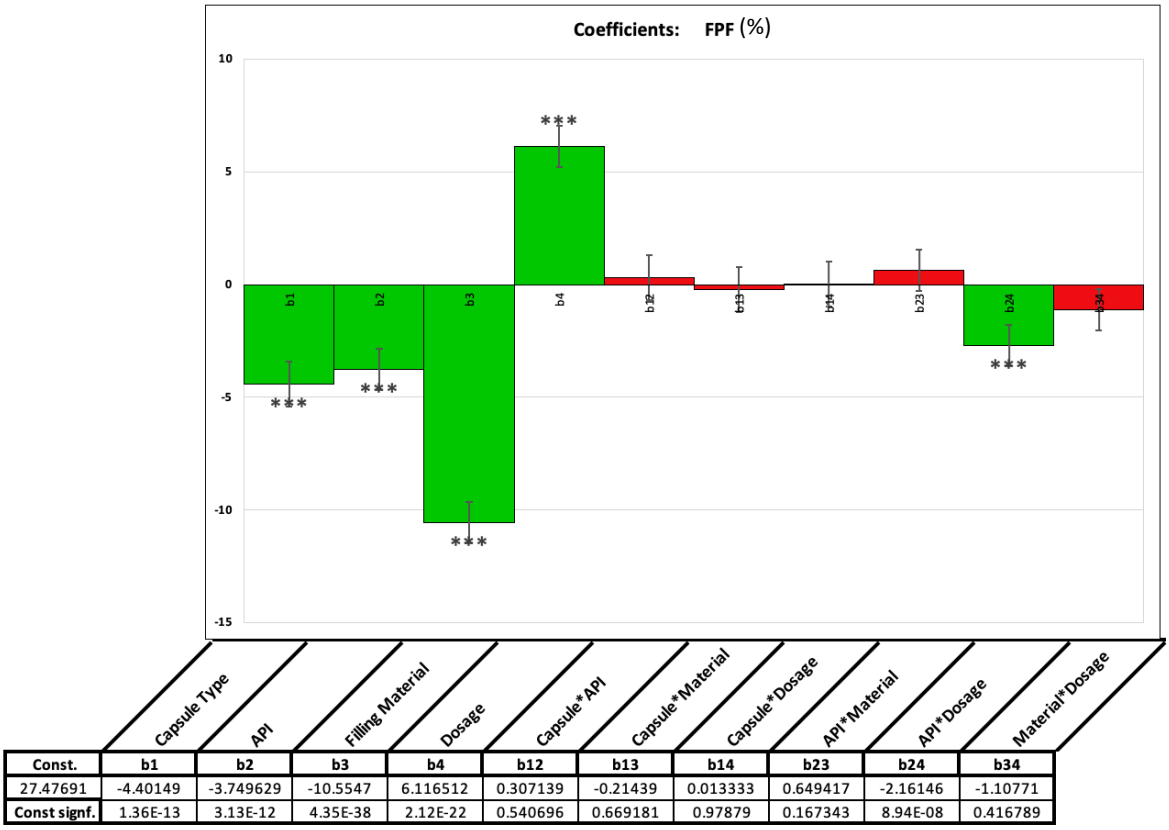

Const.	b1	b2	b3	b4	b12	b13	b14	b23	b24	b34
27.47691	-4.40149	-3.749629	-10.5547	6.116512	0.307139	-0.21439	0.013333	0.649417	-2.16146	-1.10771
Const signf.	1.36E-13	3.13E-12	4.35E-38	2.12E-22	0.540696	0.669181	0.97879	0.167343	8.94E-08	0.416789

Figure 2.15. Effect of individual variables and their combination on the FPF (%)

In detail, capsules with lower water content (HPMC and HPMC plus), the lipophilic drug (beclomethasone dipropionate) and mannitol as carrier determined an increase in FPF. This suggests a higher amount of active ingredient resulted as well as a lower water content in the capsule and a high lipophilicity of the drug afford an improved FPF (%). This results confirms what already presented in early literature [121] .

The quantification of this effects on the FPF % is graphically represented as a function of type of active ingredient and dosage in the response surface plots in Figures 2.16 and 2.17 for gelatin and HPMC capsule groups respectively both for mannitol-containing capsules (panel a) and lactose-containing capsules (panel b).

In all cases the FPF increases with dosage. For gelatin capsule group this effect is limited with lactose-containing capsules. Highest FPF can be obtained increasing both drug lipophilicity and dosage.

Both for hydrophilic and lipophilic active ingredients mannitol-containing capsules perform better than those containing lactose. HPMC capsules afford higher FPF irrespectively of the active ingredient and carrier used.

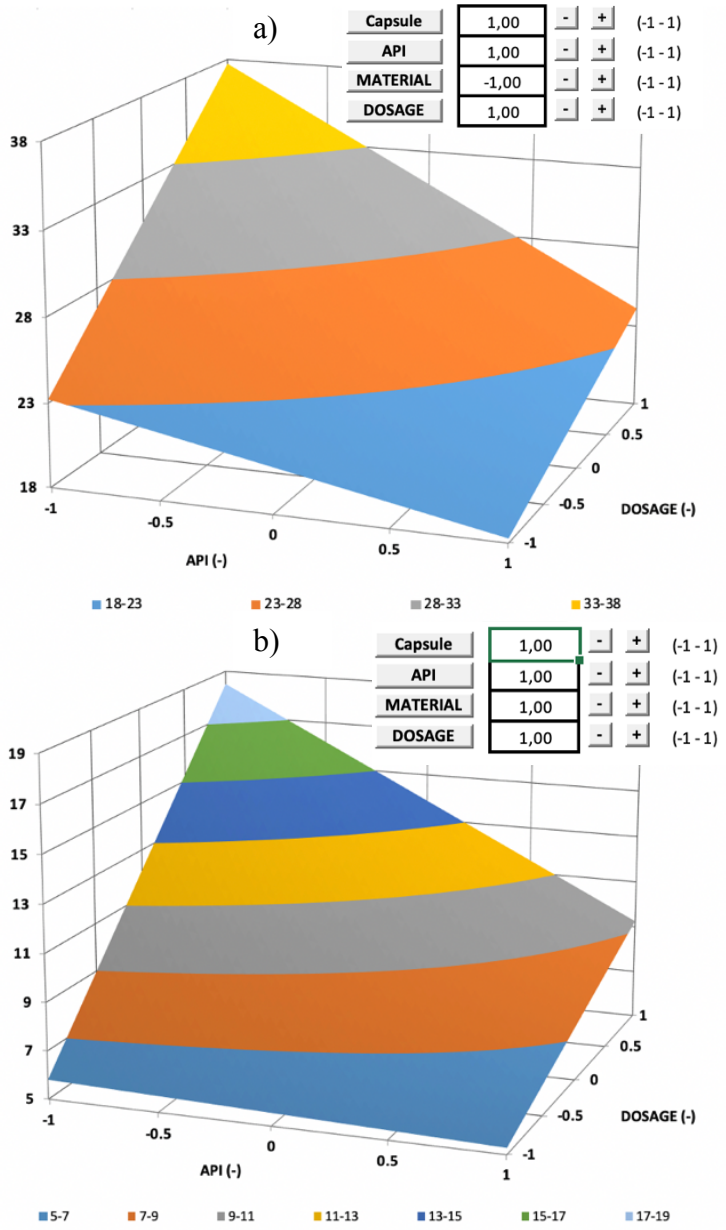

Figure 2.16. FPF% response surface upon aerosolization of powder in gelatin capsules versus different APIs and Dosage. Mannitol-containing powders (a); lactose-containing powders (b).

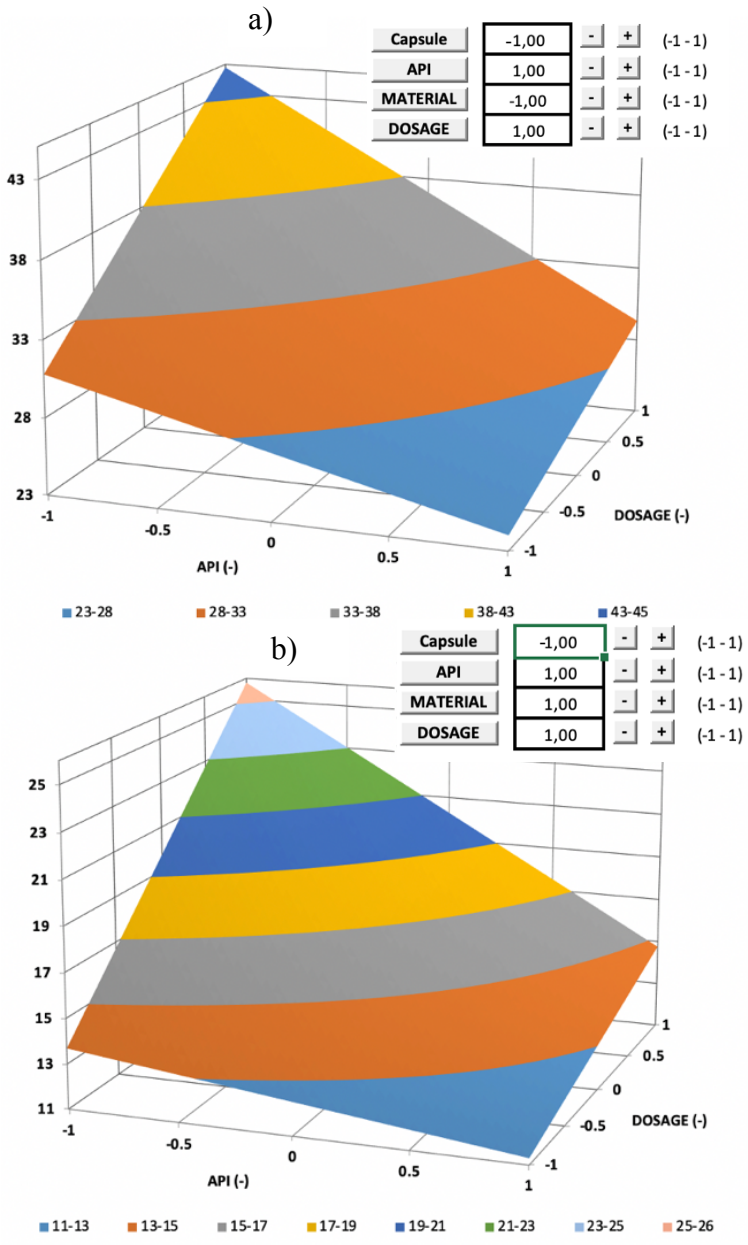

Figure 2.17. FPF% response surface upon aerosolization of powder in HPMC capsules versus different APIs and Dosage. Mannitol-containing powders (a); lactose-containing powders (b).

4.4 Capsules filling with mannitol polymorphs

In the next step of the project the filling performance of the mannitol polymorph (α, β and δ) powders crystallized using the methods described Chapter 1 (paragraphs 3.2.1) was investigated with Minima® equipment using the worst-case conditions based on the results obtained in 4.3. Conisnap® white capsules were filled with 10 mg of each mannitol forms. To eliminate possible effects stemming from different particle size differences, the powders were previously sieved through a 53 µm sieve to eliminate the fine portion. For comparison purpose a commercially available mannitol (Pearlitol® 160C) was used. It is claimed to be an almost pure β form. The powder of said product was also sieved in order to select the 53-150 µm fraction.

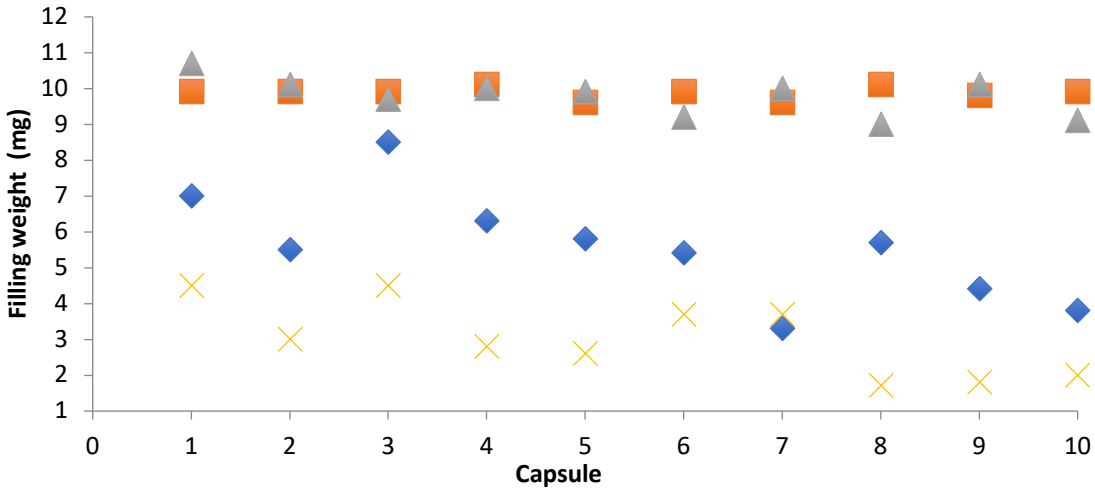

Figure 2.18. Weight of 10 capsules filled with different mannitol polymorphs and a commercially available mannitol. Triangle sieved Pearlitol® 160C; square recrystallized δ form; diamond recrystallized β form; cross recrystallized α form.

Figure 2.18 reports the results obtained upon filling 10 capsules with the different powders. It is evidenced that δ form afforded highly accurate filling, similarly to sieved Pearlitol® 160C.

The difference between the average values obtained from the two powders was not statistically significant (p value = 0.6519). On the contrary, the capsule filled with the recrystallized β form never reached the target weight giving rise to a great weight variability (higher value 8.5 mg; lower value 3.7 mg). With the recrystallized α form an even worse behavior was observed (higher value 4.5 mg; lower value 1.7 mg). The most curious aspect was represented by the significant difference ($p < 0.00001$) between commercial β form and crystallized β form.

In an attempt to explain this behavior, the flowability of the powders was investigated. The obtained data are reported in Table 2.19.

Table 2.19. Angle of repose, Carr's Index, Hausner ratio of mannitol powders. Mean value ± standard deviation (n=3).

Mannitol forms	Angle of repose [°]	Carr's Index (%)	Hausner ratio
δ form	39.8 ± 1.0	29.9 ± 1.0	1.43 ± 0.1
β form	37.6 ± 1.0	31.6 ± 0.5	1.46 ± 0.1
α form	63.4 ± 2.5	40.3 ± 3.4	1.58 ± 0.2
Sieved Pearlitol® 160C	39.4 ± 1.4	27.6 ± 0.4	1.39 ± 0.0

The α form turns out to be the one with the worst flow properties, δ form and Sieved Pearlitol® 160C gave rise to similar value and not significantly different from that of the recrystalized β form showing passable flowability.

The comparison among this value was not sufficient to justify the large differences observed among the different mannitol forms in terms of capsule filling accuracy.

These differences may be ascribed to different mechanical characteristics of the powder bed of each mannitol form, leading to different compactability during the sampling phase by the dosator of Minima equipment; it could have been possible that Minima® piston did apply a force that, in the case of α and β form, was not sufficient to obtain an aggregated powder

compact. To verify this hypothesis the force exerted by the piston in the dosator during the compaction step of the sampling phase was estimated from the Heckel equation calculated upon compacting a predefined amount of powder with the Styl'One compression simulator at the lowest compression force (0.5 kN).

4.5 Calculation of the force applied by Minima® using the Heckel equation

By means of the Heckel equation, knowing the density of the powder compact in the dosator, it was possible to calculate the value of the force applied by the capsule filling machine to obtain the powder compact that was dosed in the capsule. The density of the powder compact in the dosator was calculated measuring the height of each powder cylinder released into the capsule by the dosator knowing that the capsule diameter was 3 mm; as a first approximation the possible axial elastic recovery of the compact was disregarded.

Considering the height of the powder cylinder and the diameter of the dispenser, it was possible to calculate the volume as:

$$\text{Volume} = \pi r^2 h \qquad (2.7)$$

$$\text{density} = m/V \qquad (2.8)$$

where h = the height of the compact release by the dosator in the capsule, r = 1.5 mm, and m = average weight of each capsule (Tab.2.20).

Through the use of a Styl'One tableting simulator, 100 mg of powder were transformed into compact, maintaining the compression force at 0.5 kN and performing five replicates per polymorph. From the force values obtained from the compression of the powders, it was possible, through the Heckel equation, to calculate applied by Minima®. The density of the compacted powder was calculated using the weight and the height of the compacted powder obtained from the dosator; this density was applied to the Heckel plot constructed with the Styl'One.

Table 2.20. Results of the Heckel equation with mannitol polymorphs and calculated force values applied by the Minima® capsule filling machine. Mean values ± standard deviation (n=10).

Mannitol	Weight (mg)	Height of compact (mm)	Density of compact (g/cm^3)	Equation of Heckel: Ln(1/(1-D))	Force applied by Minima (N/mm^2)
α form	4.55±0.27	1.49±0.1	0.43±0.1	0.34±0.01	1.25±0.4
β form	6.47±0.77	2.32±0.35	0.4±0.03	0.32±0.03	2.24±0.68
δ form	8.88±0.47	2.51±0.13	0.5±0.02	0.39±0.02	0.78±0.28
Pearlitol 160C®	9.96±1.44	2.66±0.49	0.53±0.03	0.44±0.03	1.78±0.36

To investigate the force applied by the Minima® capsule filling machine, five tablets were manufactured for each mannitol polymorph using a compression force of 0.5 kN. 10 capsules were filled at a dosage of 10 mg, keeping the capsule filling machine parameters constant to obtain capsules with the same amount of powder. Table 2.20 shows the results of the Heckel equation obtained by the Styl'one software for each polymorph, which indicates the compactability of the various types of crystals.

The density of the compact was in line with the recorder weight, whereas highest computed force applied by Minima were obtained for the crystallized β form followed by the commercial β form (Pearlitol 160C). The lower value was observed for the δ form. Therefore, these results did not correlate completely with the different filling weight, indicating that the adopted approach was not useful to elucidate the observed phenomenon, likely because of the differences between the actual forces applied by Minima and those applied by Styl'one for the construction of the Heckel plot.

5 Conclusion

The goal of a formulation designed for inhalation administration is certainly to allow a constant and homogeneous delivery of the drug, in order to ensure adequate therapy. It is known that the delivery can be easily influenced by numerous factors that affect the aerosolization performance.

The purpose of this second part of the thesis was to evaluate the effect of the capsule type on the aerosolization performance *in vitro* in dry powder inhalation devices. To this end an experimental design was used.

The filling of the HPMC capsules with the powder of carrier alone is more consistent than the gelatin capsules, resulting in a lower relative standard deviation of the weight of the capsules themselves; the RSD% increases with the decrease of the particle size of the powder.

Moreover, the type of capsule does not influence the emitted fraction (EF%) and the fraction of fine particles (FPF%). The increase of either the particle size or dosage lead to an increase in EF% and a reduction in FPF.

As to the aerosolization performances of mixtures containing a lipophilic (beclomethasone dipropionate) or a hydrophilic (salmeterol xinafoate) drug, the best results in terms of higher respirable (FPF%) are obtained for mixtures using mannitol as carrier. FPF% increases by increasing the dose of active ingredient loaded.

Finally, the use of HPMC capsules favors the delivery of the drug at the level of the FFC component of the FSI, thus improving its respirability.

Chapter III

1 Introduction

1.1 Amorphous solid-state characterization

The crystalline structure is an ordered lattice which allows to minimize the distance between the molecules and therefore the free energy content of the system. As it was mentioned before, the crystalline phases can be characterized by polymorphism, i.e. the ability of many substances to crystallize in at least two crystalline phases which are chemically identical but different in the arrangement and conformation of the molecules [122]. The most stable form is the one showing the lowest solubility which often represents a problem for absorption and bioavailability of medicinal product. This issue is sometime addressed by developing formulations containing a kinetically stabilized amorphous or metastable form.

The amorphous state, unlike the crystalline one, is characterized by a high degree of disorder among the molecules [123]. In the case of amorphous substances, the energy content is higher as the molecules are located at a greater distance from each other and therefore have greater freedom of movement.

The formation of amorphous or metastable phases affects the properties of product as it can be the result of different processes. In some cases the metastable phase in the final formulation tends to recrystallize at high temperature and or high relative humidity due to the fact that water acts as a plasticizer [1]. In the pharmaceutical field the formation of amorphous phases may occur in several cases, such as [122], [124]–[126];

- Solidification of a melt, if a molten substance is cooled rapidly it does not crystallize since the molecules do not have the time to diffuse and migrate towards each other to

organize themselves in an ordered structure. The rapid cooling in fact subtracts kinetic energy and the molecules are locked in the position in which they are and maintain a disordered structure, similar to that of the liquid state.

- Grinding processes, as energy is imparted to the surface of the solid which allows the breaking of the intermolecular bonds.
- Wet granulation, in which a partial dissolution of the active substance can occur in the binding solvent and it can re-solidify in a different form compared to the starting material.
- Drying processes by nebulization, which allows to obtain a dried powder starting from an aqueous solution or suspension, thanks to the passage of the solution through a gaseous medium subjected to high temperature. During this process, the solid may not have the time to organize into an ordered structure, leading to the formation of amorphous solids. Processes such as lyophilization and spray drying can lead to the formation of the amorphous form, which tends to be less stable and more hygroscopic than the crystalline product.

The water replacement theory states that in solution the conformation of the protein is maintained by combining with water, mainly via hydrogen bonding. During the drying process, this interaction takes place between sugar and protein where the protein structure is preserved by sugar [127], [128]. To enhance the hydrogen bonding within the protein, the sugar molecules must closely fit the protein's irregular surface and therefore should preferably be in an amorphous, not crystalline state. A closely related assumption is the water entrapment theory, which defines that instead of directly hydrogen bonding with the sugar, the protein is combined with the amorphous sugar matrix via water molecules trapped at the interface [128], [129]. Despite the fact that these theories are valuable for developing a stable protein formulation in correctly selected carrier, further optimization requires more detailed knowledge of the amorphous state and the glass transition temperature for protein stabilization. When rapid kinetic processes occur, a phase change is likely to occur as there is not enough

time to allow an orderly arrangement of the structure itself. Amorphous solids generally exhibit greater solubility and dissolution rate and, sometimes, better compression characteristics than crystalline phases. However, having higher free energy, they are generally less physically and chemically stable than crystals [124]. Consequently, it is important to monitor and characterize the extent of crystallinity or degree of disorder of a system during the various processing stages, in particular during the formulation, production and storage of the pharmaceutical form [112], [113].

Over the years, various analytical techniques have been developed for the quantification of the crystalline phase of a solid and the amorphous content is inferred from the degree of crystallinity, as these techniques detect specific properties and characteristics of the crystalline material. X-ray diffraction, thermal analysis and dynamic vapor sorption (DVS) analysis are the most important techniques in the study of the solid state of crystals [68], [125], [130]–[132]. By examining the X-ray diffraction spectrum of a crystal, it is possible to trace the space group and the distribution of the atoms or ions in the unit cell. The structural determinations are based on the measurement of the intensity of the reflections given by each reticular plane of the crystal [122]. X-rays are scattered by electrons and therefore the intensity of the reflections depend on the distribution of the electron density in the planes that generated them, a distribution which is linked to the way in which the atoms are bound in the structure.

DVS is a good method to identify and quantify the polymorphs form of the same compound. as some compounds show a different behavior during water absorption at a set temperature and water content [131], [132], [130], [131].

1.2 Protein and enzyme structures

Proteins are among the most abundant biological macromolecules, present in all cell types and in all subcellular fractions. They are polymers of amino acids in which each amino acid residue is joined to the neighboring one by covalent bonds; the term "residue" emphasizes the loss of the elements of a water molecule when one amino acid joins another [133].

The structure of large molecules, such as proteins, can be described at various levels of complexity; generally four levels of structure are defined [35], [133]:

- the primary structure is made up of a sequence of amino acids joined by covalent bonds (mainly peptide bonds and disulfide bonds);
- the secondary structure describes the spatial organization of the main chain, without considering the conformation of the side chains or the relationship with other segments of the protein;
- the tertiary structure is defined as the arrangement in space of all the atoms of a protein; it considers the long-range relationships in the amino acid sequence. It is determined by the interactions that take place between amino acids distant in the sequence;
- the quaternary structure, finally, is observed in a protein consisting of two or more polypeptide subunits, arranged in three-dimensional complexes.

Considering these structural levels, it is useful to define two main groups into which proteins can be classified: fibrous proteins, which have polypeptide chains arranged in long bundles or sheets, and globular proteins, which instead have folded polypeptide chains and take on globular or spherical forms. This classification also differs functionally, in the sense that the proteins that determine the resistance, shape and external protection of the vertebrate cell are fibrous, while the enzymes and regulatory proteins are mostly globular proteins [133].

Proteins that perform different functions have different amino acid sequences; It should also be noted that thousands of genetic diseases found in humans are due to the production of defective proteins [35], [134].

Proteins are dynamic molecules, whose functions invariably depend on interactions with other molecules: most of these molecular contacts are at the basis of important physiological processes such as oxygen transport, muscle contraction and immune function. Thus, if the structure of a protein is altered, its function is also altered.

In order to perform its function, a protein, needs to establish a reversible bond with another molecule, called a ligand, which binds to a specific site, binding site, complementary to the ligand itself in terms of size, shape, charge and hydrophobic or hydrophilic character [133].

Therefore, the formulation and the process for the production of medicinal products for protein pulmonary drug delivery should be specialized in order to account for the intrinsic instability mechanism related to the protein structure. As mentioned before, the water acts as a stabilizing agent for proteins, however, when aqueous protein formulations are dried, the water surrounding proteins is removed either partly or completely. According to the Jaenicke's study, the amount of water required for full hydration has been approximated to be less than 0.25 g per one gram of protein [135]. This specific interaction is frequently related to intramolecular modification of the protein, which must adapt for binding to the ligand in order to retain it more firmly. This process also is well known as induced adjustment among a protein and its ligand takes place.

On the other hand, enzymes represent a special case of protein function: in fact, they bind and chemically transform other molecules thus catalyzing a specific reaction.

In recent years protein expression as advanced significantly so that proteins and enzymes are presently among of the most expanding pharmaceutical categories [136]. The modification of

the chemical structure of natural proteins and enzymes allows the development of more stable drug candidates with high specificity, high potency and low toxicity. This have resulted in higher development success rates comparted to small molecule, especially in clinical stages [136], [137].

Various proteins and enzymes have been identified for their potential when administered by inhalation. These include enzymes, such as lysozyme, to be used in the treatment of bacterial infection [138]–[140].

1.3 Inhalable protein formulations

The administration of peptides and proteins through the inhalation route may represent a promising and effective method for targeting the absorption at the lower airway and obtaining a systemic effect.

Macromolecules are generally more unstable than smaller molecules during their formulation manufacture and they can undergo degradation processes easily. The most common of the degradative mechanisms of proteins are denaturation and non-covalent aggregation. Denaturation consists in the loss of the native conformation with subsequent reduction of biological activity. This can be triggered by different stress mechanisms such as those occurring during the spray drying process (liquid/air interface) or also lyophilization process (liquid/ice interface), exposure to high temperature, during drying (loss of hydrogen bonds) rather than chemical factors [82]. For these reasons, various types of carriers, amino acids, surfactants, buffers solutions are often used in the formulations to reduce these stresses and slow down the degradation processes.

Carriers, mainly disaccharides, are essential for stabilizing proteins during drying (which occurs both in the case of spray drying and freeze drying). A further essential element is the non-reducing chemical activity of the selected sugar, otherwise a reaction may occur between

the anomeric carbon of the sugars and the protein amino groups which may cause the Maillard reaction.

Buffers are usually added into formulations commonly to preserve the protein stability in a specific pH range, to minimize changes upon freezing [78]. Surfactants, especially non-anionic surfactants such as polysorbate (typically used at the concentration of 0.5% w/v), can be put into the formulation to diminish the formation of aggregates at the interface. Finally, bulking agents, such as mannitol, glycine, or a combination thereof, can be added to produce a cake or to expand the amount of powder obtained; however, their addition must be accurately regulated because they tend to crystallize thus, introducing a further variable affecting the formulation performance [82].

2 Aim

The aim of this part of thesis was the investigation of the process development for the spray drying production of a powder containing mannitol as a carrier for inhalation of therapeutic protein.

The goal was first pursued through the development of the spray drying process, using a combination of sugars and sugar alcohol at different weight ratios. The selection of the most promising mixture of components was done by studying the influence of the process variables on the physico-chemical and aerodynamics characteristics of the powders obtained.

Once the new carrier was optimized, the second step was to add lysozyme as a model therapeutic and investigate the physico-chemical properties of the obtained formulation in terms of the stability and aerodynamic performance.

3 Material and method

3.1 Material

Lysozyme (EC 3.2.1.17) (L-6876), Sigma-Aldrich®, USA;

Lysozyme detection kit (LY0100), Sigma-Aldrich®, USA;

Trehalose supplied from A.C.E.F., Italy, (lot n◦ N0714801)

Raffinose supplied from A.C.E.F., Italy

Mannitol Pearlitol® SD200, Roquette, France (lot n◦ E556G)

Hydranal-Composite 5, Honeywell Fluka™, Germany (lot n°I0240)

3.2 Methods

3.2.1 Lysozyme Assay

The quantification of protein was carried out using 280 nm wavelength (Lambda 20, Perkin Elmer, USA) using the relevant calibration curve [141], [142].

The lysozyme detection kit was used to measure the activity of the protein in the powders, before and after the spray drying technique, using a suspension of *Micrococcus Lysodeikticus* bacteria as substrate of the enzyme.

The kit includes a reaction buffer (66 mM monobasic potassium phosphate, pH 6.24), *Micrococcus Lysodeikticus* substrate and standard lysozyme.

Lysozyme solution containing 40,000 IU/mg was initially prepared in a volume of cold reaction buffer to a concentration of 40,000 IU/mL. Then a 1:100 dilution was performed in reaction buffer to reach 400 IU/mL.

The cell suspension of *Micrococcus Lysodeikticus* (lot n. M3770) was prepared in Reaction buffer at a concentration of 0.01% w/v. 0.5 mg of cell suspension was weighed and added to 5 mL of buffer in a 15 mL Falcon type tube.

For each test, in addition to the samples to be analyzed, a blank, enzyme-free and positive

control were prepared.

The reading of the samples was performed at a 450nm wavelength (Lambda 20, Perkin Elmer) and monitoring the change in absorbance for 5 minutes at 30 seconds intervals in a quartz cuvette of 1 cm optical pathlength.

For the blank test, 30 µL of buffer alone were added to 800 µL of cell suspension; for the control sample, 30 µL of the lysozyme solution diluted 1:100 were added to 30 µL of buffer and 800 µL of cell suspension.

For the spray-dried samples 1 mg of powder for each sample was weighed using a balance with a sensitivity of 1µg (model MT5, Mettler Toledo); this sample was then dissolved in the reaction buffer just before reading. 30 µL of each sample were then taken and added to the individual cell suspensions.

The slope of the line obtained by reporting the absorbance change as a function of time to determine the activity of the enzyme in comparison to the control sample.

3.2.2 Spray dryer technique

The powders for inhalation were obtained through spray drying technique, using a Mini Spray Dryer® model B-290, Büchi.

For the preparation of the powders, solutions containing the sugar or sugar alcohol alone or in combination (Table 3.1) were prepared at a total concentration of 2 grams in a final volume of 100 mL of purified water and dried using the following process parameters:

• Drying temperature (Inlet): 90° C, 100° C, 110° C, 130° C or 140° C

• Aspiration: 30 $m^{3/}$h;

• Atomization air flow: 473 L/h or 601 L/h;

• Solution feeding rate: 2.0 mL/min;

• Nozzle diameter:1.4 mm or 0.5 mm.

Table 3.1. Sugar and sugar alcohol used for the production of spray dried powders.

Powder	Carrier (weight ratio)
1	Trehalose (100)
2	Trehalose-Raffinose (50:50)
3	Trehalose-Mannitol (50:50)
4	Trehalose-Mannitol (75:25)

The spray dried powders containing lysozyme were produced with mannitol and trehalose using an inlet temperature of 90 °C and atomization air flow of 473 L/h. The concentration of the feeding solution was kept at 2% w/v; this solution was obtained by dissolving in water (100 mL final volume) trehalose and mannitol in different weight ratios and adding 2ml of reaction buffer (66 mM monobasic potassium phosphate, pH 6.24) containing different amount of lysozyme as reported Table 3.2.

Table 3.2. Trehalose, mannitol and lysozyme weight ratio (relative to the solute) in the solutions used for the production of spray dried powders.

Powder	Trehalose-Mannitol (% w/w)	Lysozyme (% w/w)
5	48.75: 48.75	2.5
6	47.5:47.5	5
7	45:45	10
8	37.5:37.5	25
9	25:25	50
10	0:97.5	2.5
11	0:97.5	2.5

3.2.3 Thermogravimetric Analysis (TGA)

To determine the residual water content in the powders, a thermogravimentric analysis was performed using a TGA/DSC1 (Mettler Toledo, Switzerland). 2-6 mg of spray dried powder were placed inside a 100 µL alumina crucible and heated at a rate of 20° C/min from 25° C to 160° C under a stream of dry nitrogen (80 mL/min) inside a furnace. The mass loss, attributable to the residual moisture of the powders, was evaluated by determining the percentage change in weight as a function of the temperature.

3.2.4 Differential Scanning Calorimetry (DSC)

Differential scanning calorimetry (DSC) analysis was performed using a Mettler821e DSC model (Mettler Toledo, Ohio, USA) guided by a STARe software (Mettler Toledo, Switzerland)

The DSC traces were recorded by placing a quantity of powder between 4 mg and 6 mg inside a 40 µL aluminium crucible which was then sealed with a lid and pierced twice with a needle. The scans were performed between 25 and 280° C with a heating rate of 20° C/min under dry nitrogen flow (100 mL/min).

3.2.5 Water titration

A Karl-Fischer titrator, Mettler Toledo (model DL31), and a Hydranal-Composite 5 reagent were used for the analysis. Karl-Fisher titration is a volumetric titration of water.

The method consisted of a pre-titration, carried out automatically by the instrument, in which the solvent titration was carried out first and then the determination carried out by inserting in

the reaction vessel 25 mg of sample under magnetic stirring. The instruments gave automatically the water value in the sample.

3.2.6 Particle size distribution

Particle size distribution was performed using laser light diffraction as described in Chapter 1, Paragraph 3.2.2.2. Powders were dispersed in cyclohexane at the concentration of 1 % w/v in the presence of 0.1% w/v of Span 85 and sonicated for 3 min. Particle size distributions analysis for three dispersions of each powders were performed with an obscuration level of at least 10%.

3.2.7 *In-vitro* aerodynamic assessment

Preliminary deposition studies were carried out with FSI and RS01® (Plastiape, Italy) device as indicated in Chapter 1 and 2.

The aerodynamic diameter of the powder containing trehalose and mannitol was evaluated using the Next Generation Impactor (NGI, Copley Scientific UK).

The equipment was connected to a vacuum pump SCP5 (Copley, Scientific Ltd) and activated upon connection with the DPI. This latter was RS01® (Plastiape) with gelatin capsule (Coni-Snap® VI, size 3) filled with 30.0 ± 0.1 mg of powder. The flow rate was adjusted using a TPK Critical Flow controller (Copley Scientific, Nottingham, UK) at 60 L/min with a delivery time set at 4.0 seconds. Before starting the analysis, to ensure correct deposition of the powder and avoid rebound of particles [26], the first seven stages were filmed using a 2% w/v solution of Tween 20 in ethanol and were allowed to dry for 20 minutes to obtain the formation of a surfactant film. After actuation, the particles deposited in the Induction port, in the filter, in the

device (including the portion in the capsule) were collected using a volume of 10 mL of ultrapure water, while the powder deposited in each stage was dissolved in 5 mL of water. The filter was placed inside a crystallizer and put in an ultrasonic bath for about 5 minutes, the solution was then filtered with 0.45 μm cellulose acetate filters (VWR® International, USA). The solutions were subsequently analyzed by HPLC coupled to a refractive index detector, in order to quantify mannitol and trehalose obtained from the aerodynamic parameters.

3.2.8 High Performance Liquid Chromatography

A High Performance Liquid Chromatography (LC-10ATVP, Shimadzu Corp, Japan) system coupled to a refractive index detector (RID-10, Shimadzu Corp, Japan) was used for the quantification of trehalose and mannitol in the aerosolized samples. A Shodex OHpak SB-802.5 HQ size exclusion column was used as stationary phase, maintained at a temperature of 80° C, while ultrapure water at a flow of 1 mL/min was used as mobile phase, and a volume of 50 μL of sample was injected. A chromatographic run duration of 15 minutes was set. The peaks for trehalose and mannitol were overlapping, in fact both sugars elute at a retention time of about 10 minutes. The collected data were processed to obtain ED (Emitted dose), EF% (Emitted Fraction), FPD (Fine Particle Dose) and FPF% (Fine Particle Fraction) and Mass Median Aerodynamic Diameter, MMAD.

3.2.9 Powder X-Ray Diffraction (XRPD)

The X-ray diffraction patterns of the powders were obtained as described in Chapter 1.

The degree of crystallinity, C, was calculated for each sample using the following equation:

$$C = Rx \times 100 \qquad (3.1)$$

where *Rx* is the ratio between the area under the crystalline peaks and the total area (both areas calculated in a range 2θ 5-35°). The area under the baseline was previously subtracted to that under the crystalline peaks according to the method described by Sonneveld and Visser [143]. The areas were determined using the MiniFlex Rigaku software and the Integral Intensity Calculation program.

3.2.10 Scanning Electron Microscopy (SEM)

The morphology and surface characteristics of the spray dried particles were evaluated by Scanning Electron Microscopy with the procedure described in Chapter 1.

3.2.11 Dynamic Vapor Sorption (DVS)

Dynamic moisture absorption/desorption patterns were carried out on spray dried powders with the procedure described in Chapter 1with the following different details: about 50 mg of powder were weighed and analyzed at 25° C by in the 5-90% RH range (step size = 20% RH). The transition from one step to the next occurred when the percentage of weight variation was less than 0.0010% and, in any case, not before 30 minutes from the start of each step.

4 Results and discussion

4.1 Powders without enzyme

The data relevant to the yield and residual water content of the powders produced by spray with inlet temperature of 130° C and 1 mm nozzle diameter to select the combination of components are reported in Table 3.3. The yield % of these formulations was calculated as the ratio between the weight of the powder obtained upon spray drying process, and the total quantity of powder dissolved in the starting solution. The residual moisture content was determined by Karl Fischer titration.

Table 3.3. Percentage yield values (Recovered powder from SD), in weight ratio, of the solutions containing sugars dried by spray drying.

Sample	Composition (% w/w)	Yield (% w/w)	Water content (% w/w)
1	Trehalose	43.75	8.78
2	Trehalose-Raffinose (50:50)	57.87	5.44
3	Trehalose-Mannitol (50:50)	33.63	2.72
4	Trehalose-Mannitol (75:25)	0	-

The solution with an equiponderal amount of trehalose and raffinose gave the highest yield. No dried powder (yield equal to zero) was obtained in the case of sample n. 4, as this solution led to the formation of particles that crystallized quantitatively on the walls of the cyclone and could not be recovered in the collector. Trehalose alone or a combination with raffinose (50:50) led to powders that were not really dry. This observation suggested that the high yield of the powders obtained from sample 1 and 2 could be ascribed to the incomplete drying. The water content in the powder containing trehalose-mannitol (50:50) was instead indicative of a correct

drying.

The powders were then analyzed by DSC in order to put into evidence any possible change of the solid-state characteristics compared to the starting material.

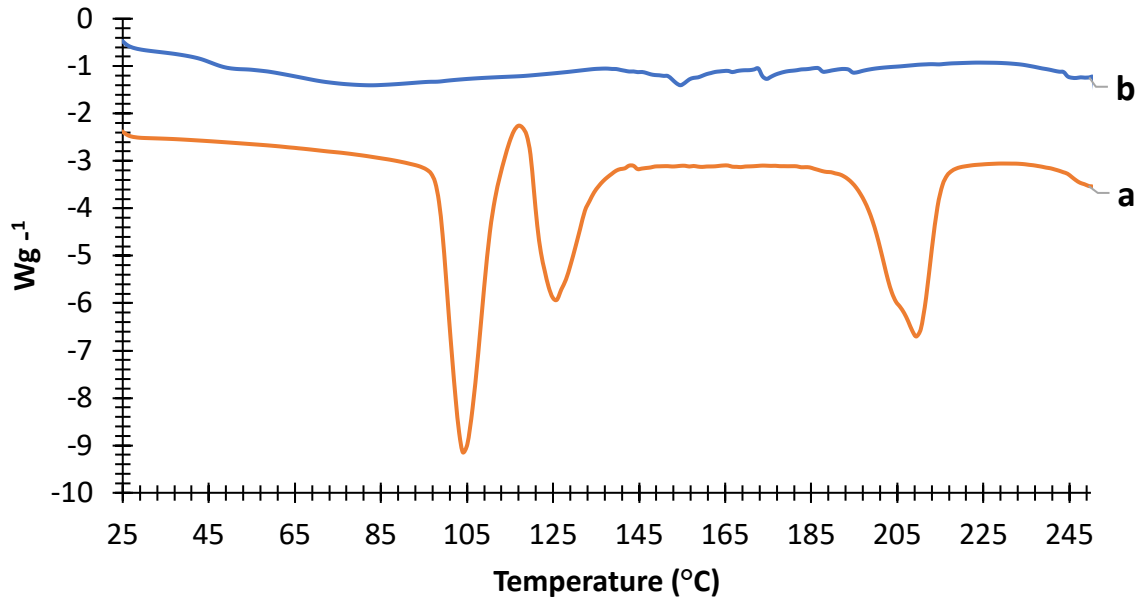

Figure 3.1. DSC traces of the trehalose powders before and after the spray drying process (a) Trehalose dihydrate starting material; (b) Spray dried trehalose.

Figure 3.1 reports the DSC traces of the trehalose starting material and spray dried powder. As for the starting material a first complex thermal event was observed between 80 and 145 °C: an endothermic peak at 105 °C followed by a small exothermic one and a second endotherm at 125° C. These phenomena are attributed to the loss of water of crystallization of the dihydrate form which represents the thermodynamically stable solid phase at standard conditions. A further endothermic event, interpreted as the final melting peak was recorded at 209 °C. The thermal analysis of trehalose powder obtained after the spray drying process suggested an amorphous solid state: no significant thermal events were recorded except a broad and slightly evident endotherm between 35 and 140 °C that was attributed to the evaporation of the residual

moisture on the powder surface.

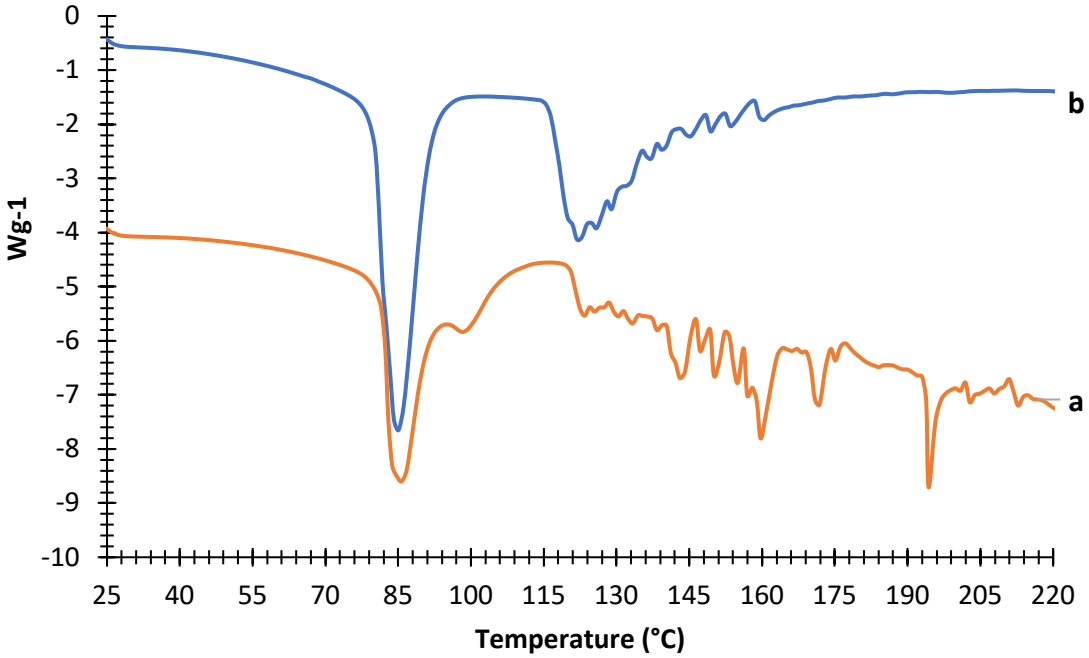

Figure 3.2. DSC traces of the trehalose dihydrate and raffinose physical mixture (50:50) (a), raffinose as a raw material (b).

Raffinose powder as raw material (Figure 3.2) showed a melting peak around 85° C followed by a marked decomposition above 120 °C. The trace of the physical mixture of trehalose-raffinose 50:50, w/w showed the presence of an endothermic peak attributable to the melting of raffinose at 85° C, then another around 100° C suggesting the dehydration of trehalose followed by a marked decomposition signal.

Figure 3.3 reports the traces of the trehalose-mannitol physical mixtures 75:25, 50:50 and also 25:75 weight ratio. Signals of thermic events relevant to the relevant transition proportional to the relative ratio of each component in the powder mixture were recorded. Only a very small shift toward lower melting temperature was recorded for mannitol, likely due to the presence of the molten trehalose. The absence of specific interaction between the sugar and the sugar alcohol was confirmed by the data of Figure 3.4 that reports the linear decrease of the melting

enthalpies of each component with the decrease of percentage of the component in the mixture.

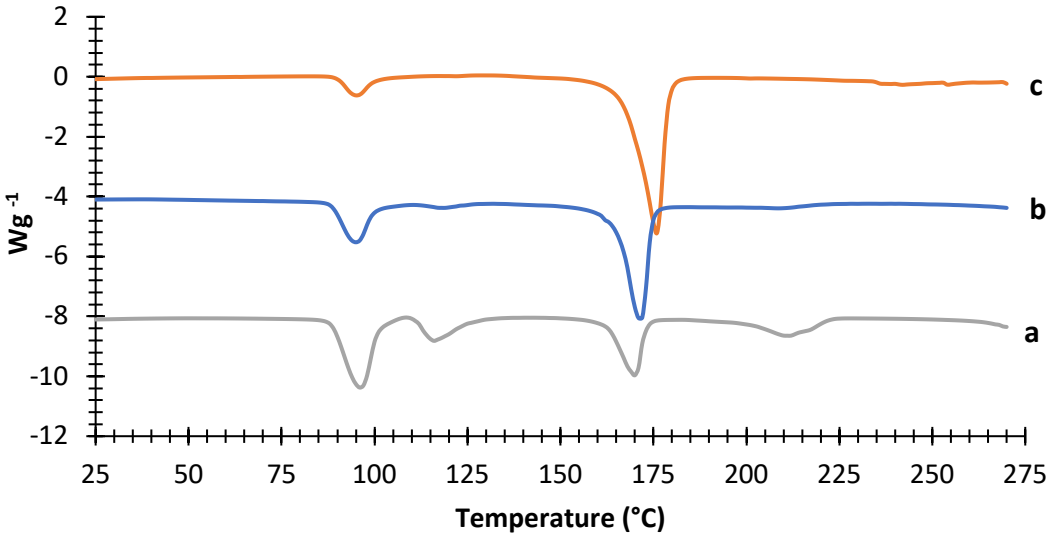

Figure 3.3. DSC trace of the physical mixtures trehalose-mannitol in the ratio 75:25 (a), 50:50 (b), 25:75 (c) w/w.

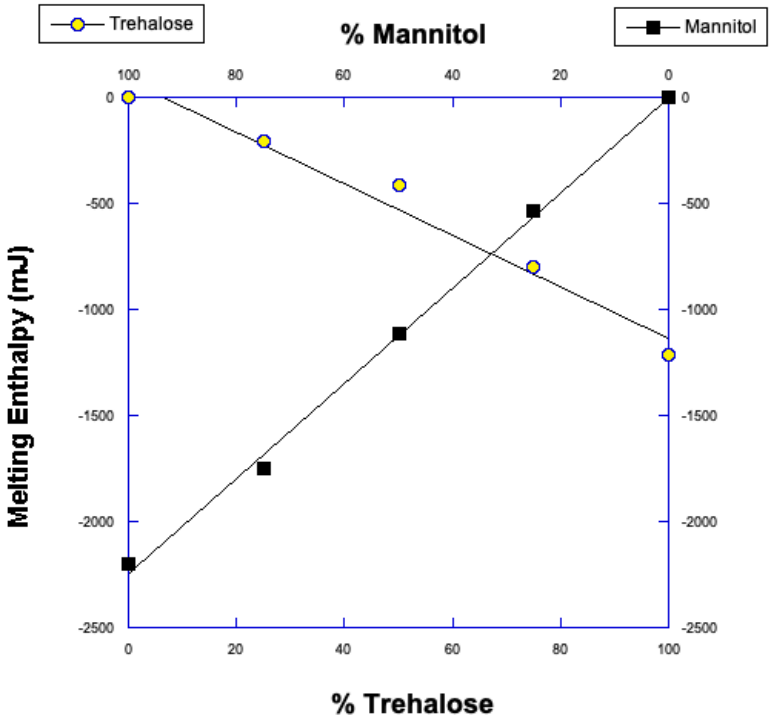

Figure 3.4. Melting enthalpy of mannitol-trehalose mixture

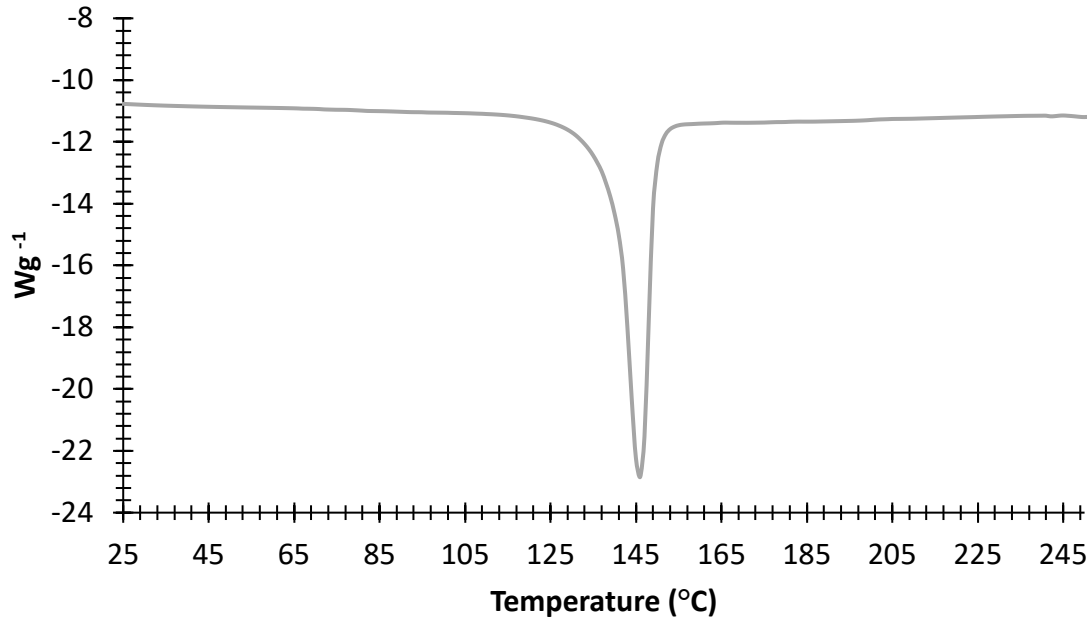

Figure 3.5. DSC trace of the spray dried powder trehalose-mannitol 50:50.

Unlike the corresponding physical mixture (Figure 3.3), the DSC for the powder containing trehalose and mannitol, obtained by spray drying (Figure 3.5), shows a single endothermic peak at 146° C attributable to the melting of mannitol suggesting two consideration: trehalose solidified in this powder as an amorphous phase following the spray drying process while mannitol crystallized as low melting δ form; the melting temperature was also in this case shifted toward a lower value as a consequence of the presence of a second component already in liquid form.

The aerodynamic performance of the first three powders was preliminary assessed through the Fast Screening Impactor (FSI). The obtained data are reported in Table 3.4.

Table 3.4. Aerosolization parameters of powders n. 1-3. FPF was expressed as a percentage of the emitted dose. Mean value ± standard deviation (n=3).

Powder	Emitted Dose (mg)	Emitted Fraction (%)	FPD (mg)	FPF (%)
Trehalose (1)	8.32 ± 0.47	83.04 ± 0.05	0.2 ± 0.1	2.45 ± 0.01
Trehalose - raffinose 50:50 (2)	7.31 ± 0.75	72.93 ± 0.08	1.4 ± 0.1	19.22 ± 0.03
Trehalose - mannitol 50:50 (3)	7.46 ± 0.70	74.79 ± 0.07	2.7 ± 0.17	36.25 ± 0.01

Whereas spray dried trehalose powder gave rise to a slightly higher Emitted Fraction (EF > 70% in all cases), the trehalose-mannitol-based powder (50:50, w/w) resulted in a significantly higher FPF.

For this reason, the trehalose-mannitol 50:50 composition was selected to study and optimize the effects of process variables on the powder physico-chemical and aerodynamic characteristics.

4.2 Optimization of process parameters

For the optimization of the process parameters the drying temperature, the atomization air flow and the diameter of the nozzle were varied.

The yield values of the powders obtained after the spray drying are reported in Table 3.5 and Table 3.6 as a function of the combination of the above three parameters.

Table 3.5. Yield values, in weight ratio, as function the drying variables using a 1.4 mm diameter nozzle in mannitol and trehalose powders 50:50 w/w.

Inlet Temperature (°C)	Nozzle diameter (mm)	Atomization air flow (L/h)	Yield (%)
110	1.4	601	39.6
120	1.4	601	21.1
130	1.4	601	22.7
130	1.4	473	38.0

Table 3.6. Yield values, in weight ratio, as a function of the drying variables using a 0.5 mm diameter nozzle in mannitol and trehalose powders 50:50 w/w.

Inlet Temperature (°C)	Nozzle diameter (mm)	Atomization air flow (L/h)	Yield (%)
90	0.5	473	45.9
100	0.5	473	40.6
110	0.5	473	37.5
130	0.5	473	35.3
140	0.5	473	29.1
110	0.5	601	31.1
130	0.5	601	31.3
140	0.5	601	13.5

A decrease in atomization air flow, at the same temperature and size of the nozzle led to higher yield values, while the inlet temperature at fixed atomization air flow affected the yield negatively. Finally, at fixed nozzle diameter and atomization air flow, the yield was inversely related the temperature.

4.3 Particle size distribution of powders

The particle size distribution of the powder produced in the optimization phase is reported in Table 3.7 and figure 3.6. for the powders prepared with a 0.5 mm nozzle and 473 L/h atomization air flow.

Table 3.7. Size distribution of mannitol-trehalose powders obtained by drying at different temperatures using a 0.5 mm nozzle and 473 L/h atomization air flow.

Inlet Temperature (°C)	Dv(10)	Dv(50)	Dv(90)
90	1.97	8.49	18.43
100	2.22	11.62	27.12
110	2.59	15.27	44.61
130	2.43	14.22	46.81
140	3.36	23.86	75.58

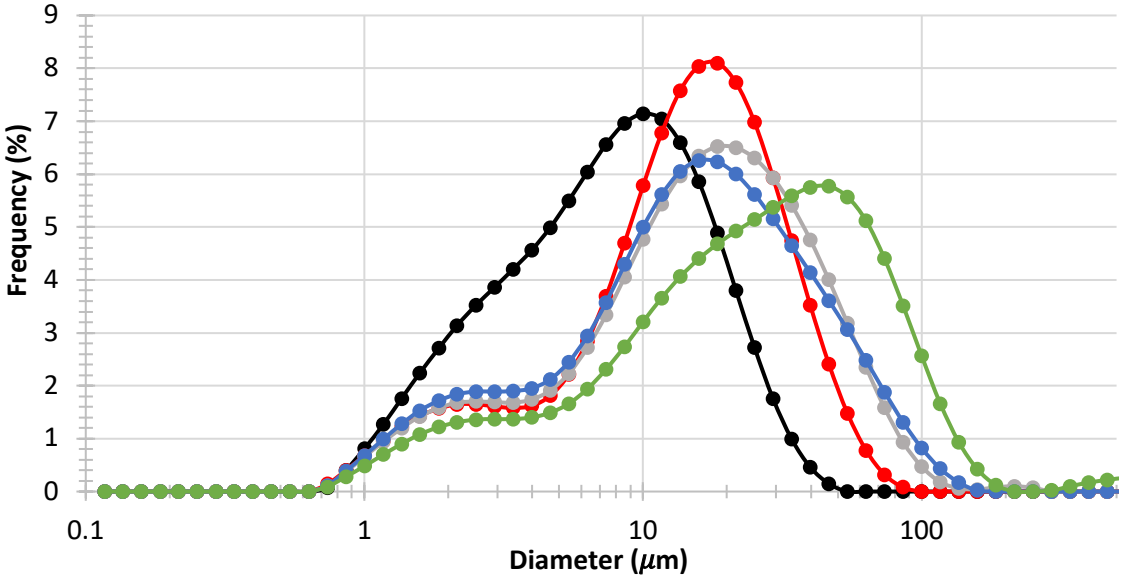

Figure 3.6. Particle size distribution curves of mannitol-trehalose powders dried at different temperatures with 0.5 mm nozzle and 473 L/h atomization air flow: black curve powder dried at 90° C; red curve powder dried at 100° C; gray curve powder dried at 110° C, blue curve powder dried at 130° C; green curve powder dried at 140° C.

A progressive increase in the particle size was observed with the increase in the drying temperature.

The data in Figure 3.6, show for all inlet temperatures, the presence of two populations of particles, one centered around 2 µm and the other between about 10 and 40 µm depending on the inlet temperature.

Table 3.8 and Figure 3.7. show the data relevant to mannitol and trehalose powders prepared with a 1.4 mm nozzle and both aspirations.

Table 3.8. Particle size distribution of powders using a 1.4 mm nozzle and atomization air flow at 601 and 473 L/h.

Inlet Temperature (°C)/ atomization air flow (L/h)	**Dv(10) µm**	**Dv(50)µm**	**Dv(90)µm**
110°C/601	3.01	18.06	52.29
120°C/601	2.49	12.7	32.97
130°C/601	7.06	38.16	91.0
130°C/473	2.68	15.68	48.8

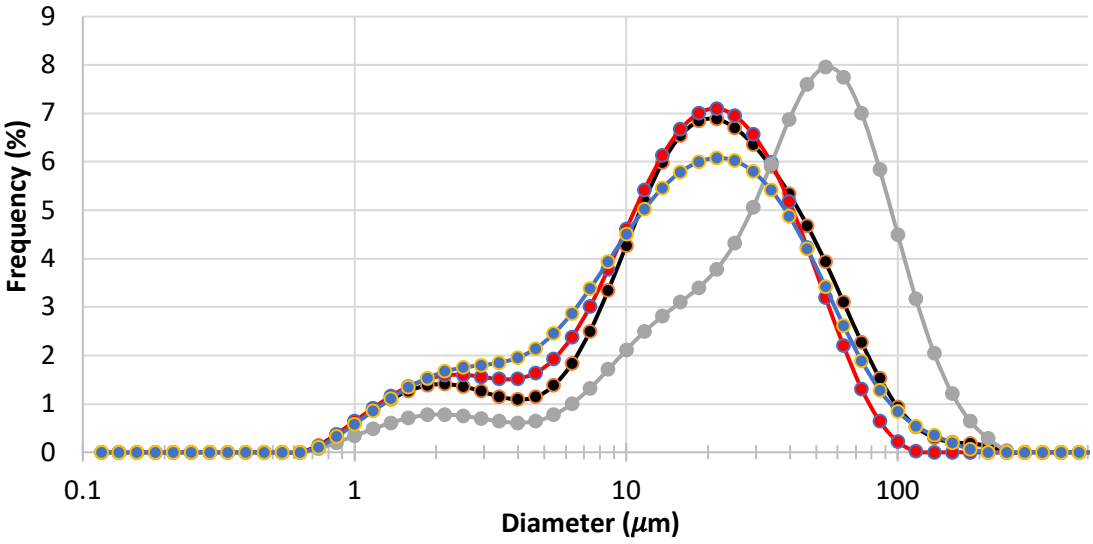

Figure 3.7. Particle size distribution curves of mannitol-trehalose powders with nozzle 1.4 mm: black curve powder dried at 110° C; red curve powder dried at 120° C; gray curve powder dried at 130° C with higher atomization air flow; blue curve powder dried at 130° C lower atomization air flow.

In this second case, no clear correlation between particle size distribution and inlet temperature with the same aspiration was found. With different aspiration at the same temperature, the value of the volumetric diameter decreased with the reduction of aspiration. Again, the presence of two particle populations was observed.

The presence of these double population of particles prompted the execution of further image analyses through scanning electron microscopy to evaluate the particle morphology and the possible presence aggregates.

4.3.1 SEM analysis

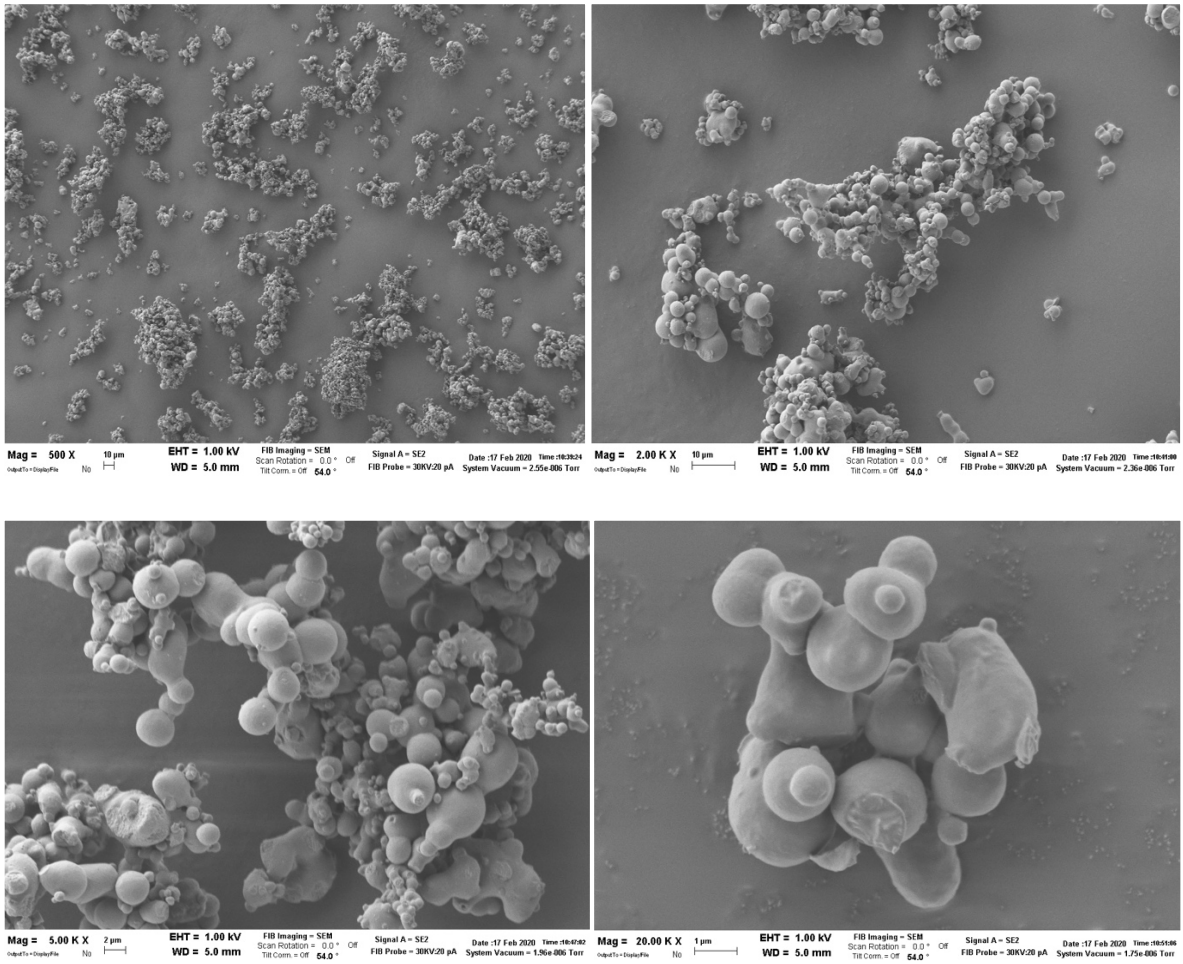

Figure 3.8. SEM pictures of the powder c trehalose-mannitol obtained at 90 °C using a 0.5 mm nozzle and atomization air flow 473 L/h.

As an example, the picture taken at different magnification of the particles obtained by spray drying at inlet temperature of 90 °C, a 0.5 mm nozzle and atomization air flow 473 L/h are reported in Figure 3.8. The particles appear as aggregates with overall dimensions greater than 10 μm of smaller spherical particles of about 1 μm diameter.

A similar situation was observed with all the prepared powders as shown as a further example in Figure 3.9 that reports the SEM picture recorded for the powder obtained at 120 °C inlet temperature, 1.4 nozzle diameter and 473 L/h atomization air flow.

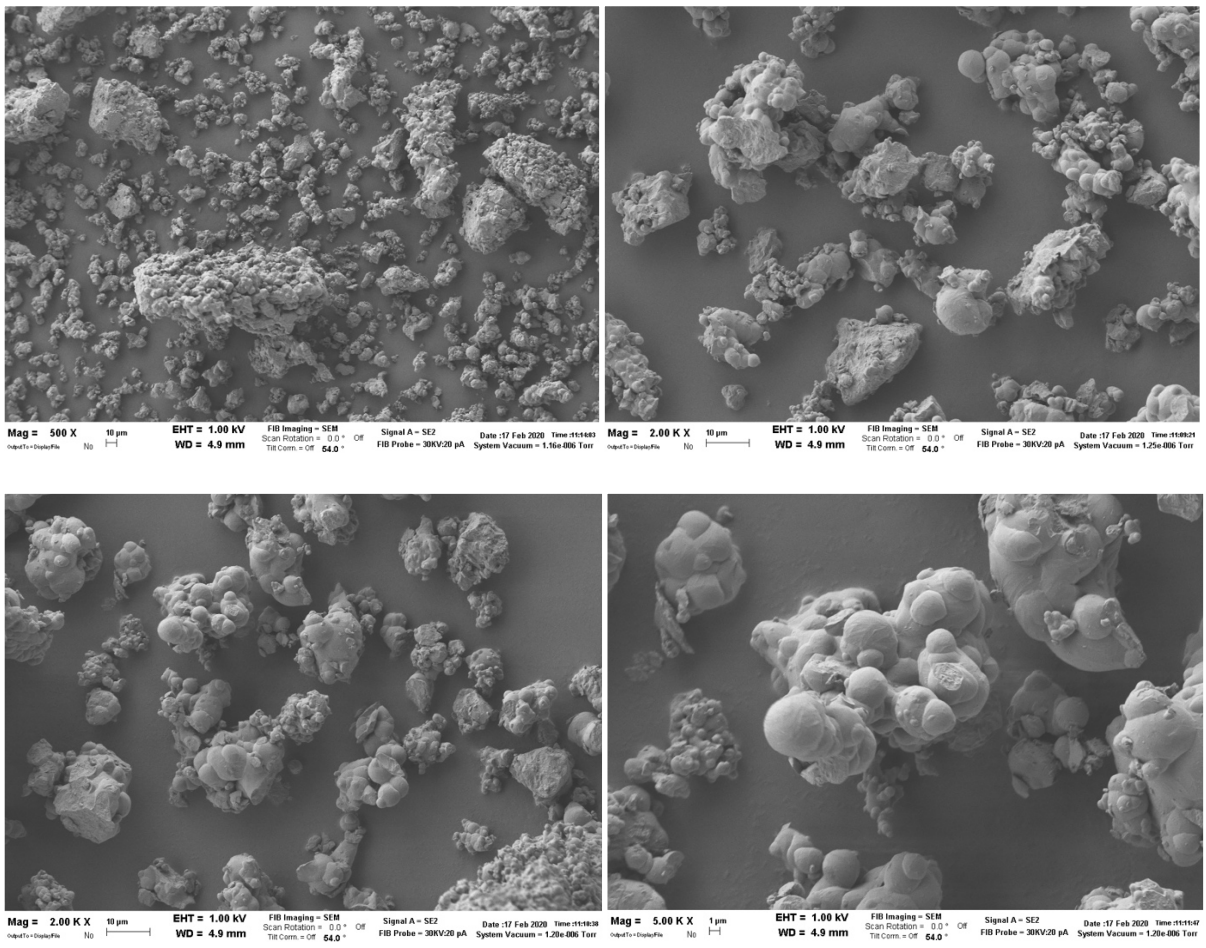

Figure 3.9. SEM picture of the powder trehalose-mannitol obtained at 120° C using a 1.4 mm nozzle and atomization air flow 473 L/h.

In general, the powders obtained with a 0.5 mm diameter nozzle and atomization air flow at 473 L/h appeared to be more consistent and more suitable in terms of particle size distribution and shape as powder for inhalation. For this reason, they were selected to carry out *in vitro* aerosolization tests.

4.3.2 In vitro aerosolization test

The evaluation of the aerodynamic behavior was carried out with a Next Generation Impactor, delivering approximately 30.0 mg of powder, as said, dried at 90, 100, 110, 130 and 140 °C obtained with a 0.5 mm diameter nozzle and atomization air flow at 473 L/h . After dispensing, the powder was collected by washing the stages with ultrapure water and analyzing the solutions using HPLC-RID. The amount of powder deposited on each stage was quantified from the area of the chromatographic peak at an elution time of 10 minutes. For the analysis a column with size exclusion was used as the stationary phase, consequently it was not possible to obtain a separation of the individual peaks of mannitol and trehalose as these sugars have molecular weights that are not sufficiently different to be distinguished.

The percentage deposition in the various stages of the impactor is presented in Figure 3.10.

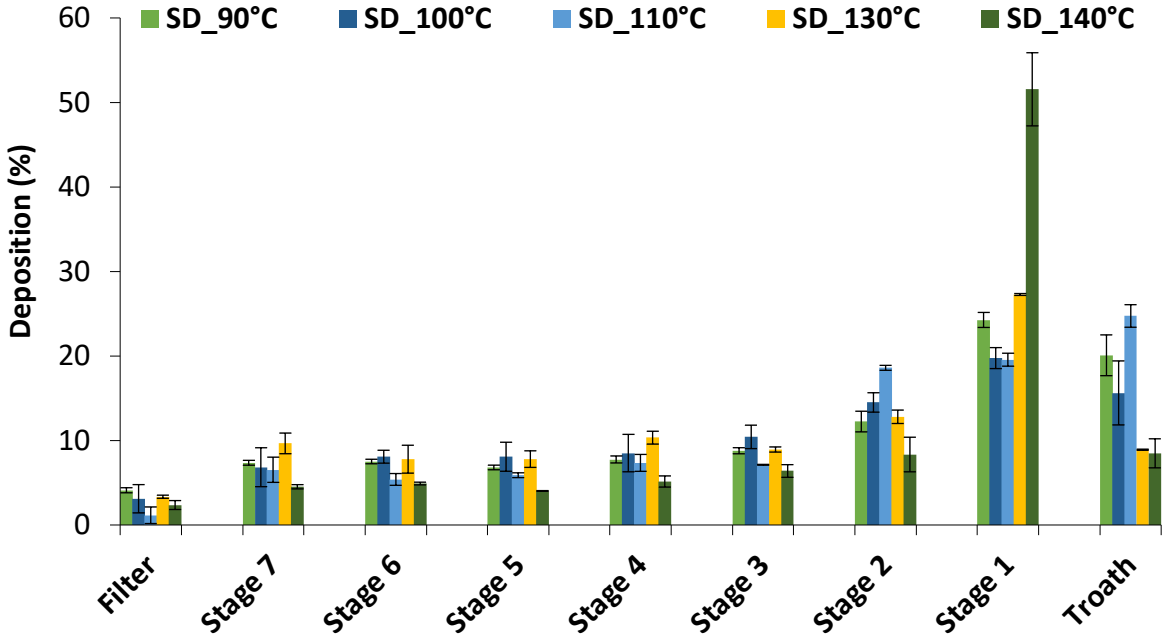

Figure 3.10. Percentage distribution of the powder trehalose-mannitol, obtained at different temperatures, in the various parts of the Next Generation Impactor.

The data in Figure 3.10 were transformed into a cumulative undersize distribution, taking into account the cut-off between one stage and the following, and subsequently processed by transforming the distribution into log-probit scale (probability% *vs* logarithm of the size). The Mass Median Aerodynamic Diameter (MMAD) was calculated from the median value of the distribution (Table 3.9).

Table 3.9. Aerodynamic parameters (EF%, FPF and MMAD) of mannitol-trehalose powders obtained by spray drying at different inlet temperatures using a 0.5 mm nozzle and 473 L/h atomization air flow. Mean values ± standard deviation.

Inlet Temperature	Emitted fraction (%)	MMAD (μm)	FPF (%)
90°C	92.98 ± 2.13	2.90 ± 0.01	66.95 ± 0.52
100°C	93.40 ± 1.93	3.66 ± 0.16	44.66 ± 0.43
110°C	96.33 ± 2.07	2.92 ± 0.15	53.50 ± 2.77
130°C	89.34 ± 0.27	3.65 ± 0.99	45.64 ± 4.66
140°C	87.84 ± 1.37	6.77 ± 0.16	36.10 ± 4.40

The Emitted dose % was in all cases close or higher than 90% indicating that almost all the loaded powder was aerosolized. Smaller MMAD was obtained at lower inlet temperatures; the respirability as expressed by the FPF paralleled the MMAD behavior. Interestingly, MMADs were in all cases lower than the geometric diameters determined by laser diffraction (Table 3.7) indicating a particularly low density of particle that was ascribed to the particle aggregation observed with the SEM analysis.

4.3.3 X-Ray Powder Diffraction

Through X-ray diffractometry it was possible to obtain information on the crystalline or amorphous structure of the powders produced at different inlet temperatures.

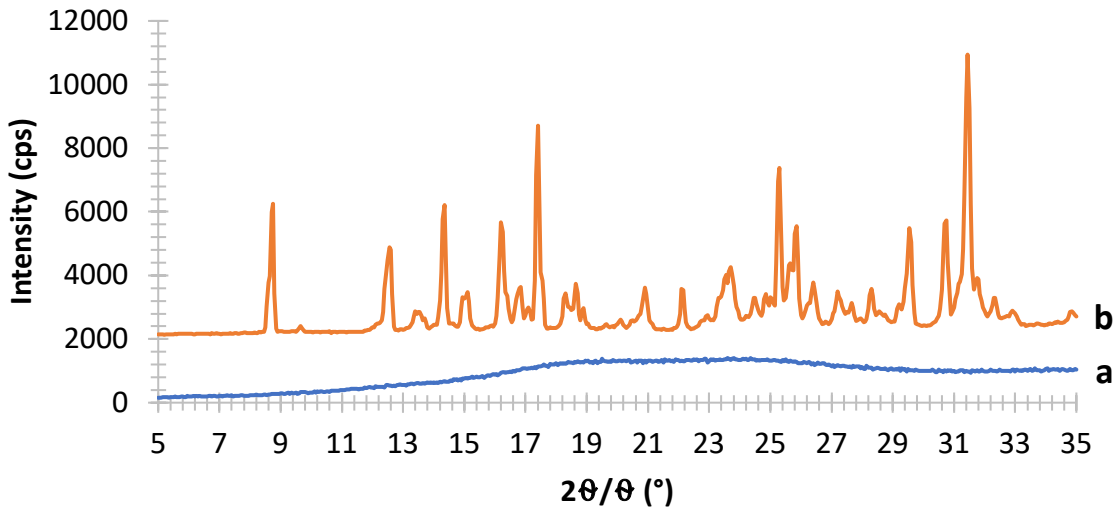

Figure 3.11. X-ray diffraction pattern of the trehalose powders before and after the spray drying process: trehalose dihydrate starting material (b) and spray dried powder obtained with an inlet temperature of 130° C, 1 mm nozzle and 601L/h atomization air flow (a).

Figure 3.11. reports the PXRD patterns of trehalose starting material and spray dried powder. It can be seen that the spray dried powder did not present any diffraction peak and presented only the typical halo of the amorphous phases were recorded. This data confirms what already observed by DSC (Figure 3.12).

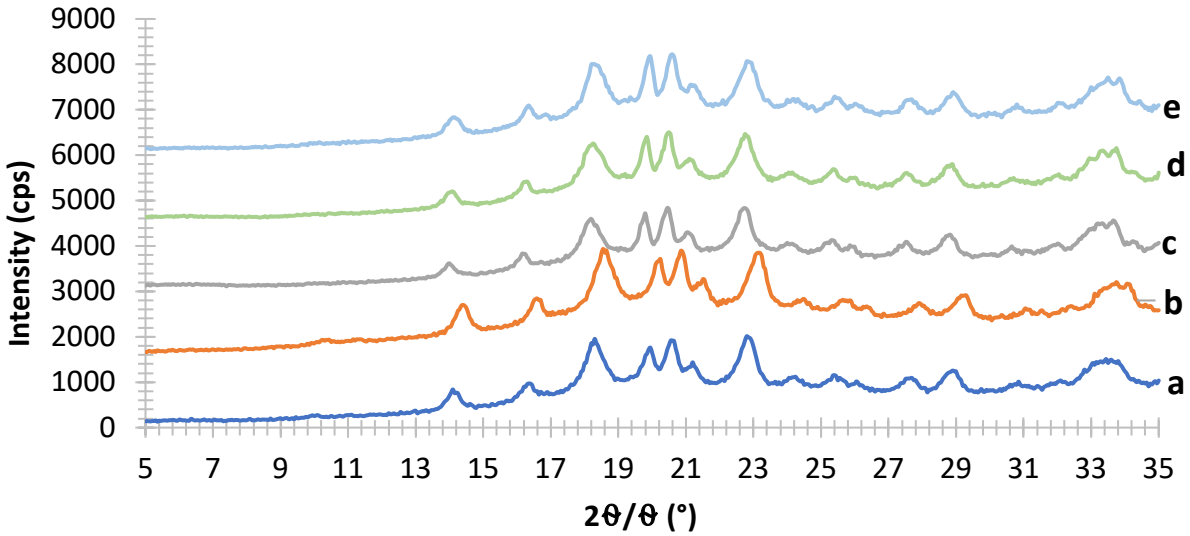

Figure 3.12. X-Ray diffraction patterns of mannitol-trehalose powders obtained by spray drying at different drying inlet temperatures with a 0.5 mm nozzle and 473 L/h atomization air flow. 90°C (a), 100°C (b), 110°C (c), 120°C (d), 130°C (e).

Figure 3.12 reports the diffraction patterns of the trehalose-mannitol powders obtained at different inlet temperatures. It can be observed that the drying temperature did not affect the structure of the solid state of these powders, being the diffraction patterns substantially superimposable peak resolution was poor due to the coexistence of an amorphous phase of trehalose (as also indicated by the DSC analysis, Figure 3.5) that determined a shift of the baseline; the small and poorly resolved peaks detected at 14.8°, 17.05°, 18.95°, 20.6°, 21.25°, 21.9° and 23.5° *2theta*, were ascribed to the presence of traces of the β form, differently to what observed for the powder analyzed by DSC (Figure 3.5) that was, however obtained with higher aspiration rate and a larger nozzle.

The degree of crystallinity for each powder was then calculate according to equation Eq 3.1. The obtained data are reported in Table 3.10. It is possible to notice how the degree of crystallinity decreased significantly, compared to the starting material, in all the powders obtained by spray drying. This analysis confirmed the fact that the trehalose spray dried powder was mainly in amorphous form, while the powders containing trehalose-mannitol had similar degree of crystallinity (between 16 and 19%) irrespectively of the inlet temperature of the spray dying process adopted.

Table 3.10. Degree of crystallinity of raw material trehalose powder and trehalose-mannitol (50:50) physical mixture or spray dried powders.

Carrier	Inlet Temperature (°C)	Nozzle diameter (mm)	Atomization air flow (L/h)	Crystallinity (%)
Trehalose dihydrate	-	-	-	57.40
Trehalose SD	130	1	473	4.4
Trehalose-Mannitol physical mixture	-	-	-	49.10
Trehalose-Mannitol	90	0.5	473	17.20
Trehalose-Mannitol	100	0.5	473	16.22
Trehalose-Mannitol	110	0.5	473	19.20
Trehalose-Mannitol	120	0.5	473	17.5

4.3.4 Dynamic Vapor Sorption

The mannitol-trehalose powders obtained by spray drying were tested in isothermal conditions by exposing them to increasing relative humidity followed by a corresponding decrease.

The isothermal graphs obtained from the DVS analyses are shown in Figure 3.13 in comparison with that of spray dried trehalose. As for this latter, it is possible to observe the powder absorbed the humidity in a liner manner up to 60% RH. Thereafter, it stabilized keeping a weight gain of about 9.2 % relative to the initial value even upon humidity decrease, indicating the complete transformation into the stable dihydrate form (theoretical water content in the dihydrate crystal 9.5%). The trehalose-mannitol powders showed different behavior depending on the inlet temperature at which they were dried. The powders produced at lower inlet temperature (90 and 100 °C) rapidly gained weight from 0 to 40 % RH reaching a value of about 4.6 % that was kept upon the humidity returned to zero. This figure is exactly the half of that recorded for trehalose alone and indicate the complete transformation of trehalose into the

dihydrate form. For the powder produced at higher inlet temperature (110, 120 and 130 °C) the weight gain occurred in a larger RH interval and afforded a final value ranging from 2.5 and 4.4 %, indicating a non-complete transformation of the trehalose that constituted half of the mass of the powder.

The DSC traces of the powder produced at 90 °C were recorded before and after DVS analysis (Figure 3.14). Before DVS, the melting temperature of mannitol was lower than that usually recorded for the thermodynamically stable β form that, according to the PXRD analysis (Figure 3.12) represented the crystal phase of these powders: an onset at 143.03 °C while the peak of 156.02 °C was in fact observed. After DVS the double peak relevant to trehalose dehydration appeared at 105-130 °C, while the melting temperature of mannitol remained at the onset temperature of 142.16 °C with the peak at 155.6 °C. This phenomenon was not observed in the physical mixture as shown in Figure 3.3 and 3.4 but confirmed what already reported in Figure 3.5 for the spray dried powder. There are no references in literature about this phenomenon that, for this reason deserves further investigation.

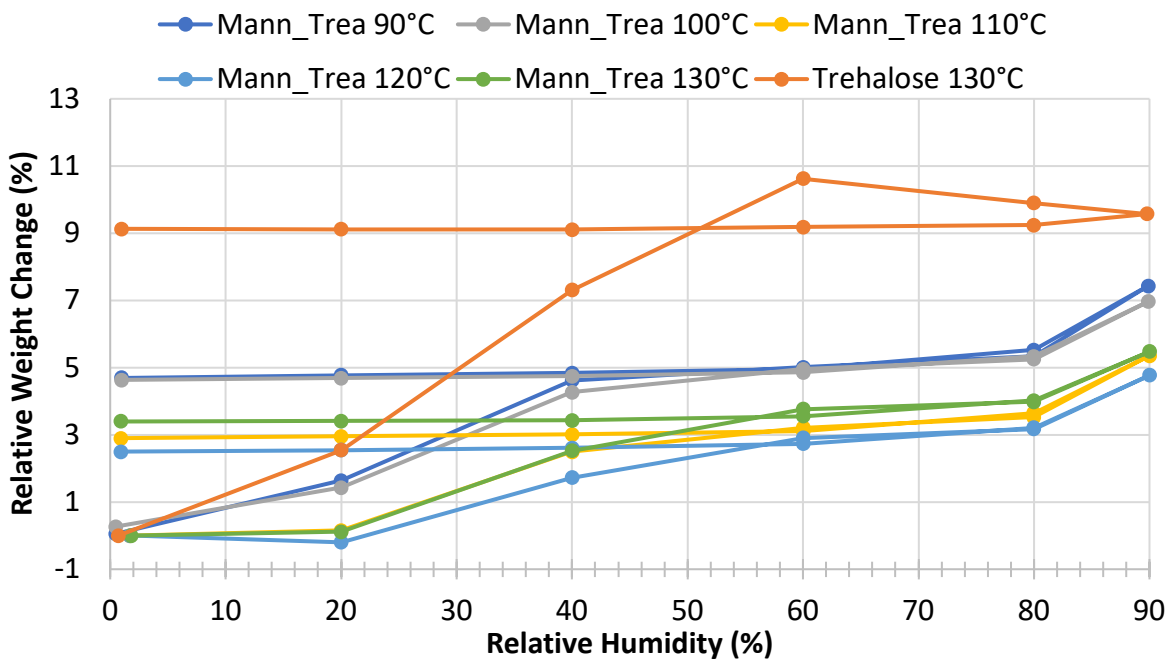

Figure 3.13. DVS profiles of powders obtained after spray drying, recorded at 25 °C in the 0-90% RH range.

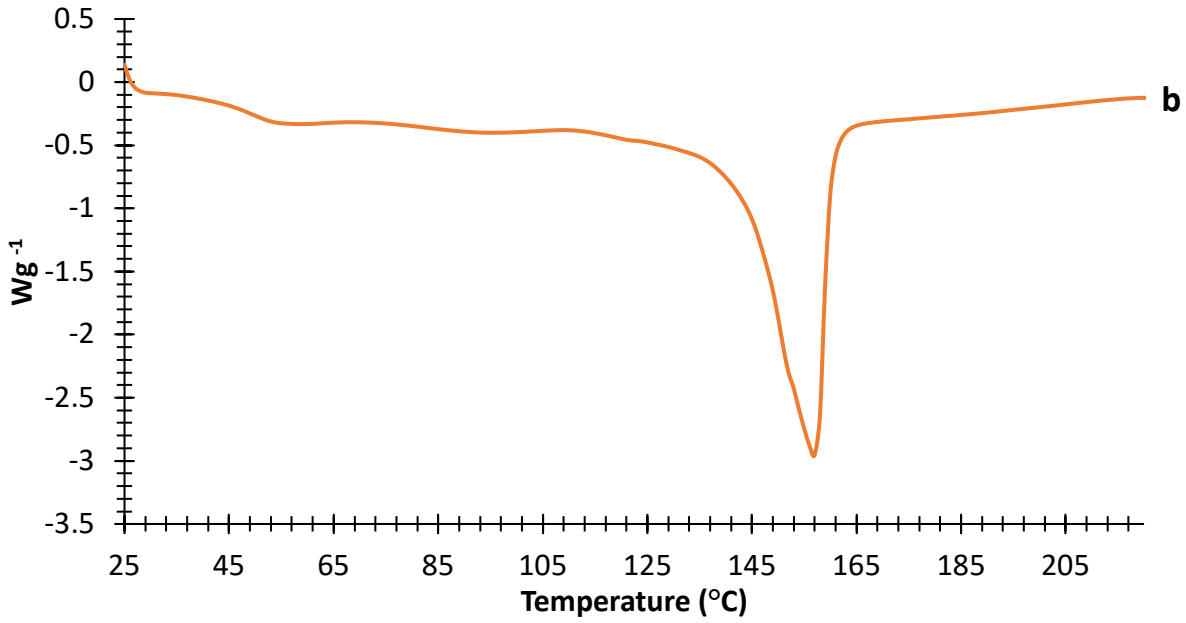

Figure 3.14. DSC trace for mannitol-trehalose powder obtained by spray drying at inlet temperature of 90 °C (b); after DVS analysis (a)

Another interesting result emerged after 10 months storage of this powder in a desiccator at the ambient temperature. Figure 3.15. No peak relevant to trehalose were observed indicating no or at least negligible transformation. This result is in agreement with those reported in the study of Hulse and co-workers [1], [76], although that perhaps did not refer a equiponderal combination of mannitol-trehalose.

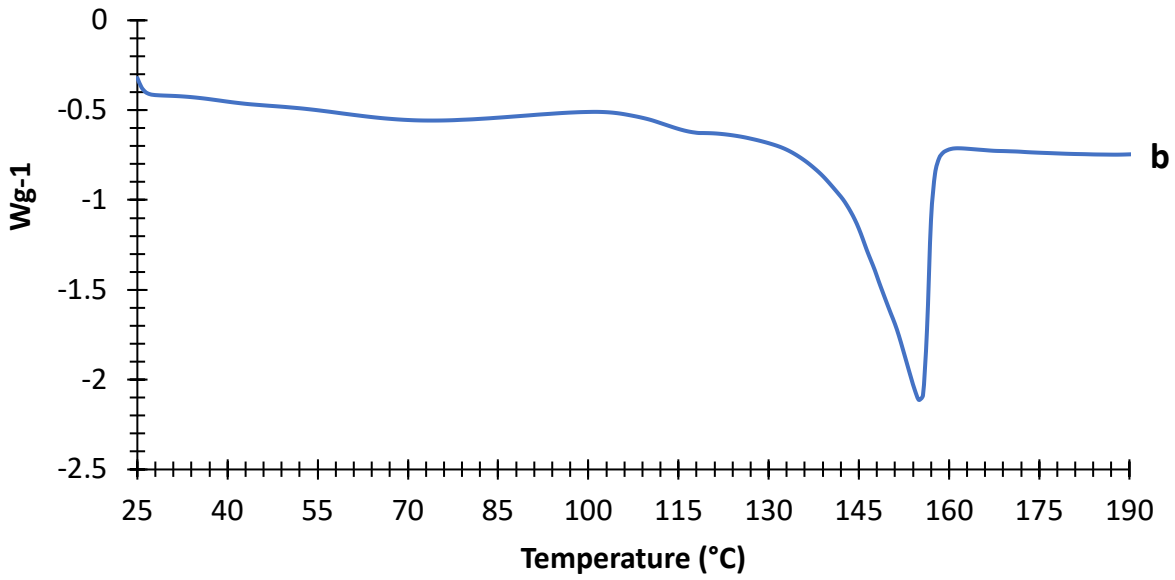

Figure 3.15. DSC trace for mannitol-trehalose powder obtained by spray drying at 90 °C stored for 10 months in desiccator at ambient temperature.

4.4 Lysozyme as a protein candidate for new carrier

Although the mannitol trehalose powders produced at inlet temperature higher than 110 °C appeared to be more stable, the powder produced at 90 °C was the best performing in terms of aerosolization. Moreover, the lower temperature is more appropriate for the drying of protein-containing solutions. Therefore, this temperature was selected (along with nozzle diameter 0.5 mm and atomization air flow 473 L/h) for the spray drying production of the lysozyme-containing powder using equiponderal amount of mannitol and trehalose as carrier. Lysozyme was mixed with the carrier in different weight ratios as reported in Table 3.2. and Table 3.11. 400 mg of powder was weighted and dissolved in 20 mL aqueous solution (18mL H_2O dissolving the carrier and 2mL reaction buffer dissolving the protein).

Table 3.11. Nominal composition and process yield of the lysozyme containing spray dried powder

Powder	Carrier (%)	Protein (%)	Yield (%)
5	Trehalose-Mannitol (48.75: 48.75)	Lysozyme (2.5)	22.52
6	Trehalose-Mannitol (47.5:47.5)	Lysozyme (5)	-
7	Trehalose-Mannitol (45:45)	Lysozyme (10)	-
8	Trehalose-Mannitol (37.5:37.5)	Lysozyme (25)	24.01
9	Trehalose-Mannitol (25:25)	Lysozyme (50)	14.02
10	Mannitol (97.5)	Lysozyme (2.5)	27.52
11	Mannitol (75)	Lysozyme (25)	29.59

The yield of the spray drying process for the different powders is reported in Table 3.11. Compared to the yield of mannitol-trehalose powders without the protein (45.9%, Table 3.6),

the formulations afforded lower yield with maximum values lower than 30%. Formulation 6 and 7 did not even afforded any powder in the collector of the spray drier. The higher yields were obtained with formulation 10 and 11 that were prepared without trehalose for comparison purpose.

4.4.1 Lysozyme activity

The lysozyme activity was measured in powders 5, 8, 10 and 11 according to the method described in paragraph 3.2.12.

To calculate the activity per mL (IU/mL) of each sample, the following formula was applied:

$$IU/ml = \frac{(\Delta A_{450}/min\ sample - \Delta A_{450}/min\ blank) \times (dilution\ factor)}{0.001 \times (volume\ sample)} \qquad (3.2)$$

Where ΔA_{450} is the difference between the value of absorbance at time zero and the value of absorbance at the selected time point which is in this case 5 minutes.

Since the concentration of the sample was known, the specific activity calculated with the following formula:

$$Specific\ activity(IU/mg) = \frac{International\ Unit/mL}{Sample\ concentration\ (mg/mL)} \qquad (3.3)$$

The obtained results are reported in Table 3.12 while Figure 3.21 depicts the variation of absorbance over time in comparison to the Blank and the Control.

Table 3.12. Activity of lysozyme-containing powders and Control.

Powder	*International Unit/mL*	*Specific activity (IU/mg)*
Control	40410	40410
5	34780	34780
8	36199	36199
10	33842	33842
11	34457	34457

Powder 8 showed the highest activity due to the higher protein content.

All powders, in particular the trehalose-mannitol containing the lower amount of lysozyme (powder 5) and the two powders of mannitol at high and low concentration of the enzyme (powder 10 and powder 11 respectively) presented a degradation kinetics that was slower compared to that that of the Control (Figure 3.16).

In particular, for powder 5 the presence of an amorphous domain may have been beneficial for lysozyme activity. This feature appeared to be related to the enzyme concentration as this effect was observed at a lower extent for powder n. 8 containing the highest lysozyme concentration, which, nevertheless, proved to be able to keep the enzyme activity at a level high enough. This finding is in agreement with data reported by Hulse et. Al. [76], who stated that the use an excipient with high glass transition temperature such as trehalose in inhalation formulations stabilize the functions of proteins during storage due to the contribution of the amorphous phase.

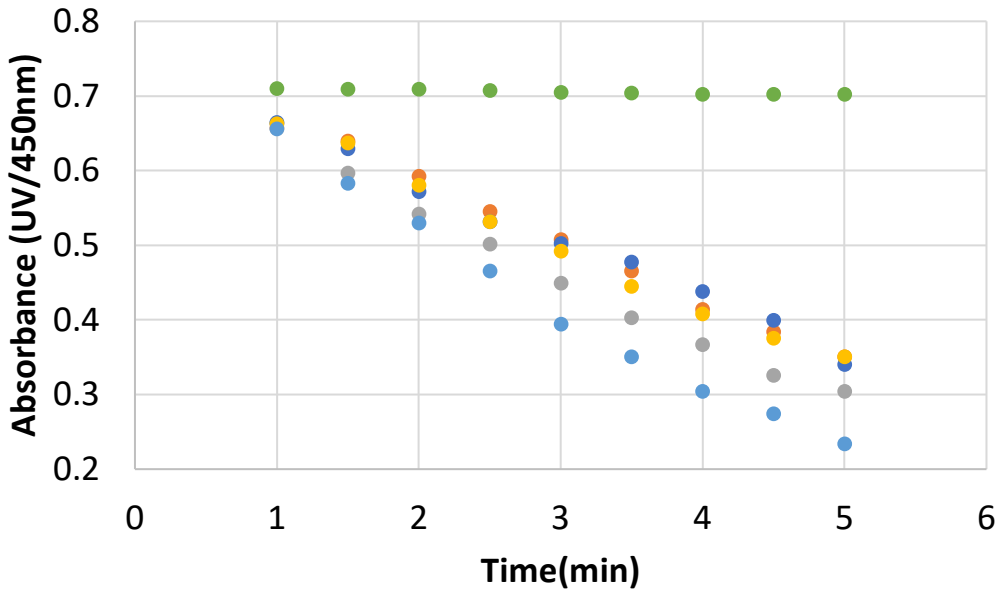

Figure 3.16. Variation of Absorbance during the lysozyme activity assay for powder produced by spray drying. Powder 5 orange bullet; powder 8 grey bullet; powder 10 deep blue bullet; powder 11 yellow bullet; Control light blue bullet; Blank green bullet.

4.4.2 In-vitro aerodynamic assessment

The evaluation of the aerodynamic behavior of these powders was carried out via Next Generation Impactor, delivering approximately 15 mg of dried powder. After dispensing, the powder was collected by washing the stages with ultrapure water and analyzing by UV spectrophotometry at 280nm wavelength.

The percentage deposition data in the various stages of the impactor are shown in Figure 3.17.

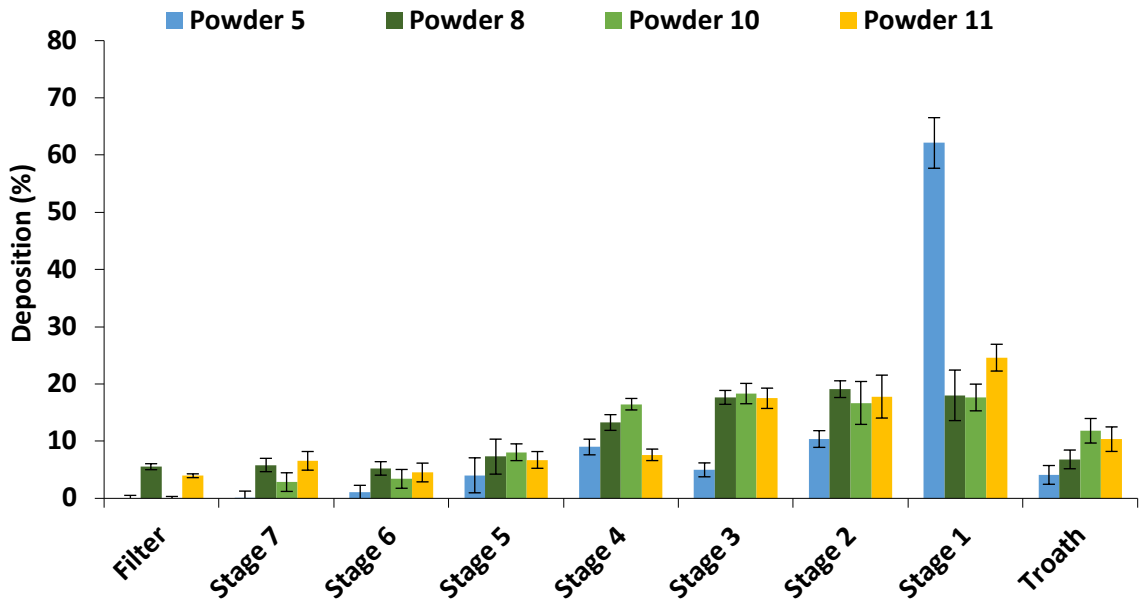

Figure 3.17. Percentage distribution in the various parts of the Next Generation Impactor of the powders containing trehalose-mannitol-lysozyme, in different concentrations. The bars represent the standard deviation.

As for the trehalose-mannitol powders without lysozyme, also in this case, the data in Figure 3.17 have been processed and also transformed into a cumulative undersize distribution o calculate the aerodynamic parameters (Table 3.13).

Table 3.13. Aerodynamic parameters (Emitted Dose %, FPF and MMAD) of mannitol-trehalose-lysozyme powders obtained by spray drying containing trehalose-mannitol-lysozyme in different concentrations.

Powder	Emitted dose (%)	MMAD (µm)	FPF (%)
5	98.97 ± 3.71	4.68 ± 0.40	38.23 ± 1.06
8	93.67 ± 1.93	2.37 ± 0.25	73.79 ± 3.21
10	96.33 ± 3.65	2.36 ± 0.02	71.62 ± 2.25
11	103.10 ± 1.70	2.64 ± 0.17	61.80 ± 1.08

The loaded powder dose compared to emitted dose almost quantitatively for all the tested powders. The MMAD was comparable and only slightly higher for powder 11. Powder 5 presented the lowest respirability, due to the highest MMAD as a consequence of a large deposition in stage 1.

Overall, this data confirmed the suitability of the approach to obtain respirable powders of lysozyme through a spray drying process: powder 8 containing 25% lysozyme, being the remaining mass an equiponderal blend of trehalose and mannitol, presented a sufficiently high activity of the enzyme and proved to be highly respirable.

5 Conclusion

From the data obtained in the third part of the thesis project, it is possible to conclude that a inhalable powder can be obtained by spray drying a solution containing trehalose and mannitol (50:50 w/w). Despite the relatively large volumetric diameter, these formulations afford an aerodynamic diameter particularly favorable for respirability. This aspect has to be considered with particular emphasis as the combination of large volumetric dimension with a small aerodynamic is a feature of value for powder for inhalation as it can be easy handled (transported, metered etc.) while keeping the good capability of lung penetration typical of micronized powders. The MMAD and therefore the particle respirability can be controlled by optimizing the three main parameters of the spray drying process, namely, drying inlet temperature, nozzle diameter and aspiration flow. Better results in this respect, are obtained by reducing all these three parameters.

The mannitol-trehalose spray dried powder proved to be a suitable formulation for the production of respirable powders containing relatively high amount of lysozyme.

As an overall conclusion, the present PhD project has evidenced that it is possible to exploit mannitol in its different polymorphic forms as carrier in formulation for inhalation in alternative to lactose.

The results reported in the present thesis, the results reported in the thesis are placed side by side with the ethical literature and provide a further contribution to the advancement of knowledge about the possible exploitation of the specific physico-chemical differences offered by mannitol polymorphs as useful tool for tuning the aerodynamic performance of small molecules with different hydrophilicity.

In addition, mannitol can be considered a first choice material for building-up , alone or in combination with other sugars, highly respirable microparticles for the next generation inhalable products taking a twofold advantage: the intrinsic low reactivity of the sugar alcohols toward protein amino groups and the peculiar capability of mannitol to afford solid particles with distinct volumetric and aerodynamic dimension.

6 Bibliography

[1] N. Shetty, D. Cipolla, H. Park, and Q. T. Zhou, "Physical stability of dry powder inhaler formulations," *Expert Opin. Drug Deliv.*, vol. 17, no. 1, pp. 77–96, 2020, doi: 10.1080/17425247.2020.1702643.

[2] H. M. Abdelaziz *et al.*, "Inhalable particulate drug delivery systems for lung cancer therapy: Nanoparticles, microparticles, nanocomposites and nanoaggregates," *J. Control. Release*, vol. 269, no. November 2017, pp. 374–392, 2018, doi: 10.1016/j.jconrel.2017.11.036.

[3] M. Malamatari, A. Charisi, S. Malamataris, and K. Kachrimanis, "Spray Drying for the Preparation of Nanoparticle-Based Drug Formulations as Dry Powders for Inhalation," *Processes*, vol. 8, no. 788, pp. 1–27, 2020, doi: doi:10.3390/pr8070788.

[4] X. Zhang *et al.*, "A Systematic Safety Evaluation of Nanoporous Mannitol Material as a Dry-Powder Inhalation Carrier System," *J. Pharm. Sci.*, vol. 109, no. 5, pp. 1692–1702, 2020, doi: 10.1016/j.xphs.2020.01.017.

[5] Y. Zhang, B. Mackenzie, J. J. Koleng, E. Maier, Z. N. Warnken, and R. O. Williams, "Development of an Excipient-Free Peptide Dry Powder Inhalation for the Treatment of Pulmonary Fibrosis," *Mol. Pharm.*, vol. 17, no. 2, pp. 632–644, 2020, doi: 10.1021/acs.molpharmaceut.9b01085.

[6] E. Quarta *et al.*, "Excipient-free pulmonary insulin dry powder: Pharmacokinetic and pharmacodynamics profiles in rats," *J. Control. Release*, vol. 323, no. February, pp. 412–420, 2020, doi: 10.1016/j.jconrel.2020.04.015.

[7] A. H. de Boer, P. Hagedoorn, M. Hoppentocht, F. Buttini, F. Grasmeijer, and H. W. Frijlink, "Dry powder inhalation: past, present and future," *Expert Opin. Drug Deliv.*, vol. 14, no. 4, pp. 499–512, 2017, doi: 10.1080/17425247.2016.1224846.

[8] J. Kozáková *et al.*, "Dry powder inhaler of colistimethate sodium for lung infections in cystic fibrosis: optimization of powder construction," *Drug Dev. Ind. Pharm.*, vol. 45, no. 10, pp. 1664–1673, 2019, doi: 10.1080/03639045.2019.1652636.

[9] Y.-H. Liao, M. B. Brown, A. Quader, and G. P. Martin, "Investigation of the physical properties of spray-dried stabilised lysozyme particles," *J. Pharm. Pharmacol.*, vol. 55, no. 9, pp. 1213–1221, 2003, doi: 10.1211/0022357021611.

[10] Y. Y. Lee, J. X. Wu, M. Yang, P. M. Young, F. Van Den Berg, and J. Rantanen, "Particle size dependence of polymorphism in spray-dried mannitol," *Eur. J. Pharm.*

Sci., vol. 44, no. 1–2, pp. 41–48, 2011, doi: 10.1016/j.ejps.2011.06.002.

[11] G. Kanojia, R. ten Have, P. C. Soema, H. Frijlink, J. P. Amorij, and G. Kersten, "Developments in the formulation and delivery of spray dried vaccines," *Hum. Vaccines Immunother.*, vol. 13, no. 10, pp. 2364–2378, 2017, doi: 10.1080/21645515.2017.1356952.

[12] R. H. Notter, "Lung surfactants Basic Science and Clinical Application," *Marcel Dekker, Inc.*, vol. 149. Marcel Dekker, Inc., New York, pp. 119–150, 2000.

[13] J. G. Weers *et al.*, "Pulmonary formulations: What remains to be done?," *J. Aerosol Med. Pulm. Drug Deliv.*, vol. 23, no. SUPPL. 2, 2010, doi: 10.1089/jamp.2010.0838.

[14] J. E. Hastedt *et al.*, "Erratum to: Scope and relevance of a pulmonary biopharmaceutical classification system AAPS/FDA/USP Workshop March 16-17th, 2015 in Baltimore, MD," *AAPS Open*, vol. 2, no. 1, p. 41120, 2016, doi: 10.1186/s41120-016-0005-2.

[15] A. Della Bella, E. Salomi, F. Buttini, and R. Bettini, "The role of the solid state and physical properties of the carrier in adhesive mixtures for lung delivery," *Expert Opin. Drug Deliv.*, vol. 15, no. 7, pp. 665–674, 2018, doi: 10.1080/17425247.2017.1371132.

[16] Q. T. Zhou, P. Tang, S. S. Y. Leung, J. G. Y. Chan, and H. K. Chan, "Emerging inhalation aerosol devices and strategies: Where are we headed?," *Adv. Drug Deliv. Rev.*, vol. 75, pp. 3–17, 2014, doi: 10.1016/j.addr.2014.03.006.

[17] A. H. De Boer and P. Hagedoorn, "The role of disposable inhalers in pulmonary drug delivery," *Expert Opin. Drug Deliv.*, vol. 12, no. 1, pp. 143–157, 2015, doi: 10.1517/17425247.2014.952626.

[18] S. Hoe, M. A. Boraey, J. W. Ivey, W. H. Finlay, and R. Vehring, "Manufacturing and device options for the delivery of biotherapeutics," *J. Aerosol Med. Pulm. Drug Deliv.*, vol. 27, no. 5, pp. 315–328, 2014, doi: 10.1089/jamp.2013.1090.

[19] M. B. Dolovich and R. Dhand, "Aerosol drug delivery: Developments in device design and clinical use," *Lancet*, vol. 377, no. 9770, pp. 1032–1045, 2011, doi: 10.1016/S0140-6736(10)60926-9.

[20] D. A. Edwards and C. Dunbar, "Bioengineering of Therapeutic Aerosols," *Annu. Rev. Biomed. Eng.*, vol. 4, no. 1, pp. 93–107, 2002, doi: 10.1146/annurev.bioeng.4.100101.132311.

[21] M. J. Telko and A. J. Hickey, "Dry Powder Inhaler Formulation," *Respir Care*, vol. 50, no. 9, pp. 1209–1227, 2005, doi: 10.2165/00128413-200615470-00016.

[22] A. G. Balducci, R. Bettini, P. Colombo, and F. Buttini, "Drug delivery strategies for

pulmonary administration of antibiotics," in *Pulmonary Drug Delivery, Advances and Challenges*, A. Nokhodchi and G. P. Martin, Eds. John Wiley & Sons Ltd., 2015, pp. 241–261.

[23] T. Peng *et al.*, "Influence of physical properties of carrier on the performance of dry powder inhalers," *Acta Pharm. Sin. B*, vol. 6, no. 4, pp. 308–318, 2016, doi: 10.1016/j.apsb.2016.03.011.

[24] N. Islam and E. Gladki, "Dry powder inhalers (DPIs)-A review of device reliability and innovation," *Int. J. Pharm.*, vol. 360, no. 1–2, pp. 1–11, 2008, doi: 10.1016/j.ijpharm.2008.04.044.

[25] Y. S. Cheng, "Mechanisms of pharmaceutical aerosol deposition in the respiratory tract," *AAPS PharmSciTech*, vol. 15, no. 3, pp. 630–640, 2014, doi: 10.1208/s12249-014-0092-0.

[26] R. R. Rajendran and A. Banerjee, "Mucus transport and distribution by steady expiration in an idealized airway geometry," *Med. Eng. Phys.*, vol. 66, pp. 26–39, 2019, doi: 10.1016/j.medengphy.2019.02.006.

[27] A. Kourmatzis, S. Cheng, and H. K. Chan, "Airway geometry, airway flow, and particle measurement methods: implications on pulmonary drug delivery," *Expert Opin. Drug Deliv.*, vol. 15, no. 3, pp. 271–282, 2018, doi: 10.1080/17425247.2018.1406917.

[28] M. Rahimi-Gorji, T. B. Gorji, and M. Gorji-Bandpy, "Details of regional particle deposition and airflow structures in a realistic model of human tracheobronchial airways: Two-phase flow simulation," *Comput. Biol. Med.*, vol. 74, pp. 1–17, 2016, doi: 10.1016/j.compbiomed.2016.04.017.

[29] A. H. De Boer, D. Gjaltema, P. Hagedoorn, and H. W. Frijlink, "Can 'extrafine' dry powder aerosols improve lung deposition?," *Eur. J. Pharm. Biopharm.*, vol. 96, pp. 143–151, 2015, doi: 10.1016/j.ejpb.2015.07.016.

[30] P. Colombo, D. Traini, and F. Buttini, "Inhalation Drug Delivery: Techniques and Products." Wiley-Blackwell, Chichester; West Sussex, UK, pp. 47–119, 2013, doi: 10.1002/9781118397145.

[31] A. Della Bella, M. Müller, A. Danani, L. Soldati, and R. Bettini, "Effect of lactose pseudopolymorphic transition on the aerosolization performance of drug/carrier mixtures," *Pharmaceutics*, vol. 11, no. 11, 2019, doi: 10.3390/pharmaceutics11110576.

[32] A. O. Shalash, A. M. Molokhia, and M. M. A. Elsayed, "Insights into the roles of

carrier microstructure in adhesive/carrier-based dry powder inhalation mixtures: Carrier porosity and fine particle content," *Eur. J. Pharm. Biopharm.*, vol. 96, pp. 291–303, 2015, doi: 10.1016/j.ejpb.2015.08.006.

[33] R. Y. Yang, R. P. Zou, A. B. Yu, and S. K. Choi, "Characterization of interparticle forces in the packing of cohesive fine particles," *Phys Rev E Stat Nonlinear Soft Matter Phys*, vol. 78, 2008, doi: 10.1103/PhysRevE.78.031302.

[34] A. Burger, J.-O. Henck, S. Hetz, J. M. Rollinger, A. A. Weissnicht, and H. Stöttner, "Energy/Temperature Diagram and Compression Behavior of the Polymorphs of d-Mannitol," *J. Pharm. Sci.*, vol. 89, no. 4, pp. 457–468, Apr. 2000, doi: 10.1002/(SICI)1520-6017(200004)89:4<457::AID-JPS3>3.0.CO;2-G.

[35] P. Heljo, "Comparison of disaccharides and polyalcohols as stabilizers in freeze-dried protein formulations," *Faculty of Pharmacy, University of Helsinki, Finland, PhD Thesis*. pp. 23–50, 2013.

[36] P. Khadka, P. C. Hill, B. Zhang, R. Katare, J. Dummer, and S. C. Das, "A study on polymorphic forms of rifampicin for inhaled high dose delivery in tuberculosis treatment," *Int. J. Pharm.*, vol. 587, no. July, p. 119602, 2020, doi: 10.1016/j.ijpharm.2020.119602.

[37] R. A. Storey and I. Ymén, "Solid State Characterization of Pharmaceuticals," *Solid State Characterization of Pharmaceuticals*. A John Wiley & Sons, Ltd, Chippenham, UK, pp. 1–31, 2011, doi: 10.1002/9780470656792.

[38] W. C. McCrone, "'Physics and chemistry of the organic solid state.' Polymorphism." New York: Wiley Interscience, New York, pp. 725–76, 1965.

[39] H. G. Brittain, "Polymorphism in Pharmaceutical Solids edited," in *Polymorphism in Pharmaceutical Solids: Second Edition*, 2009, vol. 192, pp. 1–640.

[40] A. Y. Lee, D. Erdemir, and A. S. Myerson, "Crystal polymorphism in chemical process development," *Annu. Rev. Chem. Biomol. Eng.*, vol. 2, pp. 259–280, 2011, doi: 10.1146/annurev-chembioeng-061010-114224.

[41] L. Yu and K. Ng, "Glycine Crystallization during Spray Drying: The pH Effect on Salt and Polymorphic Forms," *J. Pharm. Sci.*, vol. 91, no. 11, pp. 2367–2375, Nov. 2002, doi: 10.1002/jps.10225.

[42] M. Maldonado, M. D. Oleksiak, S. Chinta, and J. D. Rimer, "Controlling crystal polymorphism in organic-free synthesis of na-zeolites," *J. Am. Chem. Soc.*, vol. 135, no. 7, pp. 2641–2652, 2013, doi: 10.1021/ja3105939.

[43] J. Bernstein, R. J. Davey, and J. O. Henck, "Concomitant polymorphs," *Angew.*

Chemie - Int. Ed., vol. 38, no. 23, pp. 3440–3461, 1999, doi: 10.1002/(sici)1521-3773(19991203)38:23<3440::aid-anie3440>3.0.co;2-%23.

[44] B. K. Hodnett and V. Verma, "Thermodynamic vs. kinetic basis for polymorph selection," *Processes*, vol. 7, no. 5, pp. 1–12, 2019, doi: 10.3390/pr7050272.

[45] J. F. B. Black, P. T. Cardew, A. J. Cruz-Cabeza, R. J. Davey, S. E. Gilks, and R. A. Sullivan, "Crystal nucleation and growth in a polymorphic system: Ostwald's rule,: P - aminobenzoic acid and nucleation transition states," *CrystEngComm*, vol. 20, no. 6, pp. 768–776, 2018, doi: 10.1039/c7ce01960b.

[46] D. Croker and B. K. Hodnett, "Mechanistic features of polymorphic transformations: The role of surfaces," *Cryst. Growth Des.*, vol. 10, no. 6, pp. 2808–2816, 2010, doi: 10.1021/cg901594c.

[47] S. Datta and D. J. W. Grant, "Crystal structures of drugs: Advances in determination, prediction and engineering," *Nat. Rev. Drug Discov.*, vol. 3, no. 1, pp. 42–57, 2004, doi: 10.1038/nrd1280.

[48] G. M. Keserü and G. M. Makara, "The influence of lead discovery strategies on the properties of drug candidates," *Nat. Rev. Drug Discov.*, vol. 8, no. 3, pp. 203–212, 2009, doi: 10.1038/nrd2796.

[49] D. J. Hauss, "Oral lipid-based formulations," *Adv. Drug Deliv. Rev.*, vol. 59, no. 7, pp. 667–676, 2007, doi: 10.1016/j.addr.2007.05.006.

[50] L. Chen, T. Okuda, X. Y. Lu, and H. K. Chan, "Amorphous powders for inhalation drug delivery," *Adv. Drug Deliv. Rev.*, vol. 100, pp. 102–115, 2016, doi: 10.1016/j.addr.2016.01.002.

[51] D. Singhal and W. Curatolo, "Drug polymorphism and dosage form design: A practical perspective," *Adv. Drug Deliv. Rev.*, vol. 56, no. 3, pp. 335–347, 2004, doi: 10.1016/j.addr.2003.10.008.

[52] P. Colombo, P. Catellani, A. Gazzaniga, E. Menegatti, and E. Vidale, "Principi di tecnologie farmaceutiche." Casa editrice ambrosiana, Italy, pp. 519–531, 2004.

[53] A. Benassi, I. Perazzi, R. Bosi, C. Cottini, and R. Bettini, "Quantifying the loading capacity of a carrier-based DPI formulation and its dependence on the blending process," *Powder Technol.*, vol. 356, pp. 607–617, 2019, doi: 10.1016/j.powtec.2019.08.109.

[54] A. O. Shalash and M. M. A. Elsayed, "A new role of fine excipient materials in carrier-based dry powder inhalation mixtures: effect on deagglomeration of drug particles during mixing revealed," *AAPS PharmSciTech*, vol. 18, 2017, doi:

10.1208/s12249-017-0767-4.

[55] W. Kaialy *et al.*, "Characterisation and deposition studies of recrystallised lactose from binary mixtures of ethanol/butanol for improved drug delivery from dry powder inhalers," *AAPS J.*, vol. 13, no. 1, pp. 30–43, 2011, doi: 10.1208/s12248-010-9241-x.

[56] J. M. Sonnergaard, "Quantification of the compactibility of pharmaceutical powders," vol. 63, pp. 270–277, 2006, doi: 10.1016/j.ejpb.2005.10.012.

[57] A. Borde, A. Ekman, J. Holmgren, and A. Larsson, "Effect of protein release rates from tablet formulations on the immune response after sublingual immunization," *Eur. J. Pharm. Sci.*, vol. 47, no. 4, pp. 695–700, 2012, doi: 10.1016/j.ejps.2012.08.014.

[58] G. W. Canonica *et al.*, "Clinical efficacy of sublingual immunotherapy tablets for allergic rhinitis is unlikely to be derived from in vitro allergen-release data," *Expert Rev. Clin. Immunol.*, vol. 15, no. 9, pp. 921–928, 2019, doi: 10.1080/1744666X.2019.1649597.

[59] S. L. Bahna, "Is it milk allergy or lactose intolerance?," *Immunol. Allergy Clin. North Am.*, vol. 16, no. 1, pp. 187–198, 1996, doi: 10.1016/S0889-8561(05)70242-3.

[60] A. Nowak-Wegrzyn, G. Shapiro, and K. Beyer, "Contamination of dry powder inhalers for asthma with milk proteins containing lactose," *J Allergy Clin Immunol*, vol. 113, no. 3, pp. 558–60, 2004.

[61] G. L. Rossi, A. Corsico, and G. Moscato, "Occupational asthma caused by milk proteins: Report on a case," *J. Allergy Clin. Immunol.*, vol. 93, no. 4, pp. 799–801, 1994, doi: 10.1016/0091-6749(94)90261-5.

[62] D. L. Swagerty, A. D. Walling, and R. M. Klein, "Lactose intolerance," *Gac. Med. Mex.*, vol. 152, pp. 67–73, 2016, doi: 10.7748/phc2006.02.16.1.41.c595.

[63] K. Thalberg, S. Åslund, M. Skogevall, and P. Andersson, "Dispersibility of lactose fines as compared to API in dry powders for inhalation," *Int. J. Pharm.*, vol. 504, no. 1–2, pp. 27–38, 2016, doi: 10.1016/j.ijpharm.2016.03.004.

[64] G. Schaafsma, "Lactose and lactose derivatives as bioactive ingredients in human nutrition," *Int. Dairy J.*, vol. 18, no. 5, pp. 458–465, 2008, doi: 10.1016/j.idairyj.2007.11.013.

[65] J. Parkerson and D. Ledford, "Mannitol as an indirect bronchoprovocation test for the 21st century," *Ann. Allergy, Asthma Immunol.*, vol. 106, no. 2, pp. 91–96, 2011, doi: 10.1016/j.anai.2010.11.010.

[66] S. J. Nevitt, J. Thornton, C. S. Murray, and T. Dwyer, "Inhaled mannitol for cystic fibrosis," *Cochrane Database Syst. Rev.*, vol. 2020, no. 5, 2020, doi:

10.1002/14651858.CD008649.pub4.

[67] V. Vanhoorne, B. Bekaert, E. Peeters, T. De Beer, J. P. Remon, and C. Vervaet, "Improved tabletability after a polymorphic transition of delta-mannitol during twin screw granulation," *Int. J. Pharm.*, vol. 506, no. 1–2, pp. 13–24, 2016, doi: 10.1016/j.ijpharm.2016.04.025.

[68] R. R. Smith, U. V. Shah, J. V. Parambil, D. J. Burnett, F. Thielmann, and J. Y. Y. Heng, "The Effect of Polymorphism on Surface Energetics of D-Mannitol Polymorphs," *AAPS J.*, vol. 19, no. 1, pp. 103–109, 2017, doi: 10.1208/s12248-016-9978-y.

[69] M. G. Cares-Pacheco *et al.*, "Physicochemical characterization of d-mannitol polymorphs: The challenging surface energy determination by inverse gas chromatography in the infinite dilution region," *Int. J. Pharm.*, vol. 475, no. 1–2, pp. 69–81, 2014, doi: 10.1016/j.ijpharm.2014.08.029.

[70] H. M. Berman, G. A. Jeffrey, and R. D. Rosenstein, "The crystal structures of the alpha and beta forms of D-mannitol.," *Acta Crystallogr. B.*, vol. 24, no. 3, pp. 442–449, 1968, doi: 10.1107/S0567740868002530.

[71] G. Bruni *et al.*, "Physico-chemical Characterization of anhydrous D-mannitol," vol. 95, pp. 871–876, 2009.

[72] S. Focaroli *et al.*, "A Design of Experiment (DoE) approach to optimise spray drying process conditions for the production of trehalose/leucine formulations with application in pulmonary delivery," *Int. J. Pharm.*, vol. 562, no. November 2018, pp. 228–240, 2019, doi: 10.1016/j.ijpharm.2019.03.004.

[73] N. B. Carrigy *et al.*, "Amorphous pullulan trehalose microparticle platform for respiratory delivery," *Int. J. Pharm.*, vol. 563, no. March, pp. 156–168, 2019, doi: 10.1016/j.ijpharm.2019.04.004.

[74] J. L. Crisp, S. E. Dann, and C. G. Blatchford, "Antisolvent crystallization of pharmaceutical excipients from aqueous solutions and the use of preferred orientation in phase identification by powder X-ray diffraction," *Eur. J. Pharm. Sci.*, vol. 42, no. 5, pp. 568–577, 2011, doi: 10.1016/j.ejps.2011.02.010.

[75] A. Lerbret, P. Bordat, F. Affouard, M. Descamps, and F. Migliardo, "How homogeneous are the trehalose, maltose, and sucrose water solutions? An insight from molecular dynamics simulations," *J. Phys. Chem. B*, vol. 109, no. 21, pp. 11046–11057, 2005, doi: 10.1021/jp0468657.

[76] W. L. Hulse, R. T. Forbes, M. C. Bonner, and M. Getrost, "Do co-spray dried

excipients offer better lysozyme stabilisation than single excipients?," *Eur. J. Pharm. Sci.*, vol. 33, no. 3, pp. 294–305, 2008, doi: 10.1016/j.ejps.2007.12.007.

[77] S. A. Shoyele and S. Cawthorne, "Particle engineering techniques for inhaled biopharmaceuticals," *Adv. Drug Deliv. Rev.*, vol. 58, no. 9–10, pp. 1009–1029, 2006, doi: 10.1016/j.addr.2006.07.010.

[78] S. Ohtake, Y. Kita, and T. Arakawa, "Interactions of formulation excipients with proteins in solution and in the dried state," *Adv. Drug Deliv. Rev.*, vol. 63, no. 13, pp. 1053–1073, 2011, doi: 10.1016/j.addr.2011.06.011.

[79] M. A. Mensink, H. W. Frijlink, K. van der Voort Maarschalk, and W. L. J. Hinrichs, "How sugars protect proteins in the solid state and during drying (review): Mechanisms of stabilization in relation to stress conditions," *Eur. J. Pharm. Biopharm.*, vol. 114, pp. 288–295, 2017, doi: 10.1016/j.ejpb.2017.01.024.

[80] N. Grasmeijer, M. Stankovic, H. De Waard, H. W. Frijlink, and W. L. J. Hinrichs, "Unraveling protein stabilization mechanisms: Vitrification and water replacement in a glass transition temperature controlled system," *Biochim. Biophys. Acta - Proteins Proteomics*, vol. 1834, no. 4, pp. 763–769, 2013, doi: 10.1016/j.bbapap.2013.01.020.

[81] K. M. Forney-Stevens, M. J. Pelletier, E. Y. Shalaev, M. J. Pikal, and R. H. Bogner, "Optimization of a Raman microscopy technique to efficiently detect amorphous-amorphous phase separation in freeze-dried protein formulations," *J. Pharm. Sci.*, vol. 103, no. 9, pp. 2749–2758, 2014, doi: 10.1002/jps.23882.

[82] S. Ferrati, T. Wu, S. R. Kanapuram, and H. D. C. Smyth, "Dosing considerations for inhaled biologics," *Int. J. Pharm.*, vol. 549, no. 1–2, pp. 58–66, 2018, doi: 10.1016/j.ijpharm.2018.07.054.

[83] V. Vanhoorne *et al.*, "Continuous manufacturing of delta mannitol by cospray drying with PVP," *Int. J. Pharm.*, vol. 501, no. 1–2, pp. 139–147, 2016, doi: 10.1016/j.ijpharm.2016.02.001.

[84] F. R. Fronczek, H. N. Kamel, and M. Slattery, "Three polymorphs (α, β, and δ) of d-mannitol at 100 K," *Acta Crystallogr. Sect. C Cryst. Struct. Commun.*, vol. 59, no. 10, pp. 567–570, 2003, doi: 10.1107/S0108270103018961.

[85] L. Yu, N. Milton, E. G. Groleau, D. S. Mishra, and R. E. Vansickle, "Existence of a mannitol hydrate during freeze-drying and practical implications," *J. Pharm. Sci.*, vol. 88, no. 2, pp. 196–198, 1999, doi: 10.1021/js980323h.

[86] C. M. Xian Ming Zeng, Gary Peter Martin, "Particulate Interactions in Dry Powder Formulations for Inhalation." CRC Press, London, pp. 135–204, 2000.

[87] K. A. Foster, M. L. Avery, M. Yazdanian, and K. L. Audus, "Characterization of the Calu-3 cell line as a tool to screen pulmonary drug delivery," *Int. J. Pharm.*, vol. 208, no. 1–2, pp. 1–11, 2000, doi: 10.1016/S0378-5173(00)00452-X.

[88] D. M. Silva, R. Paleco, D. Traini, and V. Sencadas, "Development of ciprofloxacin-loaded poly(vinyl alcohol) dry powder formulations for lung delivery," *Int. J. Pharm.*, vol. 547, no. 1–2, pp. 114–121, 2018, doi: 10.1016/j.ijpharm.2018.05.060.

[89] C. Nunes, R. Suryanarayanan, C. E. Botez, and P. W. Stephens, "Characterization and crystal structure of D-mannitol hemihydrate," *J. Pharm. Sci.*, vol. 93, no. 11, pp. 2800–2809, 2004, doi: 10.1002/jps.20185.

[90] W. Kaialy, M. N. Momin, M. D. Ticehurst, J. Murphy, and A. Nokhodchi, "Engineered mannitol as an alternative carrier to enhance deep lung penetration of salbutamol sulphate from dry powder inhaler," *Colloids Surfaces B Biointerfaces*, vol. 79, no. 2, pp. 345–356, 2010, doi: 10.1016/j.colsurfb.2010.04.016.

[91] A. M. Boshhiha and N. A. Urbanetz, "Influence of carrier surface fines on dry powder inhalation formulations," *Drug Dev. Ind. Pharm.*, vol. 35, no. 8, pp. 904–916, 2009, doi: 10.1080/03639040802698794.

[92] M. Momin, A. Hedayati, and A. Nokhodchi, "Investigation into Alternative Sugars as Potential Carriers for Dry Powder Formulation of Budesonide," vol. 1, no. 2, pp. 105–111, 2011.

[93] G. Pilcer, N. Wauthoz, and K. Amighi, "Lactose characteristics and the generation of the aerosol," *Adv. Drug Deliv. Rev.*, vol. 64, no. 3, pp. 233–256, 2012, doi: 10.1016/j.addr.2011.05.003.

[94] N. Grabowski *et al.*, "Toxicity of surface-modified PLGA nanoparticles toward lung alveolar epithelial cells," *Int. J. Pharm.*, vol. 454, no. 2, pp. 686–694, 2013, doi: 10.1016/j.ijpharm.2013.05.025.

[95] S. Ahlberg *et al.*, "PVP-coated, negatively charged silver nanoparticles: A multi-center study of their physicochemical characteristics, cell culture and in vivo experiments," *Beilstein J. Nanotechnol.*, vol. 5, pp. 1944–1965, 2014, doi: 10.3762/bjnano.5.205.

[96] M. Kurakula and G. S. N. K. Rao, "Pharmaceutical assessment of polyvinylpyrrolidone (PVP): As excipient from conventional to controlled delivery systems with a spotlight on COVID-19 inhibition," *J. Drug Deliv. Sci. Technol.*, vol. 60, no. September, p. 102046, 2020, doi: 10.1016/j.jddst.2020.102046.

[97] L. X. Yu *et al.*, "Understanding Pharmaceutical Quality by Design," *AAPS J.*, vol. 16, no. 4, pp. 771–783, 2014, doi: 10.1208/s12248-014-9598-3.

[98] L. X. Yu, "Pharmaceutical quality by design: Product and process development, understanding, and control," *Pharm. Res.*, vol. 25, no. 4, pp. 781–791, 2008, doi: 10.1007/s11095-007-9511-1.

[99] U.S. Department of Health and Human Services Food and Drug Administration, "ICH Q8(R2) Pharmaceutical Development," *Work. Qual. by Des. Pharm.*, vol. 8, no. November, p. 28, 2009.

[100] A. A. Signore and T. Jacobs, "Good Design Practices for GMP Pharmaceutical Facilities," *Good Des. Pract. GMP Pharm. Facil.*, 2005, doi: 10.1201/9780849398537.

[101] D. Diez, M. Cetinkaya-Rundel, and C. D. Barr, "OpenIntro Statistics.pdf." openintro.org/os, Duke University, pp. 7–71, 2019.

[102] E. Faulhammer, V. Wahl, S. Zellnitz, J. G. Khinast, and A. Paudel, "Carrier-based dry powder inhalation: Impact of carrier modification on capsule filling processability and in vitro aerodynamic performance," *Int. J. Pharm.*, vol. 491, no. 1–2, pp. 231–242, 2015, doi: 10.1016/j.ijpharm.2015.06.044.

[103] S. Stranzinger *et al.*, "The effect of material attributes and process parameters on the powder bed uniformity during a low-dose dosator capsule filling process," *Int. J. Pharm.*, vol. 516, no. 1–2, pp. 9–20, 2017, doi: 10.1016/j.ijpharm.2016.11.010.

[104] N. Hertel, G. Birk, and R. Scherließ, "Particle engineered mannitol for carrier-based inhalation – A serious alternative?," *Int. J. Pharm.*, vol. 577, p. 118901, 2020, doi: 10.1016/j.ijpharm.2019.118901.

[105] M. Fink, "Continuous low-dose capsule filling of pharmaceutical inhalation powders," no. January, 2014.

[106] F. Buttini *et al.*, "Multivariate Analysis of Effects of Asthmatic Patient Respiratory Profiles on the in Vitro Performance of a Reservoir Multidose and a Capsule-Based Dry Powder Inhaler," *Pharm. Res.*, vol. 33, no. 3, pp. 701–715, 2016, doi: 10.1007/s11095-015-1820-1.

[107] P. Muralidharan, D. Hayes, and H. M. Mansour, "Dry powder inhalers in COPD, lung inflammation and pulmonary infections," *Expert Opin. Drug Deliv.*, vol. 12, no. 6, pp. 947–962, 2015, doi: 10.1517/17425247.2015.977783.

[108] F. Martinelli, A. G. Balducci, A. Rossi, F. Sonvico, P. Colombo, and F. Buttini, "'Pierce and inhale' design in capsule based dry powder inhalers: Effect of capsule piercing and motion on aerodynamic performance of drugs," *Int. J. Pharm.*, vol. 487, no. 1–2, pp. 197–204, 2015, doi: 10.1016/j.ijpharm.2015.04.003.

[109] N. Wauthoz, I. Hennia, S. Ecenarro, and K. Amighi, "Impact of capsule type on aerodynamic performance of inhalation products: A case study using a formoterol-lactose binary or ternary blend," *Int. J. Pharm.*, vol. 553, no. 1–2, pp. 47–56, 2018, doi: 10.1016/j.ijpharm.2018.10.034.

[110] M. S. Coates, D. F. Fletcher, H. K. Chan, and J. A. Raper, "The role of capsule on the performance of a dry powder inhaler using computational and experimental analyses," *Pharm. Res.*, vol. 22, no. 6, pp. 923–932, 2005, doi: 10.1007/s11095-005-4587-y.

[111] M. Šimek, V. Grünwaldová, and B. Kratochvíl, "Comparison of compression and material properties of differently shaped and sized paracetamols," *KONA Powder Part. J.*, vol. 2017, no. 34, pp. 197–206, 2017, doi: 10.14356/kona.2017003.

[112] B. Shah, V. K. Kakumanu, and A. K. Bansal, "Analytical Techniques fo Quantification of Amorphous/Crystalline Phases in Pharmaceutical Solids," *J. Pharm. Sci.*, vol. 96, no. 8, pp. 1641–1665, 2006, doi: 10.1002/jps.

[113] K. S. Khomane and A. K. Bansal, "Effect of particle size on in-die and out-of-die compaction behavior of ranitidine hydrochloride polymorphs," *AAPS PharmSciTech*, vol. 14, no. 3, pp. 1169–1177, 2013, doi: 10.1208/s12249-013-0008-4.

[114] M. Celik, *Pharmaceutical Powder Compaction Technology*, vol. 38, no. 8. 2012.

[115] E. Faulhammer *et al.*, "The effects of material attributes on capsule fill weight and weight variability in dosator nozzle machines," *Int. J. Pharm.*, vol. 471, no. 1–2, pp. 332–338, 2014, doi: 10.1016/j.ijpharm.2014.05.058.

[116] L. Riccardo, "CAT (Chemometric Agile Tool)," 2017. [Online]. Available: http://www.gruppochemiometria.it/index.php/software. [Accessed: 23-Mar-2020].

[117] C. Sun and D. J. W. Grant, "Influence of elastic deformation of particles on Heckel analysis," *Pharm. Dev. Technol.*, vol. 6, no. 2, pp. 193–200, 2001, doi: 10.1081/PDT-100000738.

[118] M. U. Ghori, "Powder Compaction: Compression Properties of Cellulose Ethers," *Br. J. Pharm.*, vol. 1, no. 1, 2016, doi: 10.5920/bjpharm.2016.09.

[119] G. Bonacucina, M. Cespi, M. Misici-Falzi, and G. F. Palmieri, "Mechanical characterization of pharmaceutical solids: A comparison between rheological tests performed under static and dynamic porosity conditions," *Eur. J. Pharm. Biopharm.*, vol. 67, no. 1, pp. 277–283, 2007, doi: 10.1016/j.ejpb.2006.12.018.

[120] M. Mönckedieck *et al.*, "Dry powder inhaler performance of spray dried mannitol with tailored surface morphologies as carrier and salbutamol sulphate," *Int. J. Pharm.*, vol. 524, no. 1–2, pp. 351–363, 2017, doi: 10.1016/j.ijpharm.2017.03.055.

[121] P. M. Young, S. Edge, D. Traini, M. D. Jones, R. Price, and D. El-Sabawi, "The influence of dose on the performance of dry powder inhalation systems," *Int J Pharm*, vol. 296, 2005, doi: 10.1016/j.ijpharm.2005.02.004.

[122] L. Yu, "Amorphous pharmaceutical solids: Preparation, characterization and stabilization," *Adv. Drug Deliv. Rev.*, vol. 48, no. 1, pp. 27–42, 2001, doi: 10.1016/S0169-409X(01)00098-9.

[123] X. Ma and R. O. Williams, "Characterization of amorphous solid dispersions: An update," *J. Drug Deliv. Sci. Technol.*, vol. 50, no. November 2018, pp. 113–124, 2019, doi: 10.1016/j.jddst.2019.01.017.

[124] S. R. Vippagunta, H. G. Brittain, and D. J. W. Grant, "Crystalline solids," *Adv. Drug Deliv. Rev.*, vol. 48, no. 1, pp. 3–26, 2001, doi: 10.1016/S0169-409X(01)00097-7.

[125] S. Dedroog, T. Pas, B. Vergauwen, C. Huygens, and G. Van den Mooter, "Solid-state analysis of amorphous solid dispersions: Why DSC and XRPD may not be regarded as stand-alone techniques," *J. Pharm. Biomed. Anal.*, vol. 178, p. 112937, 2020, doi: 10.1016/j.jpba.2019.112937.

[126] P. Pandi, R. Bulusu, N. Kommineni, W. Khan, and M. Singh, "Amorphous solid dispersions: An update for preparation, characterization, mechanism on bioavailability, stability, regulatory considerations and marketed products," *Int. J. Pharm.*, vol. 586, no. May, p. 119560, 2020, doi: 10.1016/j.ijpharm.2020.119560.

[127] J. F. Carpenter and J. H. Crowe, "An infrared spectroscopic study of the interactions of carbohydrates with dried proteins," *Biochemistry*, vol. 28, no. 9, pp. 3916–3922, 1989, doi: 10.1021/bi00435a044.

[128] F. Grasmeijer *et al.*, "New mechanisms to explain the effects of added lactose fines on the dispersion performance of adhesive mixtures for inhalation," *PLoS One*, vol. 9, 2014, doi: 10.1371/journal.pone.0087825.

[129] P. S. Belton and A. M. Gil, "IR and Raman spectroscopic studies of the interaction of trehalose with hen egg white lysozyme," *Biopolymers*, vol. 34, no. 7, pp. 957–961, 1994, doi: 10.1002/bip.360340713.

[130] P. M. Young *et al.*, "The use of organic vapor sorption to determine low levels of amorphous content in processed pharmaceutical powders," *Drug Dev. Ind. Pharm.*, vol. 33, no. 1, pp. 91–97, 2007, doi: 10.1080/03639040600969991.

[131] S. Sheokand, S. R. Modi, and A. K. Bansal, "Dynamic vapor sorption as a tool for characterization and quantification of amorphous content in predominantly crystalline materials," *J. Pharm. Sci.*, vol. 103, no. 11, pp. 3364–3376, 2014, doi:

10.1002/jps.24160.

[132] A. Della Bella, M. Müller, L. Soldati, L. Elviri, and R. Bettini, "Quantitative determination of micronization-induced changes in the solid state of lactose," *Int. J. Pharm.*, vol. 505, no. 1–2, pp. 383–393, 2016, doi: 10.1016/j.ijpharm.2016.04.015.

[133] D. L. Nelson and M. M. Cox, *Lehninger principles of biochemistry*, Fourth Edi. worth publisher, 2000.

[134] E. M. Wilson, J. C. Luft, and J. M. DeSimone, "Formulation of High-Performance Dry Powder Aerosols for Pulmonary Protein Delivery," *Pharm. Res.*, vol. 35, no. 10, 2018, doi: 10.1007/s11095-018-2452-z.

[135] R. Jaenicke, "Protein stability and molecular adaptation to extreme conditons," *Eur. J. Biochem.*, vol. 202, no. 3, pp. 715–728, 1991, doi: 10.1111/j.1432-1033.1991.tb16426.x.

[136] F. Albericio and H. G. Kruger, "Therapeutic peptides," *Future Med. Chem.*, vol. 4, no. 12, pp. 1527–1531, 2012, doi: 10.4155/fmc.12.94.

[137] J. L. Lau and M. K. Dunn, "Therapeutic peptides: Historical perspectives, current development trends, and future directions," *Bioorganic Med. Chem.*, vol. 26, no. 10, pp. 2700–2707, 2018, doi: 10.1016/j.bmc.2017.06.052.

[138] C. C. Teneback, T. C. Scanlon, M. J. Wargo, J. L. Bement, K. E. Griswold, and L. W. Leclair, "Bioengineered lysozyme reduces bacterial burden and inflammation in a murine model of mucoid Pseudomonas aeruginosa lung infection," *Antimicrob. Agents Chemother.*, vol. 57, no. 11, pp. 5559–5564, 2013, doi: 10.1128/AAC.00500-13.

[139] P. V. Gupta, A. M. Nirwane, and M. S. Nagarsenker, "Inhalable Levofloxacin Liposomes Complemented with Lysozyme for Treatment of Pulmonary Infection in Rats: Effective Antimicrobial and Antibiofilm Strategy," *AAPS PharmSciTech*, vol. 19, no. 3, pp. 1454–1467, 2018, doi: 10.1208/s12249-017-0945-4.

[140] A. Beaussart *et al.*, "Supported lysozyme for improved antimicrobial surface protection," *J. Colloid Interface Sci.*, vol. 582, pp. 764–772, 2021, doi: 10.1016/j.jcis.2020.08.107.

[141] S. Ji *et al.*, "Effect of ethanol as a co-solvent on the aerosol performance and stability of spray-dried lysozyme," *Int. J. Pharm.*, vol. 513, no. 1–2, pp. 175–182, 2016, doi: 10.1016/j.ijpharm.2016.09.025.

[142] N. Brestich, M. Rüdt, D. Büchler, and J. Hubbuch, "Selective protein quantification for preparative chromatography using variable pathlength UV/Vis spectroscopy and partial least squares regression," *Chem. Eng. Sci.*, vol. 176, pp. 157–164, 2018, doi:

10.1016/j.ces.2017.10.030.

[143] J. W. Visser and E. J. Sonneveld, "Automatic Collection of Powder Data from Photographs," *J. Appl. Crystallogr.*, vol. 8, no. June 1974, pp. 1–7, 1975.